Staphylococcal peroxidase inhibitor: structure/function analysis and studies on host-species specificity

by

Soheila Fatehi Abdoljabbar

B.S., University of Tabriz, 2010
M.S., University of Tabriz, 2014

AN ABSTRACT OF A DISSERTATION

submitted in partial fulfillment of the requirements for the degree

DOCTOR OF PHILOSOPHY

Department of Biochemistry and Molecular Biophysics
College of Arts and Sciences

KANSAS STATE UNIVERSITY
Manhattan, Kansas

2026

Abstract

Human neutrophils, the most abundant leukocytes in circulation, serve as the primary responders in the innate immune defense against bacterial pathogens. Following the opsonization of bacteria by antibodies or complement fragments, neutrophils execute killing through both extracellular traps (NETs) and intracellular phagocytosis. While neutrophils employ a diverse arsenal of granule-resident defenses including proteases, lysozymes, and antimicrobial peptides, their oxidative killing system is paramount to bacterial clearance. This oxidative process is centered on the heme-containing enzyme myeloperoxidase (MPO), the most abundant protein within the neutrophil. Myeloperoxidase as a critical component of the antibacterial arsenal of neutrophils, consumes H_2O_2 as an oxidant to convert halogen and pseudohalogen anions into cytotoxic hypohalous acids.

Following phagocytosis by neutrophils, the human pathogen *Staphylococcus aureus* secretes a potent myeloperoxidase inhibitory protein, called SPIN, as part of its immune evasion repertoire. The matured *S. aureus* SPIN polypeptide consists of only 73 residues yet contains two functional domains: whereas the 60 residue C-terminal helical bundle domain is responsible for MPO binding, the 13 residue N-terminal domain is required to inhibit MPO. Previous studies informed understanding of the SPIN N-terminal domain, but comparatively little was known about the helical domain insofar as the contribution of individual residues is concerned. To address this limitation, we carried out a residue-level structure/function investigation on the helical bundle domain of *S. aureus* SPIN. Using sequence conservation and existing structures of SPIN bound to human MPO, we selected residues L49, E50, H51, E52, Y55, and Y75 for interrogation by site-directed mutagenesis. We found that loss of L49 or E52 reduced SPIN activity by roughly an order of magnitude, but that loss of Y55 or H51 caused progressively

greater loss of inhibitory potency. Direct binding studies by SPR showed that loss of inhibitory potency in these SPIN mutants resulted from a diminished initial interaction between the inhibitor and MPO. Together, our studies provided new insights into the structure/function relationships of SPIN and identified positions Y55 and H51 as critical determinants of SPIN function.

S. aureus SPIN relies on its C-terminal α-helical bundle domain to mediate initial binding to MPO but requires a disordered N-terminal region to fold into a β-hairpin conformation to inhibit MPO activity. To further investigate the structure/function relationship of SPIN, we introduced two cysteine residues into its N-terminal region to trap SPIN in its MPO-bound conformation and characterized the modified protein, which we refer to here as SPIN-CYS. Although control experiments confirmed the presence of the disulfide bond in SPIN-CYS, solution structure determination revealed that the N-terminal region of SPIN-CYS adopted a physically constrained series of lariat-like structures rather than a well-defined β-hairpin. Nevertheless, SPIN-CYS exhibited a gain in inhibitory potency against human MPO when compared to wild-type SPIN. This gain of function persisted even in the presence of deleterious mutations within the C-terminal α-helical bundle domain. SPR studies showed that the gain in potency arose through an increase in apparent affinity of SPIN-CYS for MPO, which was driven primarily by an increased association rate with MPO when compared to wild-type SPIN. Together, this work provided new information on the coupled binding and folding events required to manifest biological activity of this unusual MPO inhibitor.

S. aureus is primarily a human pathogen, and its SPIN protein cannot inhibit MPO from many non-human species. Evaluation of the inhibitory potency of SPIN orthologs against hMPO, revealed that these proteins also exhibited significantly weaker potency compared to SPIN-

aureus. This raised questions as to whether staphylococci that prefer alternative mammalian species might produce SPIN proteins with binding preferences for MPO from those hosts. We tested this hypothesis by isolating canine MPO (cMPO) from individual and pooled abscess fluid samples and exploring its inhibition profile by different SPIN orthologs. Consistent in both trials, our results showed that SPIN proteins from known canine pathogens bind more tightly to and inhibit canine MPO more potently than human MPO. We also found that the increased affinity and potency arose from increases in the second order (i.e. association rate constant (k_a)) rate constant. Comparison of the prototypic of these inhibitors, *SPIN-delphini*, bound to canine MPO when compared to human MPO, explains the physical basis for our observation and provides support for our hypothesis. This work alongside our previous studies on SPIN/MPO interaction can be developed into a valuable model system for understanding the structure/function principles that underlie host-specific evolution of virulence proteins.

Staphylococcal peroxidase inhibitor: structure/function analysis and studies on host-species specificity

by

Soheila Fatehi Abdoljabbar

B.S., University of Tabriz, 2010
M.S., University of Tabriz, 2014

A DISSERTATION

submitted in partial fulfillment of the requirements for the degree

DOCTOR OF PHILOSOPHY

Department of Biochemistry and Molecular Biophysics
College of Arts and Sciences

KANSAS STATE UNIVERSITY
Manhattan, Kansas

2026

Approved by:

Major Professor
Dr. Brian V. Geisbrecht

Abstract

Human neutrophils, the most abundant leukocytes in circulation, serve as the primary responders in the innate immune defense against bacterial pathogens. Following the opsonization of bacteria by antibodies or complement fragments, neutrophils execute killing through both extracellular traps (NETs) and intracellular phagocytosis. While neutrophils employ a diverse arsenal of granule-resident defenses including proteases, lysozymes, and antimicrobial peptides, their oxidative killing system is paramount to bacterial clearance. This oxidative process is centered on the heme-containing enzyme myeloperoxidase (MPO), the most abundant protein within the neutrophil. Myeloperoxidase as a critical component of the antibacterial arsenal of neutrophils, consumes H_2O_2 as an oxidant to convert halogen and pseudohalogen anions into cytotoxic hypohalous acids.

Following phagocytosis by neutrophils, the human pathogen *Staphylococcus aureus* secretes a potent myeloperoxidase inhibitory protein, called SPIN, as part of its immune evasion repertoire. The matured *S. aureus* SPIN polypeptide consists of only 73 residues yet contains two functional domains: whereas the 60 residue C-terminal helical bundle domain is responsible for MPO binding, the 13 residue N-terminal domain is required to inhibit MPO. Previous studies informed understanding of the SPIN N-terminal domain, but comparatively little was known about the helical domain insofar as the contribution of individual residues is concerned. To address this limitation, we carried out a residue-level structure/function investigation on the helical bundle domain of *S. aureus* SPIN. Using sequence conservation and existing structures of SPIN bound to human MPO, we selected residues L49, E50, H51, E52, Y55, and Y75 for interrogation by site-directed mutagenesis. We found that loss of L49 or E52 reduced SPIN activity by roughly an order of magnitude, but that loss of Y55 or H51 caused progressively

greater loss of inhibitory potency. Direct binding studies by SPR showed that loss of inhibitory potency in these SPIN mutants resulted from a diminished initial interaction between the inhibitor and MPO. Together, our studies provided new insights into the structure/function relationships of SPIN and identified positions Y55 and H51 as critical determinants of SPIN function.

S. aureus SPIN relies on its C-terminal α-helical bundle domain to mediate initial binding to MPO but requires a disordered N-terminal region to fold into a β-hairpin conformation to inhibit MPO activity. To further investigate the structure/function relationship of SPIN, we introduced two cysteine residues into its N-terminal region to trap SPIN in its MPO-bound conformation and characterized the modified protein, which we refer to here as SPIN-CYS. Although control experiments confirmed the presence of the disulfide bond in SPIN-CYS, solution structure determination revealed that the N-terminal region of SPIN-CYS adopted a physically constrained series of lariat-like structures rather than a well-defined β-hairpin. Nevertheless, SPIN-CYS exhibited a gain in inhibitory potency against human MPO when compared to wild-type SPIN. This gain of function persisted even in the presence of deleterious mutations within the C-terminal α-helical bundle domain. SPR studies showed that the gain in potency arose through an increase in apparent affinity of SPIN-CYS for MPO, which was driven primarily by an increased association rate with MPO when compared to wild-type SPIN. Together, this work provided new information on the coupled binding and folding events required to manifest biological activity of this unusual MPO inhibitor.

S. aureus is primarily a human pathogen, and its SPIN protein cannot inhibit MPO from many non-human species. Evaluation of the inhibitory potency of SPIN orthologs against hMPO, revealed that these proteins also exhibited significantly weaker potency compared to SPIN-

aureus This raised questions as to whether staphylococci that prefer alternative mammalian species might produce SPIN proteins with binding preferences for MPO from those hosts. We tested this hypothesis by isolating canine MPO (cMPO) from two separate abscess fluid samples and exploring its inhibition profile by different SPIN orthologs. Consistent in both trials, our results showed that SPIN proteins from known canine pathogens bind more tightly to and inhibit canine MPO more potently than human MPO. We also found that the increased affinity and potency arose from increases in the second order (i.e. association rate constant (k_a)) rate constant. Comparison of the prototypic of these inhibitors, *SPIN-delphini*, bound to canine MPO when compared to human MPO, explains the physical basis for our observation and provides support for our hypothesis. This work alongside our previous studies on SPIN/MPO interaction can be developed into a valuable model system for understanding the structure/function principles that underlie host-specific evolution of virulence proteins.

Table of Contents

List of Figures

List of Tables

Acknowledgements

I would like to express my deepest appreciation to my advisor, Dr. Brian V. Geisbrecht. Your support, kindness, humility, and encouragement have meant more to me than words can express. Throughout my Ph.D., you have always made me feel capable and confident, never intimidated, and you consistently highlighted my strengths and encouraged me to keep moving forward. Your support during one of the most important times in my life when I was expecting my baby, meant so much to me and my family. I will never forget your understanding and kindness during that time. You taught me not just how to perform experiments, but how to think critically about them, how to design them carefully, and how to approach them with confidence and curiosity. Those lessons will stay with me throughout my career. You allowed me to feel comfortable coming to you at any time, whether it was about my research or my personal life, and I always received thoughtful and supportive feedback from you. You always brought joy to us with your great sense of humor, wherever you were present. You are truly the kind of mentor anyone would hope to have, and I feel incredibly fortunate and honored to have trained under your guidance. Thank you for believing in me and helping me achieve this goal in my life which I have long been waiting for.

I would like to thank Dr. Erika R. Geisbrecht. Even though you were not my mentor, your impact on my life and my personal growth was no less than that of my advisor. Your support, kindness, and presence were truly heartwarming and uplifting. If I become a professor one day, I hope to treat the people around me the way you and Brian treated me.

I would like to thank my committee members, Dr. Om Prakash, Dr. Brandon Lee Garcia, and Dr. Jeffery Comer, for their support and kindness throughout my journey.

I would like to express my sincere gratitude to Dr. Ming Shun Chen for responding so promptly to my email regarding a sabbatical position and for providing me with the opportunity to come to the United States, and to Dr. Yoonseong Park for training me in his laboratory for four and a half years. Without the extensive training I received under his supervision, I would not have been able to accomplish my Ph.D. in such a short time.

I would like to thank our family in San Diego, Dr. Ali Shafiee, Dr. Gelare Asadi, and Dr. Mahnaz Sahebjamee, for their presence, kindness, and support.

I would like to thank my family in Iran: my dear mother, for her endless love, encouragement, and belief in me from childhood until now; and my dear brother, Saeed, who has been a wonderful friend and constant support throughout my life. I am deeply grateful for their love, which I have relied on in every moment of my life. As they often say, I am the first thing they think about when they wake up and the last thing they think about before they go to bed-and I think of them the same way.

I would like to thank my dear husband, Omid, for rising in my life like the sun and surrounding me with his endless loyalty, support, friendship, kindness, calmness, and love. I love you and your beautiful soul deeply, and I cherish every moment of being with you and learning from you. Thank you for being who you are.

And finally, I would like to thank my little baby, my beautiful flower, my daughter, Hannah, for being such a calm and understanding baby, which made the completion of my Ph.D. possible.

Dedication

To my mother: thank you for teaching me to live without fear. When I was pressured to take a different path, you were the one that encouraged me to follow my heart and my love for academia. I owe my greatest joys to you, without your guidance, I would not have found my way to this degree, nor would I have been blessed with Omid and Hannah. This achievement is as much yours as it is mine.

Chapter 1 - Introduction

NEUTROPHIL RECRUITMENT

Neutrophils are the most abundant leukocytes in humans and are early acting cellular constituents of the innate immune response to bacteria [1,2]. Resting neutrophils circulate freely in the blood in an inactive state but exhibit major morphological and behavioral changes upon sensing any number of stimuli that lead to their activation. A pillar of the activated neutrophil's response to bacteria is phagocytosis, which serves to envelop these potentially harmful microorganisms within an intracellular compartment where they can ultimately be killed and destroyed. Maturation of the nascent phagosome is an orchestrated process [2,3]. It involves fusion of the bacteria-laden compartment with several types of cytosolic granules, each of which contains various aspects of the neutrophil's antibacterial arsenal of peptides, proteins, and enzymes [2,4]. This not only mobilizes an array of antibacterial peptides like α-defensins, it also establishes the NADPH oxidase/myeloperoxidase (MPO) system for producing cytotoxic oxidants (e.g. HOCl) and liberates a series of chymotrypsin-like serine proteases, including neutrophil elastase (NE), cathepsin-G (CG), and proteinase-3 (PR3), that are collectively known as the neutrophil serine proteases (NSPs) [4–7]. Together, these systems generate a formidable antibacterial environment within the matured phagosome that is believed to exhibit synergistic potency when compared to its various components in isolation [8].

NEUTROPHIL DEGRANULATION

Although killing bacteria with the phagosome provides a mechanism for isolating host cells from the neutrophil's indiscriminate biochemical arsenal, it is not the only antibacterial response following activation. Neutrophil granule contents can also be directly released into the extracellular environment through a process known as degranulation [2,4]. Freed from the

restrictions of the phagosome, various antibacterial activities can thus manifest themselves across a broader area, albeit at lower concentrations. Separately, certain granule components are also key constituents of neutrophil extracellular traps (NETs) [9]. These webs of decondensed chromatin decorated with antimicrobial proteins serve to ensnare extracellular bacteria and restrict their mobility. NETs are thought to promote killing by increasing the local concentration of antimicrobial proteins [10,11], although this topic remains an area of active investigation. Nevertheless, neutrophils exhibit multiple, overlapping bacterial killing mechanisms that operate both within the cell as well as in the extracellular environment.

BACTERIAL IMMUNE EVASION STRATEGIES

Invading bacteria must contend with the neutrophil's highly diversified and formidable antibacterial arsenal. Thus, there is heavy selective pressure on these bacteria to evolve the physical and biochemical means for inhibiting, evading, or escaping from neutrophil attack. Whereas evidence for bacterial evasion of neutrophils has been available since at least the pioneering work of van de Velde in the mid-1890's [12], studies from the last two decades focused on the pathogen bacterium *Staphylococcus aureus* have greatly expanded our understanding of the breadth of neutrophil evasion mechanisms [13]. Several *S. aureus* evasion mechanisms targeting neutrophil cell-surface receptors important to sensing chemotactic cues have been described [14–16]. This includes the fundamental observation by Spaan et al. that the prototypic neutrophil evasion molecule, Panton-Valetine Leukocidin (PVL), binds to the cell-surface C5a receptors, C5aR and C5L2 [17]. However, more recent work has identified two families of *S. aureus* innate immune evasion proteins, known as SPINs and EAP proteins, that target key antibacterial enzymes normally found within neutrophil granules, namely MPO and NSPs.

SPIN: A UNIQUE MYELOPEROXIDASE INHIBITOR EXPRESSED BY STAPHYLOCOCCI

Myeloperoxidase (MPO) is a cornerstone of the neutrophil antibacterial arsenal, whereby it consumes H_2O_2 to generate cytotoxic hypohalous acids, most notably HOCl [5,18]. Since MPO is the most abundant antimicrobial enzyme within neutrophils and reaches concentrations estimated near 1 mM within the phagosome [19], de Jong et al. hypothesized that it would be an attractive target for a staphylococcal innate immune evasion strategy. By screening a specialized phage library that displayed only secreted *S. aureus* proteins, de Jong et al. identified a small, 73-residue protein that bound tightly to human MPO with an apparent K_d of ~10 nM [20]. The authors subsequently named this protein Staphylococcal Peroxidase INhibitor, or SPIN, since it potently blocked the peroxidase activity of MPO in functional assays [20]. Expression of SPIN by *S. aureus* increased by nearly an order of magnitude following phagocytosis by neutrophils, suggesting that the primary role of SPIN lies in inhibiting MPO within the phagosome [20]. Consistent with this model, *S. aureus* cells lacking SPIN were more susceptible to killing by isolated human neutrophils than were cells overexpressing SPIN [20].

THE STRUCTURE/FUNCTION RELATIONSHIPS OF THE SPIN PROTEIN

Structural studies of *S. aureus* SPIN, either free or bound to a recombinant form of human MPO, revealed that this small protein consists of two functionally unique domains [20,21]. The ~60-residue C-terminal region adopts a compact, α-helical bundle fold (Figure 1.1A). Although studies on this domain in isolation showed that it mediates initial high-affinity binding to MPO, it cannot inhibit MPO on its own [21]. The ~13-residue N-terminal region is disordered in the absence of ligand [21], but folds into a β-hairpin conformation following MPO

binding (Figure 1.1A-D) [20]. Several peptides designed to mimic this region did not appear to bind MPO or inhibit its activity [21]. However, the N-terminal segment of SPIN is required to inhibit MPO [20,21]. Examination of the crystal structure of *S. aureus* SPIN bound to a recombinant form of human MPO (rhMPO) revealed that the SPIN N-terminus inserts into the MPO active site channel, apparently blocking access to the MPO active site (Figure 1.1A-D) [20]. This observation, combined with the studies mentioned earlier in this paragraph, led to the "bind-fold-inhibit" model for SPIN function [21,22]. Although this model has certain limitations that have been pointed out by recent studies (e.g. [23]), it nevertheless served as a useful framework for understanding the structure/function properties of SPIN for several years.

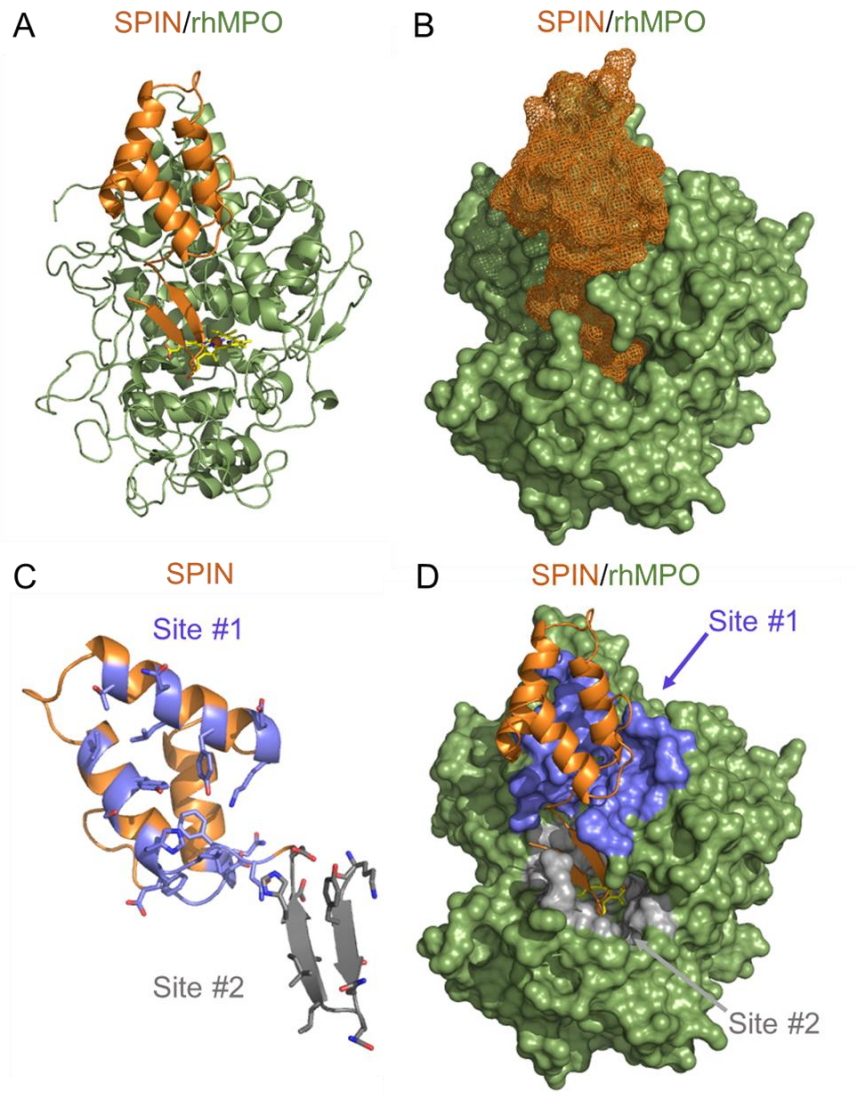

Figure 1.1. Structure of SPIN bound to rhMPO.

(A) Cartoon representation of the *S. aureus* SPIN (orange) bound to rhMPO (olive). (B) SPIN is drawn as an orange space-filling mesh and rhMPO is an olive molecular surface. The N-terminal β-hairpin of SPIN inhibits MPO by restricting access to the catalytic heme which is a key determinant of MPO inhibition by SPIN. (C) Two distinct rhMPO/SPIN-aureus interaction interfaces. Interface/Site #1 (light purple) represents the residues within the α-helical bundle domain. Interface/Site #2 (silver) is comprised of residues within the β-hairpin domain. The ball-and-stick models represent the sidechains of residues that form contacts with rhMPO in the structure. (D) Representation of the SPIN/rhMPO structure. The two distinct SPIN-binding surfaces on MPO are colored according to panel C [22].

IDENTIFICATION AND CHARACTERIZATION OF SPIN HOMOLOGS FROM OTHER STAPHYLOCOCCI

Shortly after the discovery of SPIN from *S. aureus*, Ploscariu et al. identified a cohort of SPIN orthologs from other closely related staphylococcal species [24]. The initial outcome of these efforts was the structure/function characterization of SPIN from *S. delphini* [24]. These authors showed that *S. delphini* SPIN binds and inhibits human MPO, albeit ~6.5-fold weaker than *S. aureus* SPIN. This loss in potency appeared to arise from weakening specific interactions at the SPIN/MPO interface: comparison of the crystal structures of recombinant human MPO bound to either *S. delphini* or *S. aureus* SPIN revealed either minor positional changes in key sidechains or substitution to different residues altogether (Figure 1.2A-D). Ultimately, this led to broader questions regarding which SPIN residues were most important for mediating initial binding of this inhibitor to MPO.

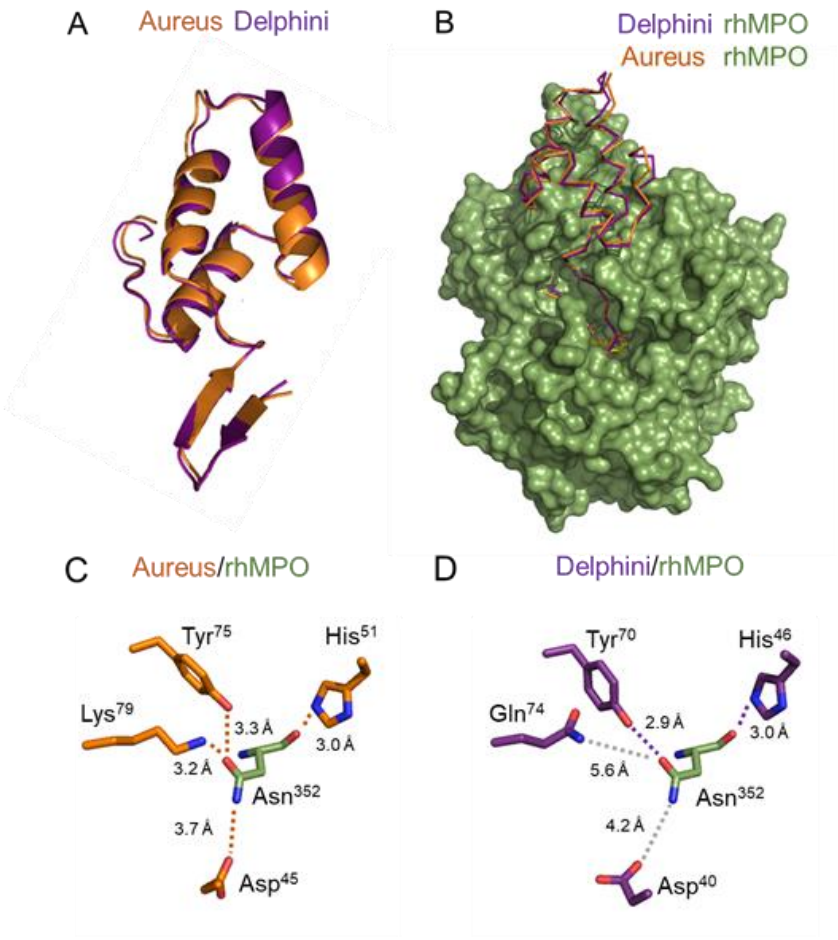

Figure 1.2. Structural characterization of rhMPO/SPIN-delphini.

The cocrystal structure of rhMPO/*SPIN-delphini* solved to 2.4 Å limiting resolution [24]. (A) Superposition of SPIN-aureus (orange) and *SPIN-delphini* (purple) drawn as ribbon diagrams. (B) Superposition of the crystal structure of rhMPO/*SPIN-delphini* with that of rhMPO/SPIN-aureus. The SPIN proteins are drawn as Cα wires using the same coloring scheme as panel A. (C) SPIN-aureus residues (carbon atoms colored orange) and the contacts formed with Asn^{352} of rhMPO (carbon atoms colored olive). Likely polar interactions, along with their distances, are shown as orange dashed lines. (D) *SPIN-delphini* residues (carbon atoms colored purple) and the contacts formed with Asn^{352} of rhMPO. Likely polar interactions and distances are shown as purple dashed lines, while interactions that fail to form due to excessive distance are shown as grey dashed lines [24].

Using the same crystal structures of *S. aureus* and *S. delphini* SPIN bound to human MPO as a guide, we examined a multiple sequence alignment of SPIN orthologs to identify candidate residues for study by site-directed mutagenesis. We focused our attention on residues

within the SPIN α-helical bundle domain since this region of SPIN is required for MPO binding. The detailed explanation of this study can be found in chapter 2.

BIND-FOLD-INHIBIT MECHANISM FOR MPO INHIBITION BY SPIN

Initial structure/function investigations on SPIN were broadly consistent with a "bind-fold-inhibit" mechanism for MPO inhibition [20–22]. A central feature of this mechanism is that the SPIN N-terminal domain acts as a molecular plug, preventing the unimpeded exchange of substrates and products with the MPO active site (Figure 1.1). However, Leitgeb and coworkers noted that many MPO substrates are approximately the same size as water and suggested that such substances might still access the MPO active site to some degree, even in the presence of SPIN [23]; consistent with this premise, they observed that SPIN does not fully block halide oxidation by MPO [23]. These observations suggested that SPIN must fit rather loosely in the MPO active site. They also raised questions about how the N-terminus of SPIN folds following initial MPO binding. A subsequent computational study by Zhang et al. employed atomistic molecular dynamics simulations to investigate this issue [25]; these authors concluded that binding and folding of the *S. aureus* SPIN N-terminus is a highly cooperative process [25]. This observation suggested that restricting the conformational landscape accessible to the SPIN N-terminus might have functional consequences. To investigate this issue experimentally, we introduced a stabilizing disulfide bond into the N-terminal region of *S. aureus* SPIN and characterized the structure and function of this disulfide-insertion mutant. The outcomes of this study can be found in chapter 3.

SPIN orthologs are distributed across several bacterial species closely related to *S. aureus* [24]. While *S. aureus* is recognized as a versatile pathogen capable of colonizing both humans and livestock (such as dairy cattle), multiple staphylococcal species encoding SPIN-like

sequences, including *S. delphini*, *S. intermedius*, *S. schleiferi*, and *S. pseudintermedius*, are primarily known as pathogens of livestock and/or companion animals [26]. Consistent with this, SPIN-aureus demonstrates a pronounced binding selectivity and inhibitory potency toward myeloperoxidase derived from its human host, yet it lacks any detectable interaction with or inhibition of murine MPO and many others [20]. Additionally, it is noteworthy that SPIN orthologs from S. *delphini*, *S. intermedius*, *S. schleiferi*, and *S. pseudintermedius* fail to bind with or inhibit human MPO with the same affinity or potency as the SPIN-aureus [24]. Therefore, we hypothesized that these SPIN variants may instead exhibit a similar selectivity for MPO derived from their preferred hosts. To test this hypothesis, we isolated canine MPO from abscess fluid samples obtained for veterinary diagnostic purposes and explored its inhibition profile by different SPIN orthologs. The details of this study can be found in chapter 4.

Chapter 2 - Staphylococcal Peroxidase Inhibitor (SPIN): Residue-Level Investigation of the Helical Bundle Domain

This chapter has been published as a journal article in the journal of Archives of Biochemistry and Biophysics 758 (2024) 110060

Soheila Fatehi[1], Timothy J. Herdendorf[1], Nicoleta T. Ploscariu[1], Brian V. Geisbrecht[1,$]

[1]Department of Biochemistry & Molecular Biophysics
Kansas State University
Manhattan, KS 66506 U.S.A.

[$]Address Correspondence To:
Brian V. Geisbrecht, Ph.D.
141 Chalmers Hall
1711 Claflin Road
Manhattan, KS 66506 U.S.A.
E-mail: geisbrechtb@ksu.edu

ABSTRACT

Myeloperoxidase is a critical component of the antibacterial arsenal of neutrophils, whereby it consumes H_2O_2 as an oxidant to convert halogen and pseudohalogen anions into cytotoxic hypohalous acids. Following phagocytosis by neutrophils, the human pathogen *Staphylococcus aureus* secretes a potent myeloperoxidase inhibitory protein, called SPIN, as part of its immune evasion repertoire. The matured *S. aureus* SPIN polypeptide consists of only 73 residues yet contains two functional domains: whereas the 60 residue C-terminal helical bundle domain is responsible for MPO binding, the 13 residue N-terminal domain is required to inhibit MPO. Previous studies have informed understanding of the SPIN N-terminal domain, but comparatively little is known about the helical domain insofar as the contribution of individual residues is concerned. To address this limitation, we carried out a residue-level structure/function investigation on the helical bundle domain of *S. aureus* SPIN. Using sequence conservation and existing structures of SPIN bound to human MPO as a guide, we selected residues L49, E50, H51, E52, Y55, and Y75 for interrogation by site-directed mutagenesis. We found that loss of L49 or E52 reduced SPIN activity by roughly an order of magnitude, but that loss of Y55 or H51 caused progressively greater loss of inhibitory potency. Direct binding studies by SPR showed that loss of inhibitory potency in these SPIN mutants resulted from a diminished initial interaction between the inhibitor and MPO. Together, our studies provide new insights into the structure/function relationships of SPIN and identify positions Y55 and H51 as critical determinants of SPIN function.

KEYWORDS

Myeloperoxidase, Inhibitor, *Staphylococcus aureus*, Immune Evasion, Structure/Function

1. INTRODUCTION

Human neutrophils play an essential and early role in the innate immune response to bacterial pathogens [1,2]. Neutrophils contribute to killing of bacteria intracellularly with the phagosome, as well as extracellularly following formation of neutrophil extracellular traps (NETs). Although bacterial killing involves diverse antibacterial molecules derived from neutrophil granules [4], enzymatic generation of oxidants within the phagosome is paramount. As the bacteria-containing phagosome matures, membrane-resident NADPH oxidase consumes O_2 to ultimately generate H_2O_2, which is subsequently used by the abundant intraphagosomal enzyme myeloperoxidase (MPO) to convert halides (e.g. Cl^-) or pseudohalides (e.g. SCN^-) anions into cytotoxic oxidant species, including HOCl [5,18]. According to known rate constants for the relevant reactions, the high concentrations of MPO within the phagosome are believed capable of generating HOCl at rates near 134 mM/min following phagocytosis [19]. Thus, efficient generation of this potent antibacterial environment is a cornerstone of a robust innate immune response.

Many successful bacterial pathogens have developed means to escape opsonization and killing by the innate immune system. Among such bacteria, *Staphylococcus aureus* appears particularly adept at immune evasion. Work from throughout the last two decades has identified nearly two dozen different proteins produced by *S. aureus* to block opsonization by complement fragments, as well as chemotaxis and subsequent phagocytosis by neutrophils (Reviewed in [27,28]). More recent studies have revealed an elaborate staphylococcal innate immune evasion program that appears to function with the phagosome. This includes a family of potent and selective inhibitors of Neutrophil Serine Proteases (NSPs) known as EAP proteins [29], as well as a novel class of MPO inhibitor known as SPIN (Staphylococcal Peroxidase Inhibitor) [20]. *S.*

aureus cells deficient in EAP proteins were less infectious in a mouse model of liver abscess formation when compared to wild-type cells [29], while *S. aureus* cells deficient in SPIN were more susceptible to killing by isolated neutrophils when compared to SPIN-expressing bacteria [20]. Although the contributions of EAP proteins and SPIN to *S. aureus* survival within the phagosome remain to be fully understood, the long-standing proposal of functional synergy between NSPs and MPO [8] suggests that inhibiting both systems simultaneously might be required to meaningfully influence the overall process of bacterial killing.

Since SPIN shares no sequence relationships with other known proteins [20], detailed structure/function studies were required to provide insight into its mechanism of MPO inhibition. Although SPIN from *S. aureus* consists of only 73 residues (Figure 2.1A), a 2.4 Å crystal structure of SPIN bound to a recombinant form of human MPO revealed that the inhibitor is comprised of two functional domains (Fig. 1B). Whereas the 60 residue C-terminal domain of SPIN assumes an α-helical bundle fold, its short, 13 residue N-terminal region adopts a β-hairpin structure when bound to MPO [20]. Significantly, this β-hairpin is almost completely buried within the MPO active site channel. Consistent with this observation, studies using an N-terminal deletion mutant of SPIN showed that this truncation still binds tightly to MPO, yet lacks the ability to inhibit MPO activity [21]. Together, these observations led to the proposal that SPIN acts as a molecular plug to prevent free exchange of substrates and products with the MPO active site [20,21]. A more recent kinetic investigation has shown that SPIN cannot completely block MPO activity for small acceptor substrates such as halides, but that it becomes a more effective inhibitor as the size of the substrate increases [23]. This suggests that if SPIN indeed acts as a molecular plug, it must fit somewhat loosely within the MPO active site channel.

Although the N-terminus of SPIN is required for inhibition, synthetic peptides corresponding to this region alone do not appear to bind or inhibit MPO activity [21]. Moreover, an N-terminally truncated form of SPIN also binds MPO with comparable affinity to the full-length molecule (c.f. ~10 nM vs ~30 nM) [21]. Together these observations suggest that the α-helical bundle region of SPIN is the main determinant of MPO binding. Unfortunately, little is currently known about the residues within the SPIN α-helical bundle region that mediate its interactions with MPO. This represents a significant barrier to understanding how SPIN initially binds to MPO. It also prevents a deeper appreciation of other relevant issues, including the selectivity of SPIN for human MPO versus MPO from other species [20,22,24].

Following the initial discovery of SPIN, we reported the identification of a panel of SPIN orthologs from various staphylococcal species closely related to *S. aureus* [24]. This provided insights into the sequence conservation status of various residues across the entire SPIN protein, including the α-helical bundle domain (Figure 2.1A). In this report, we used this sequence conservation data and available structural information on the SPIN/MPO complex [20,21,23,24] (Figure 2.1B) to identify a cohort of residues that might contribute to the SPIN/MPO interaction. We then tested our hypothesis through a combination of site-directed mutagenesis, enzyme inhibition measurements, and direct binding studies. The outcome of this investigation allowed us to assign potential roles for each of these residues. Our results further show that loss of critical positions diminishes SPIN function primarily by slowing the initial interaction of the inhibitor with its target enzyme, MPO.

2. EXPERIMENTAL

2.1. Proteins

Native human myeloperoxidase that had been isolated from quiescent human neutrophils was obtained from Planta Natural Products. The enzyme was reconstituted (10 mM HEPES (pH 7.4), 150 mM NaCl), and stored until further use according to the manufacturer's recommendations.

All SPIN proteins were obtained in recombinant form according to the general methods described previously [21]. Briefly, gene fragments encoding the matured form of *S. aureus* SPIN, or various site-directed mutants, were subcloned into the prokaryotic expression vector pT7HMT [30] and obtained from GenScript. Following overexpression in cells of *E. coli* strain BL21(DE3), the recombinant SPIN was isolated from a clarified cell extract using immobilized metal ion affinity chromatography. The target protein was cleaved from the his-tag by digestion with TEV protease, and separated from the protease and remaining digestion products by a second round of immobilized metal ion affinity chromatography where the unbound fraction was collected. Final purification was achieved by size-exclusion chromatography using a Superdex 30 26/60 column attached to an AKTA format FPLC (Cytiva Life Sciences). Following confirmation of purity by SDS-PAGE, each protein was buffer exchanged in to ddH_2O, separated into aliquots, and lyophilized for long-term storage.

2.2. Circular Dichroism Spectropolarimetry

Circular dichroism spectropolarimetry (CD) was used to examine the structural integrity of SPIN proteins containing single, double, and triple mutations by comparison to wild -type SPIN. All experiments were conducted on a Jasco J-815 CD spectrophotometer using a 1-mm path-length jacketed cylindrical quartz cuvette. All proteins were dissolved in ddH_2O and their concentrations were determined based on absorbance at 280 nm using a DeNovix DS-11 spectrophotometer. Measurements were then conducted using a final protein concentration of 25

μM. All spectra were obtained from 260 to 190 nm at scan rate of 50 nm min^{-1} with a 1 nm step interval. An average of five scans for each sample was used to obtain a composite CD spectrum, prior to subtracting a blank measurement. The subtracted spectrum was smoothed with a Savitsky−Golay algorithm using Spectra Analysis software provided by the manufacturer (Jasco Inc., Easton, MD) [31].

2.3. Myeloperoxidase Activity Assay

Myeloperoxidase activity within the peroxidase cycle was measured using a coupled colorimetric assay consisting of MPO, H_2O_2, vanillic acid (VA), and 4-aminoantipyrine (AAP) [32]. In this reaction sequence, the oxidized AAP condenses with VA to form a quinoneimine dye such that two quinoneimines are formed for each molecule of H_2O_2 consumed. Reactions were carried out in a neutral pH buffer system (50 mM sodium phosphate (pH 7.0)) at 25 °C and followed spectrophotometrically in a $Versa_{max}$ tunable microplate reader at 510 nm (ε: 6.98 $mM^{-1}cm^{-1}$) [33].

2.4. Steady-State Kinetic Analysis of Myeloperoxidase

Initial velocities of the MPO reaction (2.12 nM enzyme) were measured spectrophotometrically via a plate-based assay outlined above. Briefly, 170 μL of mixture containing 4.24 nM MPO, 7 mM VA and 5mM AAP were added to 170 μL of buffer containing H_2O_2 concentrations ranging from ~ 5 μM to ~ 1.1 mM and the formation of the quinoneimine product at 25 °C was followed at 510 nm. From these data, initial velocities were determined and converted to k_{cat} values using the extinction coefficient of the quinoneimine, MPO concentration and the stoichiometry of substrate to product (1 H_2O_2:2 quinoneimine). Replicate data (a minimum of n=3 technical replicates) were fitted to the Michaelis-Menten equation with

an additional substrate inhibition component (uncompetitive inhibition) to determine the k_{cat}, K_m and K_I with respect to H_2O_2 using GraphPad Prism.

$$y = \frac{k_{cat}*[S]}{K_m + ([S] * [1 + \frac{[S]}{K_I}])}$$

2.5. Steady-state Inhibition of Myeloperoxidase by SPIN proteins

The half-maximal inhibition concentration (IC_{50}) for various SPIN proteins was determined using the plate-based assay described above. Briefly, MPO (4 nM), VA (7 mM), AAP (5 mM) and various concentrations of SPIN proteins were incubated for 90 min at room temperature in sodium phosphate buffer. Following the incubation, 170 µL of each sample above were mixed with 170 µL of sodium phosphate buffer containing ~112 µM H_2O_2. 170 µL of the complete reaction mixture were added to the read plate and the formation of the quinoneimine product at 25 °C was followed at 510 nm. Initial velocities were converted to k_{cat} values as described above, and the replicate data (a minimum of n=3 technical replicates) were fitted to an IC_{50} equation containing four variables using GraphPad Prism. The y_{max} was fixed to the average value of uninhibited rates with the y_{min}, $logIC_{50}$ and hillslope allowed to float.

$$y = \frac{y_{min} + (y_{max} - y_{min})}{(1+ 10 \wedge ((logIC_{50} - x)*hillslope))}$$

2.6. Surface Plasmon Resonance

Surface Plasmon Resonance was used to investigate interactions between each SPIN protein and immobilized human MPO according to the general methods described previously [20,21,24]. All experiments were conducted using a Biacore T-200 instrument (Cytiva Life

Sciences) at 25°C. HBS-T was used as a running buffer (20 mM HEPES (pH 7.4), 140 mM NaCl, and 0.005% (v/v) Tween-20) with a flow rate of 30 µL/min.

The biosensor surface was established on a CMD-200M sensor chip (Xantec Bioanalytics GmbH) by coupling MPO to three separate flow cells via amine coupling according to the manufacturer's recommendations. To activate the surface, equal volumes of N-hydroxysuccinimide (NHS; 0.1 M in ddH_2O) and N-ethyl-N'-(dimethylaminopropyl) carbodiimide hydrochloride (EDC; 0.4M in ddH_2O) were mixed immediately prior to injection onto a naïve surface. Subsequently, 20 µg/mL MPO (prepared in 10 mM sodium acetate (pH 5.5)) was injected to allow the coupling of protein-borne amine groups to the surface esters through amide bond formation. Finally, 1 M ethanolamine (pH 8.5) was injected to deactivate any uncoupled NHS-esters. The levels of MPO immobilization were 855.1, 798.4, and 701 Resonance Units (RU) on the three experimental flow cells. One flow cell was activated but immediately inactivated by ethanolamine and served as the reference.

Serial two-fold dilutions (1.93-1000 nM) of each SPIN protein were injected over the flow cells. A contact time of 3 min was used, followed by a 5 min dissociation phase. To regenerate the surface following each injection, a 0.5 min pulse of 0.1 M glycine (pH 10.0) containing 1 M NaCl was applied. To determine rate constants more accurately for more severely affected mutants, higher concentrations of certain SPIN proteins were injected over the surface (2.43-10,000 nM for L49A and E50A and 3-50,000 nM for H51A, L49A/E52A, Y55A, and H51A/Y55A/Y75A). Reference subtracted sensorgram series were processed using Biacore T-200 Evaluation Software v3.2.1 (Cytiva Life Sciences). Data were analyzed globally using a two-state reaction model with local fitting of R_{max}. The fitted binding curves were then imported and graphed using GraphPad Prism.

2.7. Miscellaneous

Amino acid sequence alignments were performed using Clustal Omega [34]. Representations of secondary structure as a function of amino acid sequence were generated using EsPript [35]. Images of protein structures were rendered using PyMol (https://pymol.org/). Analyses of protein-protein interfaces were carried out using the EBI-PISA server (https://www.ebi.ac.uk/pdbe/pisa/) [36]. Statistical analyses were performed using GraphPad Prism 10 (https://www.graphpad.com/).

3. RESULTS

3.1. Selection of Residues for Investigation and Generation of SPIN Mutants

In an earlier analysis of the SPIN/MPO cocrystal structure [20,21], we identified SPIN residues H43, D44, and D45 as positions of potential significance since these residues are buried at the protein-protein interface, form hydrogen bonds and/or salt bridges with groups derived from MPO, and are conserved across a panel of SPIN orthologs [24]. Characterization of a SPIN mutant wherein all three of these positions were changed to alanine revealed that this protein maintains high-affinity MPO binding, yet lacks the ability to inhibit MPO activity [21]. Although the loss of inhibition in this mutant is noteworthy, the fact that it retains high-affinity MPO binding (K_D ~30 nM) suggests that other residues are potentially more important insofar as MPO binding is concerned. Therefore, we reevaluated the SPIN/MPO cocrystal structure and identified two additional sets of residues for further investigation. The residues in each set are either adjacent to one another in sequence (Set 1) or lie in close physical proximity in the SPIN tertiary structure (Set 2), and each of these residues is either highly conserved or invariant among known SPIN orthologs (Figure 2.1A-B). Furthermore, residues from both sets are buried at the protein-protein interface and form hydrogen bonds with groups derived from MPO

(Figure 2.1C). Set 1 consists of L49, E50, H51, and E52, while Set 2 consists of Y55 and Y75 (Figure 2.1A&C).

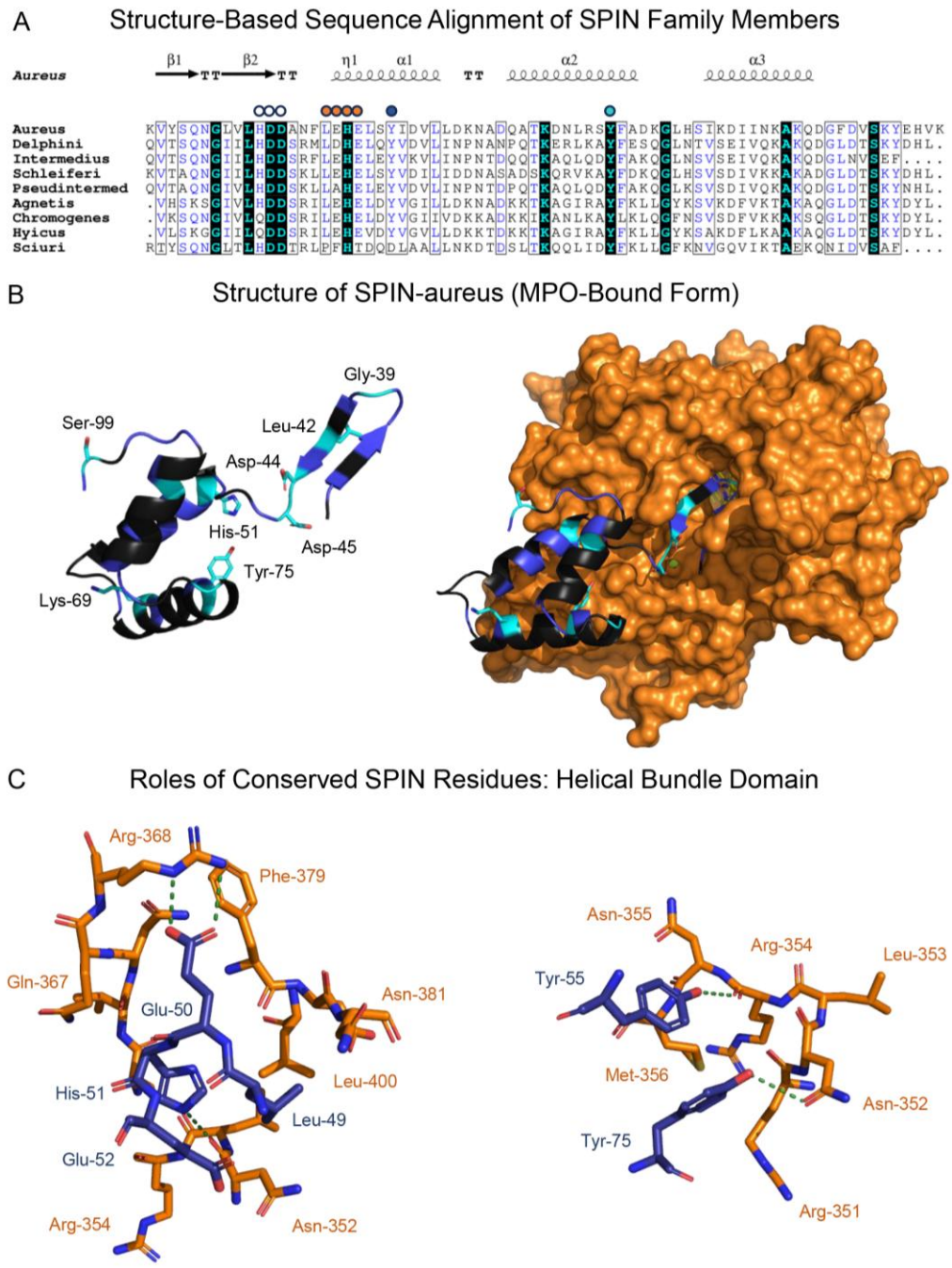

Figure 2.1. Sequence and Structural Properties of the Staphylococcal Peroxidase Inhibitor, SPIN.

(A) Structure-based sequence alignment of the SPIN family members, as rendered by EsPript [35]. Secondary structure elements of the MPO-bound form of *S. aureus* SPIN [20] are depicted above a multiple-sequence alignment of a cohort of SPIN orthologs [24]. Invariant residues are shown with a shaded background, while residues found in seven of nine sequences are outlined with a box. Residues H43, D44, and D45 of *S. aureus* SPIN are illustrated with a hollow circle above. Residues L49, E50, H51, and E52 are illustrated with a filled orange circle. Residues Y55 and Y75 are illustrated with a filled blue circle. (B) Structure of the MPO-bound form of *S. aureus* SPIN. The SPIN polypeptide is depicted as ribbon diagram in the left image. Invariant residues are labeled and shown as ball-and-stick models with their carbon atoms in light blue, while the boxed residues from panel A are colored dark blue. The structure of SPIN bound to human MPO is shown in the right image. MPO is drawn as an orange molecular surface, while its active site heme is colored with its carbon atoms in yellow. (C) Representation of the role(s) of conserved SPIN residues in MPO binding. Residues from SPIN are drawn with their carbon atoms in dark blue, while residues from MPO are drawn with their carbon atoms in orange. Hydrogen bonds are represented by green dashed lines. The left image depicts the interactions formed by SPIN residues L49, E50, H51, and E52, while the right image depicts the interactions formed by SPIN residues Y55 and Y75.

To test the functional contributions of these residues, we first prepared site-directed alanine substitution mutants for each residue within Set 1 (i.e. L49A, E50A, H51A, and E52A) and Set 2 (Y55A and Y75A). We also prepared one double mutant (i.e. L49A/E52A) and one triple mutant (i.e. H51A/Y55A/Y75A). Each mutant protein was obtained in yields comparable to the wild-type SPIN protein and exhibited similar behavior when analyzed by SDS-PAGE (Figure 2.2A). In addition, the CD spectrum of each mutant was essentially indistinguishable from that of the wild-type protein (Figure 2.2B). This suggested that these mutations did not adversely affect the overall structural properties of the SPIN proteins. Therefore, we proceeded to characterize this panel of SPIN mutants and compare their properties to those of wild-type SPIN.

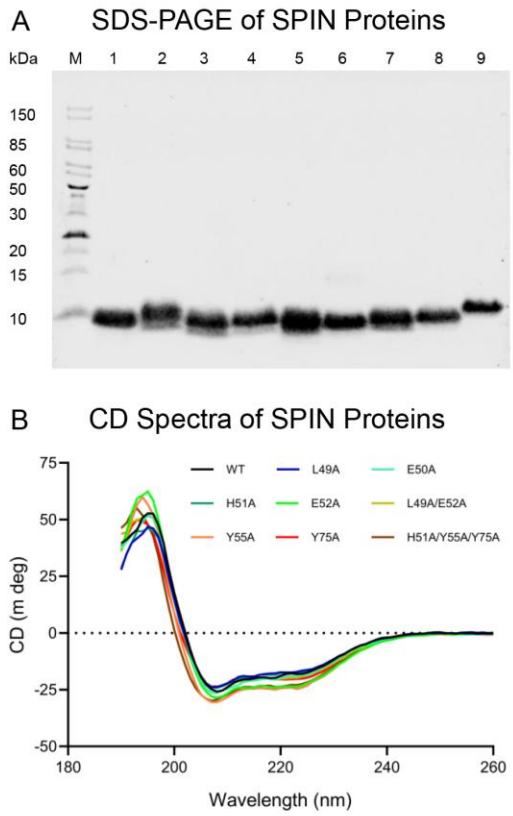

Figure 2.2. Physical Characterization of Site-Directed Mutants of *S. aureus* SPIN.

(A) SDS-PAGE of purified *S. aureus* SPIN proteins. Seven micrograms of each protein were loaded in each well, separated, and visualized by staining with Coomassie blue. A mixture of standard proteins was loaded in the left-most well with sizes indicated in kDa. Individual samples correspond to: 1, wild-type; 2, L49A; 3, E50A; 4, H51A; 5, E52A; 6, L49A/E52A; 7, Y55A; 8, Y75A; and 9, H51A/Y55A/Y75A. (B) Circular Dichroism spectropolarimetry analysis *S. aureus* SPIN variants at pH 7.4. Five spectra were collected for each sample, and were averaged, buffer-subtracted, and subjected to spectral smoothing as described in *Materials & Methods*. The processed spectra were plotted on the same graph to allow for direct comparison. A legend identifying each sample is inset.

3.2. Mutation of SPIN Residues Found at the MPO Interface Results in Loss of Inhibitory Activity

Having confirmed the structural integrity of our mutant SPIN proteins, we investigated the functional consequence of each mutation by quantifying the potency of each SPIN mutant against MPO. We employed a microplate-format colorimetric activity assay that monitors the MPO peroxidase cycle and determined the apparent k_{cat} of the enzyme across a dilution series of

each SPIN mutant (*please see Experimental 2.3-2.5*). We then fitted the replicate data for each SPIN mutant to a four-parameter dose-response curve and calculated the IC_{50} and corresponding confidence interval (Table 2.1).

Table 2.1. Functional Properties of SPIN Variants as Assessed by Enzyme Assay and Surface Plasmon Resonance[a,b]

SPIN Variant	IC_{50} (nM)[a]	K_D (nM)	k_{a1} ($M^{-1}s^{-1}$) x 10^4	k_{d1} (s^{-1}) x 10^{-3}	k_{a2} (s^{-1}) x 10^{-3}	k_{d2} (s^{-1}) x 10^{-3}
WT	7.4 (6.9-7.9)	20.9 ± 2.3	47.4 ± 3.9	23.6 ± 1.7	3.5 ± 0.3	2.5 ± 0.3
L49A	37.8 (34.3-41.8)	287.0 ± 31.7	2.5 ± 0.4	20.2 ± 2.9	3.8 ± 0.3	2.1 ± 0.3
E50A	8.9 (8.1-9.9)	28.3 ± 4.9	27.9 ± 6.5	22.2 ± 7.0	4.1 ± 0.7	2.3 ± 0.5
H51A	1193.0 (997.4-1505.0)	-	-	-	-	-
E52A	64.4 (58.9-70.2)	492 ± 56.2	1.7 ± 0.4	18.6 ± 5.5	4.1 ± 1.3	3.2 ± 1.0
L49A/E52A	268.5 (153.0-627.7)	19830 ± 1424	0.015 ± 0.005	12.1 ± 4.0	6.0 ± 1.8	1.9 ± 0.3
Y55A	181.1 (126.5-321.5)	-	-	-	-	-
Y75A	9.6 (8.4-10.9)	41.1 ± 18	21.0 ± 5.2	19.9 ± 8.1	3.8 ± 1.3	3.2 ± 1.5
H51A/Y55A/Y75A	-	-	-	-	-	-

We began by characterizing the mutants within Set 1 (Figure 2.3A & Table 2.1). Although the E50 sidechain forms a pair of hydrogen bonds with MPO (Fig. 1C), the E50A mutant displayed an IC_{50} value identical to SPIN-WT (c.f. 8.9 nM vs 7.4 nM). However, each of the remaining Set 1 mutants were significantly diminished when compared to SPIN-WT. Both L49A (37.8 nM) and E52A (64.4 nM) were impaired by roughly one order of magnitude. Simultaneous loss of both sidechains appeared to cause a greater than additive effect, since the L49A/E52A mutant lost approximately 36-fold in potency (268.5 nM). The H51A mutant was the most severely impacted, however, as it displayed an IC_{50} value roughly 180-fold weaker than SPIN-WT (1193 nM). This observation was consistent with both the invariant nature of this histidine across a panel of SPIN orthologs (Figure 2.1A), as well as the role of this sidechain at the SPIN/MPO interface (Figure 2.1**Error! Reference source not found.**C).

We then characterized the mutants within Set 2 (Figure 2.3B & Table 2.1). Although Y75 is invariant across SPIN orthologs (Figure 2.1A) and its sidechain forms a hydrogen bond with MPO (Figure 2.1C), the Y75A mutant displayed a wild-type-like IC_{50} value (9.6 nM). By contrast, removal of the Y55 sidechain resulted in a significant loss of function, since the Y55A mutant was diminished by roughly 24-fold when compared to SPIN-WT (181.1 nM). This result was somewhat surprising, since the Y55 position is not invariant, and its sidechain forms a comparable hydrogen bond with MPO to that of Y75 (Figure 2.1C). Simultaneous loss of Y55, Y75, and H51 resulted in the greatest loss of function, though, as the H51A/Y55A/Y75A protein failed to exhibit saturable inhibition of MPO even at concentrations greater than 20 μM protein. This result was consistent with previous observations on the H51A and Y55A mutants, both of which are significantly diminished on their own (Table 2.1).

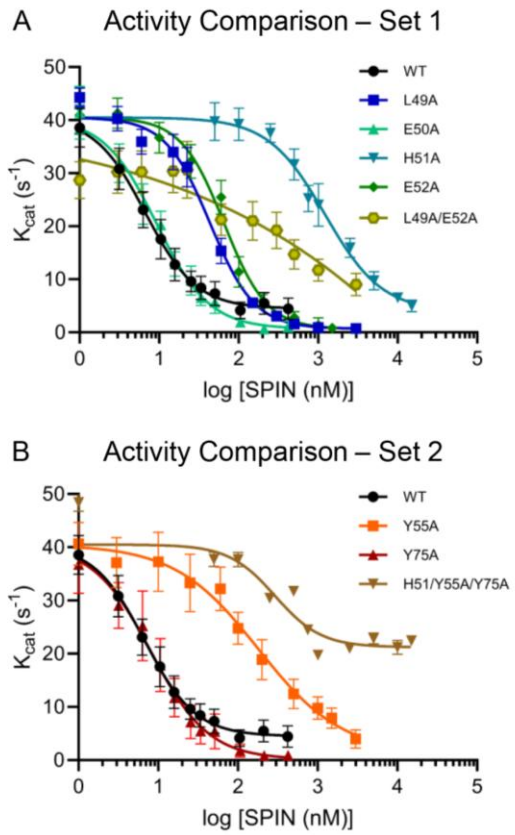

Figure 2.3. MPO Inhibitory Properties of Various *S. aureus* SPIN Mutants.

The MPO-inhibitory properties of wild-type *S. aureus* SPIN were compared to Set 1 and Set 2 site-directed mutants. A minimum of nine independent replicates were conducted on each mutant prior to fitting the data to a four-parameter dose-response inhibition curve. The outcome of curve fitting is shown in Table I. Data points are shown as the mean plus or minus the standard deviation. (A) Comparison of wild-type SPIN with Set 1 mutants consisting of L49A, E50A, H51A, H52A, and the L49A/E52A double mutant. A legend is inset. (B) Comparison of wild-type SPIN with Set 2 mutants consisting of Y55A, Y75A, and the H51A/Y55A/Y75A triple mutant. A legend is inset.

3.3. Loss of Inhibitory Activity in SPIN Mutants Results from Diminished Association Rates with MPO.

We previously showed that SPIN orthologs with decreased potency against human MPO also bind human MPO more weakly [24]. Therefore, we hypothesized that the loss of function exhibited by the SPIN mutants described above was likely due to diminished binding to MPO. To test this idea, we characterized the interaction of each SPIN mutant with immobilized human MPO using SPR (Fig. 4, Fig. S1 & Table I). Although we utilized a Langmuir binding model to evaluate SPIN/MPO binding in earlier work [20,21,24], we employed here a two-state interaction model similar to Leitgeb *et al.* [23]. This decision was made because structural studies of SPIN in both the free and MPO-bound state have shown that the SPIN protein undergoes a conformational change upon binding MPO [20,20,22]; moreover, the two-state model also results in notably improved fitting of the sensorgram series, as judged by lower normalized residual values (i.e. χ^2/R_{max}). Using this approach, we determined an apparent affinity of 20.9 nM for SPIN-WT binding to immobilized human MPO (Figure 2.4A). This value corresponds well to our earlier reports of ~10 nM for SPIN-WT binding to recombinant human MPO [20,21], and similar values of ~9-16 nM for binding to the neutrophil-derived form of human MPO used here and in previous studies [21,24].

Amongst Set 1 mutants (Figure 2.4B-F), we found that E50A (28.3 nM) displayed binding properties comparable to SPIN-WT. Both L49A (287 nM) and E52A (492 nM) were again diminished by roughly one order of magnitude, while the L49A/E52A double mutant exhibited a greater than additive loss of affinity for MPO (19,830 nM). H51A bound immobilized MPO too weakly to be fitted to a kinetic model, however, even when a higher concentration range of analyte was used (Fig. S1). Among Set 2 mutants (Figure 2.4G-I), we found that Y75A (41 nM) displayed binding properties comparable to SPIN-WT, while Y55A bound MPO too weakly to be fitted to a kinetic model. Similarly, binding of the H51A/Y55A/Y75A triple mutant to immobilized MPO could not be evaluated even at higher concentrations (Fig. S1). Nevertheless, when the observations from both Set1 and Set 2 mutants were considered together, we noted that the trend of weaker affinity for MPO correlating with weaker inhibition of MPO remained.

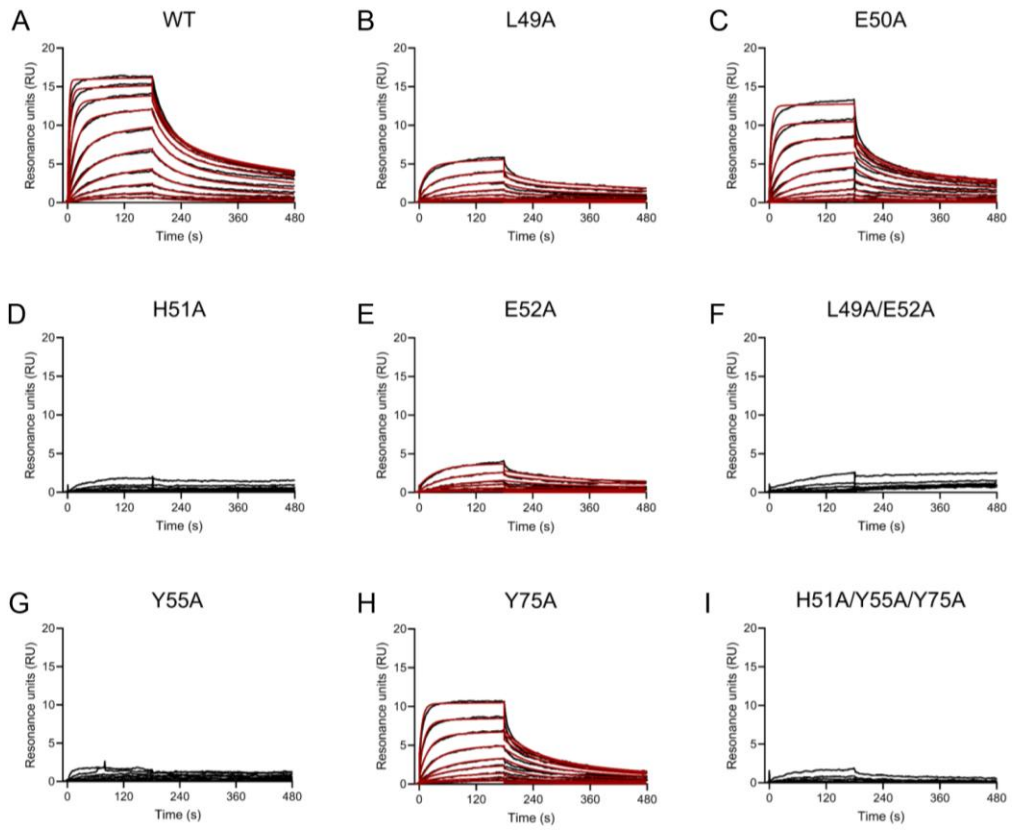

Figure 2.4. MPO Binding Properties of Various *S. aureus* SPIN Mutants as Assessed by SPR.

The binding properties of wild-type SPIN to immobilized human MPO were compared to those of Set 1 and Set 2 mutants. Reference-subtracted sensorgrams (black traces) were obtained for each sample following injection of a two-fold dilution series, using 1 μM as the highest concentration. Sensorgram series were fitted globally to a two-state binding model (red traces). The outcome of fitting is shown in Table I. (A) wild-type *S. aureus* SPIN (B) L49A (C) E50A (D) H51A (E) E52A (F) L49A/E52A (G) Y55A (H) Y75A (I) H51A/Y55A/Y75A.

The two-state model we employed to evaluate our SPR data incorporates two sets of rate constants linked to one another (Figure 2.5). In this mechanism, only the initial association is a bimolecular event described by a second order rate constant, whereas the remaining steps are unimolecular events described by first-order rate constants (Figure 2.5A). Since several of our SPIN mutants displayed statistically significant losses in affinity for MPO (Figure 2.5B & Table 2.1), we wondered whether this was attributable to changes in one or more of these rate

constants as opposed to a combination of various parameters. Interestingly, we found that loss of affinity for MPO by our SPIN mutants resulted from a statistically significant reduction in the initial association rate with MPO (Figure 2.5C & Table I). This was true for both mildly affected mutants, such as E50A and Y75A ($p < 0.001$), and for those with greater loss of function also, such as L49A and E52A ($p < 0.0001$). By contrast, we did not find any consistent differences amongst the first-order rate constants in the binding model (Figure 2.5D-F & Table 2.1). Although the more severely diminished mutants, including H51A and Y55A, could not be analyzed in this fashion, these observations strongly suggest that the conserved SPIN residues found at the interface with MPO play critical roles in driving the initial interaction of these two proteins.

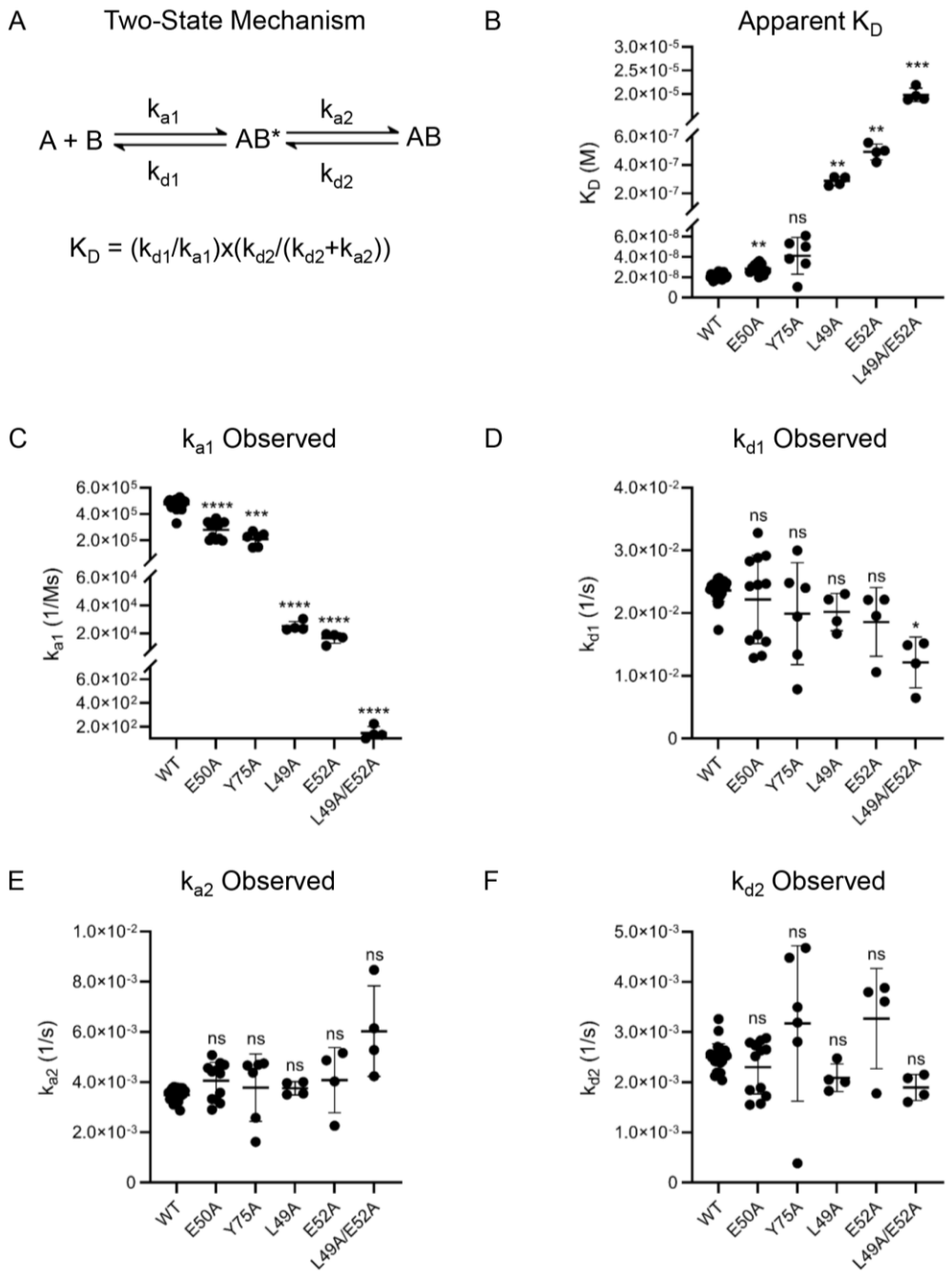

Figure 2.5. Comparative Analysis of MPO-Binding Parameters from Various *S. aureus* SPIN Mutants.

MPO binding parameters for wild-type SPIN and various mutants were compared to one another to derive potential roles for each residue. The mean value for each experimental group was compared to that of the wild-type SPIN control to arrive at an assessment of statistical significance using a one-way Brown-Forsythe and Welch ANOVA: n.s, not significant; *, $p < 0.05$; **, $p < 0.01$; ***, $p < 0.001$; ****, $p < 0.0001$. (A) A description of the two-state

mechanism used to analyze SPIN binding to immobilized human MPO. Value k_{a1} is a second order rate constant, while values k_{d1}, k_{a2}, and k_{d2} are first order rate constants. The relationship yielding the apparent K_D is shown below the mechanism. (B) Comparison of the apparent K_D for wild-type SPIN and those mutants where binding to MPO could be fitted to the two-state model. (C) Comparison of the apparent k_{a1} for wild-type SPIN and those mutants where binding to MPO could be fitted to the two-state model. (D) Comparison of the apparent k_{d1} for wild-type SPIN and those mutants where binding to MPO could be fitted to the two-state model. (E) Comparison of the apparent k_{a2} for wild-type SPIN and those mutants where binding to MPO could be fitted to the two-state model. (F) Comparison of the apparent k_{d2} for wild-type SPIN and those mutants where binding to MPO could be fitted to the two-state model.

4. DISCUSSION

The *S. aureus* innate immune evasion arsenal is comprised of numerous secreted proteins, many of whom display potent enzyme inhibitory properties. These include a series of complement inhibitors that prevent assembly and activity of C3 convertases [37–41] and family of highly potent NSP inhibitors [29,42–45], several of whom exhibit the unusual ability of inhibiting two NSPs simultaneously [46,47]. However, SPIN is unique among these proteins in that it blocks activity of an oxidant-generating enzyme, MPO [20]. Because SPIN had a novel function when it was discovered [20], extensive structure/function studies were needed to provide insight into its mode of action [20,21]. Collectively, this work revealed that SPIN follows a "bind then inhibit" mechanism. In this model, the SPIN α-helical bundle domain drives initial interaction with MPO, allowing its otherwise disordered N-terminus to fold into an inhibitory β-hairpin that is needed to block MPO activity [21,22]. Although work from our group and others have firmly established the α-helical bundle domain as the MPO-targeting motif [21,23], relatively little is known about the contributions of residues within this α-helical bundle to MPO binding. In this report, we identified several SPIN residues essential for high-affinity inhibition and showed that loss of these sidechains diminishes the initial binding rate of SPIN with human MPO.

Since there are several crystal structures available for the SPIN/MPO complex [20,21,23], we used these as a starting point to identify candidate residues for mutagenesis. We selected multiple positions within two different aspects of the compact SPIN surface (~500 $Å^2$) that mediates MPO binding for a residue-level alanine scan (Figure 2.1 & Figure 2.2). From this, we determined that H51 plays the most important role within site 1, while Y55 plays the most important role within site 2 (Figure 2.3). These two residues are found in the first α-helix of SPIN, and their sidechains are separated by only ~4-5 Å distance. It is noteworthy that H51 is invariant across SPIN orthologs, while Y55 would be if not for a single ortholog: the SPIN protein from *S. sciuri* contains a tyrosine to aspartate substitution, yet also fails to bind or inhibit human MPO [24]. Thus, H51/Y55 appears to be a hotspot in determining MPO binding and inhibition. On the other hand, we found that positions peripheral to H51 and Y55, including L49, E50, E52, and Y75 appear to make ancillary contributions to MPO binding. Despite high levels of sequence conservation (e.g. L49, E52, and Y75) and/or clearly defined interactions in structures of the SPIN/MPO complex (e.g E50), removal of these sidechains resulted in either weak (< ~10-fold) or modest (~10-fold) loss of function. Thus, levels of sequence conservation and/or structural information alone are not fully predictive of residue function for SPIN proteins.

Characterization of our SPIN mutants by SPR provided additional insights into formation of the SPIN/MPO complex. Foremost, we found that the inhibitory potency of each mutant (as judged by its IC_{50}) varied directly as a function of its affinity for human MPO (Figure 2.4 & Table 2.1). Whereas similar trends had been reported previously amongst a panel of SPIN orthologs [24], to our knowledge this is the first time that such observations have been made within a single SPIN sequence (in this case SPIN from *S. aureus*). Furthermore, we

noticed that decreasing affinity for human MPO among the SPIN mutants resulted from a statistically significant reduction in the initial association rate with the enzyme (Figure 2.5), whereas we saw no conclusive trends within any of the first order rate constants that described the SPIN/MPO interaction. Although we could not obtain SPR data on the most severely diminished mutants (i.e. H51A and Y55A), our observations suggest that the primary role of the residues interrogated here lies in promoting the initial association of SPIN with MPO. Finally, while we prepared only one double mutant in this investigation, studies on the L49A/E52A variant suggest that insights into more complex aspects of the SPIN mechanism might be discernable via combinatoric mutagenesis. For example, this double mutant was significantly diminished in its ability to inhibit MPO, owing to a dramatically weakened affinity for the enzyme (Figure 2.3, Figure 2.4, Figure 2.5 & Table 2.1). However, this loss in affinity appeared to come from not only a lowered initial association rate, k_{a1}, but also a decrease in k_{d1} and an increase in k_{a2}. As these latter two rate constants presumably describe the conformational changes associated with folding the N-terminal β-hairpin [21], future studies on additional double mutants could help dissect the events that link initial binding of the α-helical bundle domain to folding of the otherwise disordered N-terminus which is required to inhibit MPO.

During the initial characterization of *S. aureus* SPIN, we used both SPR and a bead-based Alpha Assay to derive an apparent affinity of SPIN for MPO in the 2-10 nM range [20]. In subsequent structure/function work on the same SPIN protein [21] as well as a panel of SPIN orthologs [24], we reported comparable apparent affinities for either recombinant or human neutrophil-derived MPO in the range of 10-20 nM. These values are consistent with the value of ~20 nM we report here (Table 2.1), as well as the observed potency of SPIN in enzyme kinetic studies described both here and elsewhere [20,21,24]. By contrast, Leitgeb et. al recently

suggested that the affinity of *S. aureus* SPIN for leukocyte-derived human MPO was several orders of magnitude tighter and likely less than 5 pM [23]. This value was determined by SPR, albeit not by conventional coupling of the ligand to the sensorchip surface but through a capture strategy based upon a biotinylated-DNA conjugate [23]. Although the observations of these investigators should be taken at face value, we think such an apparent affinity for MPO makes little biological sense within the context of the phagosome. Since production of the SPIN protein by *S. aureus* is dramatically upregulated following phagocytosis, the principle site of SPIN action seems to be within the phagosomal compartment [20]. However, MPO is the most abundant protein in human neutrophils and has been estimated to reach concentrations approaching 1 mM within the phagosome [19]. With such an abundance of MPO present, we believe there would be little evolutionary advantage for the pathogen to express a single digit-picomolar affinity inhibitor as opposed to one with more modest affinity, but which is produced in greater quantities. Although it may well be the case that the affinity of SPIN for MPO lies in the picomolar range, we note that a value in the low nanomolar range would also be more consistent with other *S. aureus* innate immune evasion proteins that bind to abundant host targets (e.g. complement C3 and C4) and various bioactive fragments thereof [37–41].

CONFLICTS OF INTEREST

The authors declare that they have no conflicts of interest with the contents of this article.

ACKNOWLEDGEMENTS

We are thankful to Samiksha Khadka and Ping Li (Department of Chemistry, Kansas State University) for helpful discussions during parts of this investigation. This work was

supported by Grant R35GM140852 from the National Institute of General Medical Sciences to B.V.G.

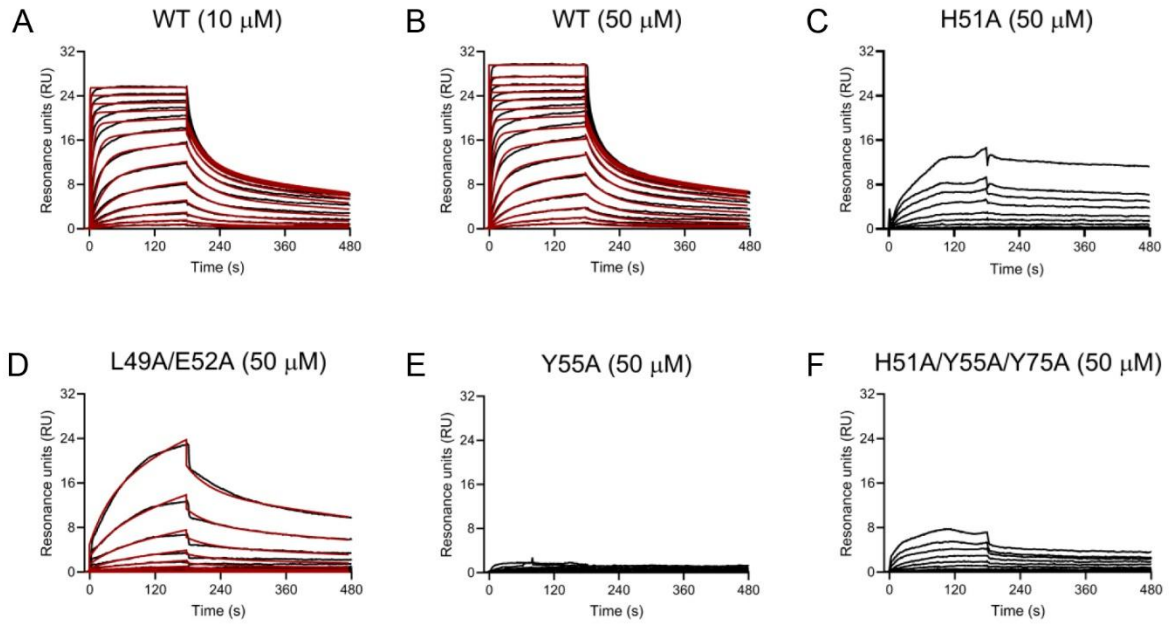

Figure S2. MPO Binding Properties of Wild-Type and Various *S. aureus* SPIN Mutants as Assessed by SPR.

The binding properties of wild-type SPIN to immobilized human MPO were compared to those of Set 1 and Set 2 mutants. Reference-subtracted sensorgrams (black traces) were obtained for each sample following injection of a two-fold dilution series, using the concentrations given in parenthesis as the highest concentration. Sensorgram series were fitted globally to a two-state binding model (red traces). (A) wild-type *S. aureus* SPIN, with a highest concentration of 10 μM (B) wild-type *S. aureus* SPIN, with a highest concentration of 50 μM. (C) H51A, with a highest concentration of 50 μM (D) L49A/E52A, with a highest concentration of 50 μM (E) Y55A, with a highest concentration of 50 μM (F) H51A/Y55A/Y75A, with a highest concentration of 50 μM. In the cases of H51A, Y55A, and H51A/Y55A/Y75A, the sensorgram series could not be fit to the two-state binding model.

Chapter 3 - Staphylococcal Peroxidase Inhibitor (SPIN): Investigation of the Inhibitory N-terminal Domain via a Stabilizing Disulfide Insertion

Soheila Fatehi[1,*], Nitin Mishra[1,*], Timothy J. Herdendorf[1], Om Prakash[1], Brian V. Geisbrecht[1,$]

[1]Department of Biochemistry & Molecular Biophysics
Kansas State University
Manhattan, KS 66506 U.S.A.

[*]These two authors contributed equally to this work.

[$]Address Correspondence To:
Brian V. Geisbrecht, Ph.D.
141 Chalmers Hall
1711 Claflin Road
Manhattan, KS 66506 U.S.A.
E-mail: geisbrechtb@ksu.edu

ABSTRACT

Staphylococcus aureus secretes an array of small proteins that inhibit key enzyme-catalyzed reactions necessary for proper function of the human innate immune system. Among these, the Staphylococcal Peroxidase Inhibitor, SPIN, blocks the activity of myeloxperoxidase (MPO) and thereby disrupts the HOCl-generating system of neutrophils. Previous studies on *S. aureus* SPIN have shown that it relies on a C-terminal α-helical bundle domain to mediate initial binding to MPO, but requires a disordered N-terminal region to fold into a β-hairpin conformation to inhibit MPO activity. To further investigate the structure/function relationship of SPIN, we introduced two cysteine residues into its N-terminal region to trap SPIN in its MPO-bound conformation and characterized the modified protein, which we refer to here as SPIN-CYS. Although control experiments confirmed the presence of the disulfide bond in SPIN-CYS, solution structure determination revealed that the N-terminal region of SPIN-CYS adopted a physically constrained series of lariat-like structures rather than a well-defined β-hairpin. Nevertheless, SPIN-CYS exhibited a gain in inhibitory potency against human MPO when compared to wild-type SPIN. This gain of function persisted even in the presence of deleterious mutations within the C-terminal α-helical bundle domain. Surface plasmon resonance studies showed that the gain in potency arose through an increase in apparent affinity of SPIN-CYS for MPO, which was driven primarily by an increased association rate with MPO when compared to wild-type SPIN. Together, this work provides new information on the coupled binding and folding events required to manifest biological activity of this unusual MPO inhibitor.

KEYWORDS

Myeloperoxidase, Inhibitor, Structure/Function, *Staphylococcus aureus*, Immune Evasion

1. INTRODUCTION

Neutrophils are the most abundant leukocytes in humans and are critical components the innate immune response against bacterial pathogens (Reviewed in [1,2]). Following opsonization of bacteria by either complement fragments or antibodies, neutrophils engulf the bacteria into their phagosomal compartment and thereafter mobilize their granule-resident defenses to affect intracellular killing. Although neutrophils possess a diverse portfolio of antibacterial molecules including proteases, lysozymes, and antimicrobial peptides [1,2], they are perhaps best known for their oxidative killing system wherein the heme-containing enzyme, myeloperoxidase (MPO), plays an essential role [5,18]. MPO is the most abundant protein in neutrophils and is present at unusually high levels within the phagosome, where it catalyzes the rapid generation of cytotoxic levels of HOCl and other hypohalous acids [19]. However, this potent killing mechanism is thought to have exerted strong selective pressure on microorganisms to evolve strategies for escaping its action. Indeed, the Gram-positive bacterium *Staphylococcus aureus* and several closely related staphylococcal species secrete a small (~8.4 kDa), but potent MPO inhibitor known as SPIN (for Staphylococcal Peroxidase Inhibitor) [20,24]. Studies on *S. aureus* showed that expression of the gene encoding SPIN is induced upon exposure to oxidant and following bacterial phagocytosis, strongly suggesting that SPIN functions primarily within the phagosome [20]. Furthermore, cells of an *S. aureus* strain deficient in SPIN are also more readily killed by isolated human neutrophils than are cells of an isogenic control strain [20]. Together, these data suggest that SPIN contributes to *S. aureus* survival within the human neutrophil phagosome by inhibiting HOCl generation via MPO.

SPIN from *Staphylococcus aureus* shares no significant sequence identity with any other proteins [20,21], aside from the orthologs from other closely related bacteria mentioned above

[24]. Therefore, extensive structure/function studies were required to understand its apparently unique mode of action as an MPO inhibitor (Reviewed in [22]). Despite its small size of only ~73 residues, the initial X-ray crystal structure of SPIN bound to a recombinant form of human MPO strongly suggested that SPIN consists of two functional domains: an MPO-binding/targeting α-helical bundle domain of ~60-residues at its C-terminus, and an inhibitory ~13-residue β-hairpin that lies at its N-terminus [20]. The N-terminal β-hairpin presented a paradox, though, as it lacks obvious stabilizing structural features such as disulfide bonds; consistent with this, NMR studies on the full-length SPIN protein in the absence of MPO revealed that this N-terminal region is in fact disordered prior to MPO binding [21,48]. Subsequent characterization of a SPIN mutant lacking the N-terminal region showed that this protein retains near wild-type binding affinity, but is completely devoid of the ability to inhibit MPO [24]. This led us to propose an ordered "bind, fold, then inhibit" mechanism for inhibition of MPO by SPIN [21,22].

Visualizing the structure of SPIN bound to recombinant human MPO as a molecular surface has been particularly informative in suggesting a physical basis for SPIN function [20,22]. In such representations, the SPIN N-terminus appears to serve as a molecular plug that occludes free solute exchange through the enzyme active site channel leading to the catalytic heme [20]. However, as pointed out by Leitgeb and coworkers [23], many biologically-relevant substrates of MPO, including the initial oxidant, H_2O_2, as well as halide anions, notably Cl^- and Br^-, are roughly the same size as H_2O [23]. This suggested that it might still be possible for solutes like these to enter the MPO active site. Using an array of complementary biophysical and kinetic methods, Leitgeb et al. showed that SPIN does not fully block halide oxidation by MPO [23]. Therefore, their observations showed that the molecular plug model is not entirely

accurate. Nevertheless, the same authors also found that SPIN becomes an increasingly effective inhibitor as the size of the substrate to be oxidized increases [23]. Collectively the data presented by Leitgeb et al. seemed to suggest that the inhibitory N-terminal β-hairpin of SPIN fits rather loosely inside the MPO active site channel even though it occupies much of the volume available. Whether this "loose fitting" inhibition goes so far as to involve a complete unfolding of the SPIN β-hairpin while the α-helical bundle domain remains associated with MPO has yet to be addressed through experimental methods. For that matter, little is known of how the SPIN N-terminus folds and inserts into the MPO active site channel following initial binding to the enzyme.

Zhang et al. recently described a series of atomistic molecular dynamics simulations investigating the coupled binding and folding mechanism of the SPIN N-terminus [25]. These authors concluded that binding and folding of the *S. aureus* SPIN N-terminus is a highly cooperative process. Considering their observations, we wondered if restricting the structural landscape accessible to the SPIN N-terminus might result in functional consequences. It is well-documented that the *S. aureus* SPIN N-terminus lacks biochemical features that lead to intrinsic stabilization of the β-hairpin seen in its MPO-bound form [20–22]. However, we were able to leverage existing structural information to generate a mutant of *S. aureus* SPIN that contains an intramolecular disulfide bond within its N-terminus. In this report, we characterize the structure of this disulfide-insertion mutant, which we refer to as SPIN-CYS. We show that this disulfide results in a mild gain-of-function in MPO inhibitory potency that is driven by an increase in its apparent affinity for MPO, primarily by increasing the association rate of the inhibitor for MPO. We also find that gain-of-function caused by this disulfide insertion remains even when other residues critical for mediating initial MPO binding have been removed by site-directed

mutagenesis [49]. Together, this work provides new insights into how the structural features of the SPIN N-terminus influence its function as the essential determinant of MPO inhibition in this unusual staphylococcal innate immune evasion protein.

2. EXPERIMENTAL

2.1. Proteins

Native myeloperoxidase isolated from purulent human sputum was obtained from Elastin Products Corp., while enzyme isolated from quiescent human neutrophils was obtained from Planta Natural Products. Both enzymes were reconstituted (10 mM HEPES (pH 7.4), 150 mM NaCl), and stored until further use according to the manufacturer's recommendations.

All SPIN proteins were obtained in recombinant form according to the general methods described previously [21]. Gene fragments encoding the matured form of *S. aureus* SPIN, as well as various truncation and site-directed mutants, were subcloned into the bacterial expression vector pT7HMT [30] and obtained from GenScript. Following overexpression in *E. coli* strain BL21(DE3) cells, the recombinant SPIN protein was isolated from a clarified cell extract using immobilized metal ion affinity chromatography. The target recombinant protein was cleaved from the affinity tag by digestion with TEV protease. Thereafter, it was separated from the TEV protease and residual digestion products by a second round of immobilized metal ion affinity chromatography wherein the unbound fraction was collected and processed further. Final purification was achieved by size-exclusion chromatography using a Superdex 30 26/60 column attached to an AKTA format FPLC (Cytiva Life Sciences). Following confirmation of purity by SDS-PAGE, each protein was buffer exchanged into ddH_2O, separated into aliquots, and lyophilized for long-term storage.

Isotopically enriched forms of SPIN-CYS for NMR studies were expressed in *E. coli* strain BL21(DE3) cells using minimal media enriched with either $^{15}NH_4Cl$ and/or [^{13}C]-glucose according to the general methods described in an earlier publication [41]. These forms of SPIN were overexpressed, purified, and processed for long-term storage as described above.

2.2. Solution NMR spectroscopy

Isotopically ^{15}N- and/or ^{13}C-labeled forms of SPIN-CYS were dissolved at concentrations of ~1 mM in a buffer containing 50 mM sodium phosphate (pH 6.5) with 5% (v/v) D_2O as a lock solvent and placed in a 5 mm NMR tubes. All NMR measurements were conducted at a temperature of 25 °C using a 600 MHz Bruker Avance Neo NMR instrument equipped with a 5 mm HCN triple resonance cryogenically cooled probe. To facilitate the assignment of both backbone and sidechain resonances, various multidimensional spectra were collected. ^{15}N-HSQC, Dipsi-TOCSY, (H)C(CCO)NH, and H(CCCO)NH spectra were employed for identifying spin systems, while HNCA, HNCACB, HN(CA)CO, HNCO, and HN(CO)CA spectra were utilized for the sequential assignment of SPIN-CYS. Additionally, ^{15}N-edited NOESY spectra were recorded with mixing times of 60, 100, and 150 ms to allow for a semi-quantitative calculation of distances between nuclei. All triple resonance NMR experiments were acquired using non-uniform sampling. Uniformly sampled data were obtained using reconstruction methods such as hmsIST, SMILE, NMRPipe IST, and RIST as implemented in the NMRPipe software [50].

Peak picking and resonance assignments were carried out using CARA NMR software. These assignments were then used to predict dihedral angles and secondary structure using TALOS-N [51]. Structure calculation was performed using Cyana v2.1 [52] with hydrogen-bonding constraints introduced during the final structure calculation. These constraints were

obtained experimentally from $^{1}H–^{15}N$ HSQC spectra collected over a 24-hour period on a sample dissolved in 100% (v/v) D_2O. 20 of the 300 lowest energy structures were selected for preparation of the final structural ensemble. Cyana v2.1 [52], PyMOL, PROCHECK_NMR [53], and the Protein Structure Validation Software Suite (PSVS) were used to assess structure quality. Chemical shifts, structural restraints (distance, dihedral, and H-bonding restraints), and atomic coordinates have been deposited in the BMRB (entry no. 52103) and RCSB (PDB ID 9BD0).

2.3. Steady-State Kinetic Measurement of Myeloperoxidase Inhibition by SPIN Proteins

A coupled colorimetric assay consisting of H_2O_2, vanillic acid (VA), and 4-aminoantipyrine (AAP) was used to measure MPO activity within the peroxidase cycle [32]. In this reaction, oxidized AAP condenses with VA to form a quinoneimine dye that is followed spectrophotometrically at 510 nm (Ɛ: 6.98 $mM^{-1}cm^{-1}$) [33]. To quantify MPO activity, 170 µL of a chromogenic assay mixture consisting of 4.24 nM MPO (enzyme from Planta Natural Products), 7 mM VA and 5mM AAP were added to 170 µL of 50 mM sodium phosphate buffer (pH 7.0) containing H_2O_2 concentrations ranging from ~ 5 µM to ~ 1.1 mM; the formation of the quinoneimine product was then followed spectrophotometrically in a 96-well plate format. Triplicate data (n = 3) were fit to a Michaelis-Menten equation with an additional substrate inhibition component (uncompetitive inhibition) to determine the k_{cat}, K_m and K_I with respect to H_2O_2.

$$y = \frac{k_{cat}*[S]}{K_m + ([S] * [1 + \frac{[S]}{K_I}])}$$

To investigate inhibition of MPO by SPIN proteins, an H_2O_2-free reaction mixture analogous to that described above was prepared and incubated with varying concentrations of SPIN proteins for 1.5 h at room temperature. Complete reactions were prepared in a 96-well plate by rapidly mixing 170 µL of each sample above with an equal volume of ~112 µM H_2O_2 in 50 mM sodium phosphate buffer (pH 7.0); the absorbance was then followed continuously every 25 seconds for 30 min at 25 °C using a $Versa_{max}$ tunable microplate reader. Each inhibition assay was performed in at least three sets of three replicates and the IC_{50} values were estimated by fitting the data to an IC_{50} equation containing four variables (i.e. y_{max} (fixed to the average value of uninhibited rates), y_{min}, $logIC_{50}$ and hillslope (allowed to float)) using GraphPad Prism.

$$y = \frac{y_{min} + (y_{max} - y_{min})}{(1+ 10 \wedge ((logIC_{50} - x)*hillslope))}$$

2.4. Surface Plasmon Resonance

Protein-protein interactions between the SPIN mutants and MPO were investigated by Surface Plasmon Resonance using a Biacore T-200 instrument (Cytiva Life Sciences) and the general methods described earlier [6-8]. All experiments were performed at 25 °C using HBS-T as a running buffer and a flow rate of 30 µL/min. Replicate biosensors were created on three separate experimental flow cells of a CMD-200M chip (Xantec Bioanalytics GmbH) using standard NHS/EDC chemistry to couple human MPO (20 µg/mL in 10 mM sodium acetate (pH 5.5)) to the surface. Two different sensor chips were used in this study. MPO obtained from Elastin Products Corp was used to assess binding of SPIN-CYS, SPIN-WT, and SPIN-dN; the final ligand densities on each flow cell were 1041.7, 758.5, and 643.8 resonance units (RU),

respectively. MPO obtained from Planta Natural Products was used to assess binding of all other SPIN variants; the final ligand densities on each flow cell were 855.1, 798.4, and 701 RU, respectively. One flow cell on each chip was activated by NHS/EDC and immediately quenched by ethanolamine to serve as the reference surface. Two-fold serial dilutions (1.93-1,000 nM) of each SPIN protein were injected over the flow cells with a contact time of 3 min, followed by a 5 min dissociation phase. For the L49A-CYS and E52A-CYS mutants (1.93-2,000 nM), as well as the Y55A-CYS mutant (3-50,000 nM), higher concentration ranges were used to obtain a more accurate estimation of the apparent rate constants. A 0.5 min pulse of 0.1 M glycine (pH 10.0) containing 1 M NaCl was applied to regenerate the surface between injection cycles. Kinetic evaluation was performed on each reference-subtracted injection series using Biacore T-200 evaluation software (Cytiva). A two-state binding model was used to determine the apparent rate constants (i.e. k_{a1}, k_{d1}, k_{a2}, and k_{d2}) and equilibrium constant (i.e. K_D) from the resulting fits.

2.5. Miscellaneous

Representations of secondary structure as a function of amino acid sequence were generated using EsPript [35]. Images of protein structures were rendered using PyMol (https://pymol.org/). Analyses of protein-protein interfaces were carried out using the EBI-PISA server (https://www.ebi.ac.uk/pdbe/pisa/) [36].

3. RESULTS

3.1. Rationale for and Structural Characterization of a Disulfide-Insertion Mutant in S. aureus SPIN

The "bind, fold, then inhibit" mechanism for SPIN action is an ordered process [21,22]: the C-terminal α-helical bundle domain is responsible for initial MPO binding while the

previously disordered N-terminal region folds into the β-hairpin structure required to inhibit MPO catalytic activity. The N-terminal region of SPIN is comprised of only 13 residues and examination of its structure in the MPO-bound state reveals no obvious features to stabilize the β-hairpin in the absence of MPO [20,20]. Interestingly, the sidechains of positions V34 and D44 lie at opposing ends of the SPIN β-hairpin yet are only ~3.6 Å distance from one another in the MPO-bound structure [20]. Therefore, we hypothesized that inserting a pair of cysteine residues at positions V34 and D44 would create a disulfide bond, stabilize the SPIN β-hairpin in its MPO-bound conformation, and thereby promote inhibitory activity (Figure 3.1A).

To investigate this possibility, we overexpressed and purified a V34C/D44C double mutant in *S. aureus* SPIN (hereafter SPIN-CYS). Characterization of the recombinant protein using an Ellman assay revealed no free sulfhydryls in the sample (*Data Not Shown*); since SPIN has no other naturally occurring cysteine residues, and because the protein behaved as a monomer in solution, this result suggested that the sidechains of C34 and C44 had indeed oxidized to form the intended disulfide bond. Thereafter, we expressed and purified $^{15}N/^{13}C$ isotopically labeled SPIN-CYS and collected its 3D HNCACB spectrum; this experiment showed Cβ resonances at 43.6 and 43.5 ppm for C34 and C44, respectively, which matched well the expected value of 43 ppm (^{13}C) if the residue were in a disulfide bond (Fig. S1) [54]. We then used heteronuclear NMR methods to solve the solution structure of SPIN-CYS (Figure 3.1B, Figure 3.1C & Table 3.1). Examination of a representative solution from the ensemble of the 20 lowest-energy structures showed that the C-terminal helical bundle domain of SPIN is not affected by the two mutations, and that the sidechains of C34 and C44 do indeed form a disulfide bond consistent with the observations described above. Although the N-terminal region of SPIN-CYS adopts a more constrained conformation resembling a β-hairpin in certain

solutions (Figure 3.1B), comparison of the entire ensemble reveals significant structural differences in this area albeit with a more compact character distance-wise than would be expected in the absence of the disulfide (Figure 3.1C).

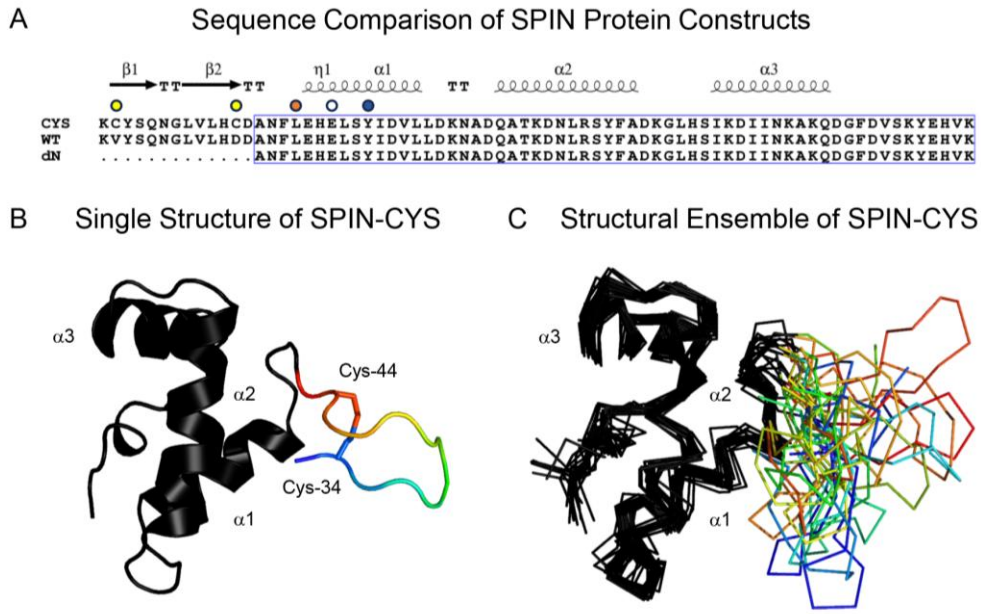

Figure 3.1. Sequence of the Staphylococcal Peroxidase Inhibitor, SPIN, and Solution Structure of the Disulfide-Insertion Mutant, SPIN-CYS.

(A) Sequence alignment of *S. aureus* SPIN proteins investigated here, as rendered by EsPript [35]. Secondary structure elements of the MPO-bound form of *S. aureus* SPIN [20] are shown above the sequence alignment, where the residues corresponding to the α-helical bundle domain are enclosed in a blue rectangle. Residues V34 and D44, which were replaced by cysteines in SPIN-CYS, are illustrated with yellow circles. The locations of residues utilized in mutagenesis studies are indicated: L49, orange circles; E52, clear circles; and Y55, blue circles. (B) Structure of a representative solution from the NMR structure calculation for SPIN-CYS. The SPIN polypeptide is depicted as a black ribbon diagram. Residues comprising the N-terminal region are colored from C34 (blue) to D45 (red), with the inserted disulfide shown in ball and stick convention. Supporting data pertaining to structure solution and calculation are shown in Table 3.1. (C) Ensemble of the 20 lowest-energy structure solutions for SPIN-CYS, as determined by NMR. The color scheme is identical to that used in Panel B, except that the N-termini for individual solutions are depicted with single colors. Note that only Cα positions are shown for purposes of clarity.

Table 3.1. Statistics for SPIN-CYS NMR Solution Structure[a]

PDB Accession Code	9BD0
NOE-based distance restraints	
Intra-residue ($i = j$)	134
Sequential ($\|i-j\| = 1$)	321
medium range ($1 < \| i - j \| < 5$)	281
Long Range ($\|i-j\| \geq 5$)	56
Total	792
Hydrogen bond distance restraints	10
Dihedral angle restraints (Φ and Ψ)	100
Restraint Violations	
NOE > 0.2 Å	11.85
NOE > 0.5 Å	0.25
Dihedral angle > 5°	0
RMSD from the mean structure (Å)[b]	
Main chain	0.88 ± 0.29
Heavy atoms	1.52 ± 0.32
RMSD from experimental restraints	
NOE-based distance restraints (Å)	0.032 ± 0.001
Dihedral angle restraints (°)	0.683 ± 0.114
Deviations from ideal geometry	
RMS deviation for bond angles (°)	0.2
RMS deviation for bond lengths (Å)	0.001
Ramachandran analysis (PROCHECK-NMR)	
Most favored regions (%)	88.6
Additionally allowed regions (%)	10.2
Generously allowed regions (%)	1.2
Residues in disallowed regions	0
Protein Structure Validation Suite Analyses[c]	
PROCHECK G-factor (all dihedral)	-0.90 N/A (-5.32)
PROCHECK G-factor (phi/psi)	-0.35 N/A (-1.06)
Verify3D	0.17 ± 0.03 (-4.65)
ProsaII (-ve)	0.31 ± 0.11 (-1.41)
MolProbity clashscore[d]	14.21 ± 5.84 (-0.91)
MolProbity clashcore Analysis[e]	26.60

[a]Statistics presented for the 20 lowest energy structures of the ensemble.

[b]Calculated using Cyana 2.1.

[c]Values in parentheses are Z-scores as calculated by version 1.5.

[d]Clashscore obtained from the PSVS server.

[e]Clashscore obtained from Molprobity server version 4.5.1.

To further explore the structural differences between SPIN-CYS and wild-type *S. aureus* SPIN (hereafter SPIN-WT) in this N-terminal region, we compared the HetNOE values and relaxation rates (i.e. R2/R1) across the polypeptide backbone of the two proteins [48]. Whereas the average HetNOE value within the 13-residue N-terminal region of SPIN-CYS is 0.482 (Figure 3.2A), the average value within the same residues of SPIN-WT is considerably lower at 0.169 (Figure 3.2B). By contrast, the average HetNOE values across the ~60-residue helical bundle domain of SPIN-CYS and SPIN-WT are in good agreement with one another at 0.788 and 0.786, respectively. Similarly, the average R2/R1 ratio within the N-terminal region of SPIN-CYS is 3.057 (Figure 3.2C), but is 2.512 for the corresponding region of SPIN-WT (Figure 3.2D). The average R2/R1 values across the helical bundle domains of SPIN-CYS and SPIN-WT are 3.923 and 3.614, respectively. Considering these data in total, the observed increase in HetNOE enhancement and relaxation ratio (R2/R1) in the N-terminus of SPIN-CYS relative to SPIN-WT strongly suggests that the introduction of the disulfide greatly restricted the overall conformational flexibility of the N-terminus even though the structure solution itself does not reveal the presence of a β-hairpin structure as initially anticipated.

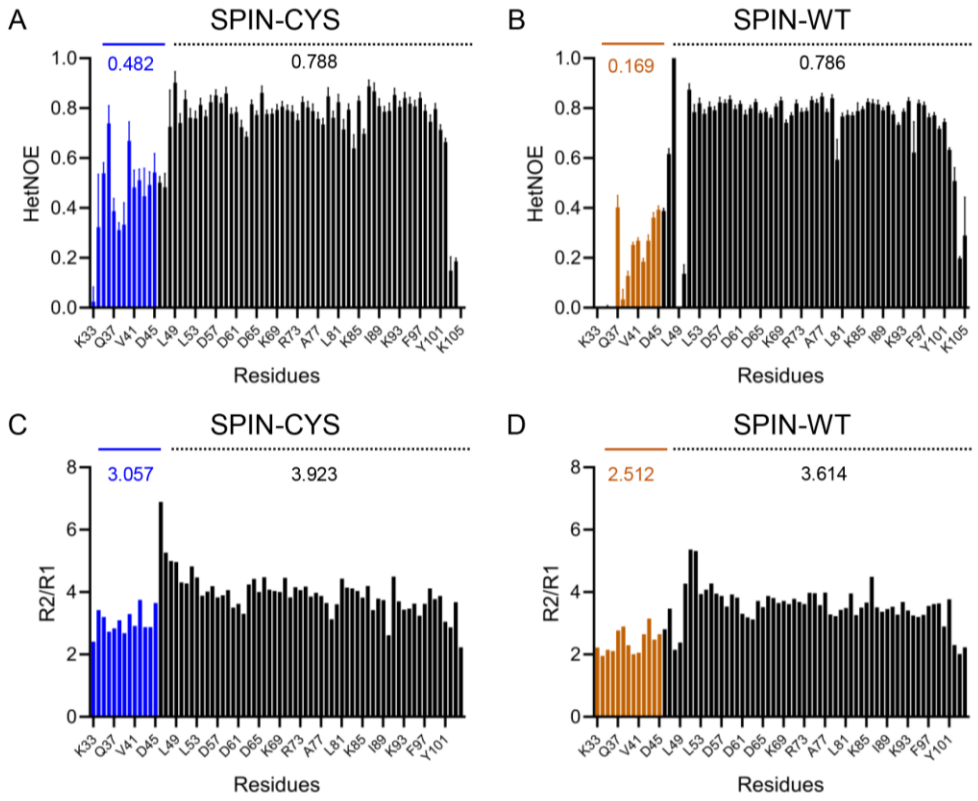

Figure 3.2. Solution Dynamic Properties of SPIN Proteins as Assessed by NMR.

(A) Residue-level hetNOE values for SPIN-CYS. Values for residues comprising the N-terminal region are shown in blue, while those within the C-terminal α-helical bundle domain are shown in black. Average values within each region appear at the top of the panel. (B) Identical information to Panel A, except for the SPIN-WT protein. Here, the values for residues comprising the N-terminal region are shown in orange. (C) Residue-level values for the ratio of observed ^{15}N-R2 (transverse relaxation rate) and ^{15}N-R1 (longitudinal relaxation rate) for SPIN-CYS. Values for residues comprising the N-terminal region are shown in blue, while those within the C-terminal α-helical bundle domain are shown in black. Average values within each region appear at the top of the panel. (D) Identical information to Panel C, except for the SPIN-WT protein. Here, the values for residues comprising the N-terminal region are shown in orange.

3.2. Disulfide Insertion in the N-terminus of S. aureus SPIN Increases its Inhibitory Potency Against MPO

We continued our characterization of SPIN-CYS to examine whether the constrained structural properties of its N-terminus might influence function of this protein as an MPO

inhibitor. As an initial assessment, we compared the potency of SPIN-CYS versus that of SPIN-WT in a chromogenic assay that measures the peroxidase cycle of human MPO [13, 20, 21]. We performed assays in triplicate across a two-fold dilution series of SPIN proteins ranging from ~32 μM to 1 nM and fit the observed MPO activity to a four-parameter dose-response curve to determine apparent IC_{50} values and the associated confidence intervals (Figure 3.3A & Table 3.2). Interestingly, we observed an enhancement of MPO inhibition for SPIN-CYS (IC_{50} 3.6 nM) when compared to SPIN-WT (IC_{50} 6.6 nM). Although this enhancement is only roughly ~1.8-fold, the associated confidence intervals derived from curve fitting do not overlap with one another, suggesting that the observed change potency is significant (Table 3.2). To further validate the accuracy of these findings, we compared the potencies of three SPIN orthologs from *S. delphini*, *S. schleiferi*, and *S. intermedius* in the same assay since these proteins had been reported to exhibit weaker dose-dependent inhibition of human MPO in a previously used method for assessing the MPO peroxidase cycle [24] (Figure 3.3A). Consistent with our previously published observations, we found that SPIN-delphini (IC_{50} 44 nM) is ~6.5-fold weaker than SPIN-WT, while both SPIN-schleiferi (IC_{50} 102 nM) and SPIN-intermedius (IC_{50} 125 nM) are weaker still than SPIN-delphini but comparable to one another [24]. Thus, we concluded that the difference observed between SPIN-CYS and SPIN-WT represents a *bona fide* change in potency.

Because the absolute change in potency resulting from the disulfide insertion is modest, we sought to further substantiate its influence on SPIN function. In that regard, we recently completed a residue-level analysis of the α-helical bundle domain of SPIN-WT that identified several residues, including L49, E52, and Y55, required for maximal MPO binding and inhibition [49]. We therefore prepared a series of site-directed mutants wherein the L49A,

E52A, and Y55A mutations were incorporated into the SPIN-CYS framework. We then compared the properties of these new proteins with the L49A, E52A, and Y55A mutants that lacked the disulfide insertion (Figure 3.3B & Table 3.2). Consistent with our data on SPIN-CYS versus SPIN-WT, we found that the N-terminal disulfide results in a ~1.3-fold gain for L49A-CYS (IC_{50} 29.1 nM), a ~1.9-fold gain for E52A-CYS (IC_{50} 33.5 nM), and ~2.2-fold gain (IC_{50} 83.3 nM) in inhibitory potency for Y55A-CYS. Thus, the disulfide insertion also provides a gain of function in these SPIN variants despite the presence of the otherwise deleterious mutations.

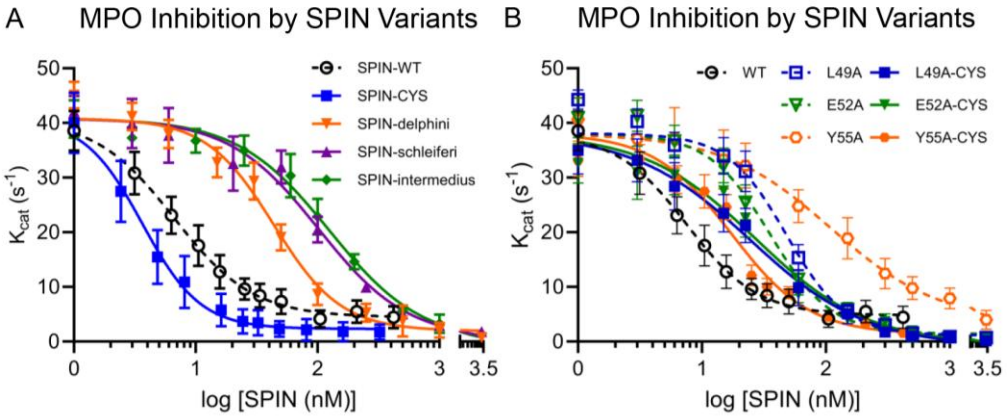

Figure 3.3. MPO Inhibitory Properties of Various *S. aureus* SPIN Mutants.

(A) The inhibitory properties of SPIN-CYS were compared to SPIN-WT, SPIN-delphini, SPIN-schleiferi, and SPIN-intermedius in an enzyme assay designed to interrogate the peroxidase cycle of MPO. A minimum of nine independent replicates were conducted on each inhibitor prior to fitting the respective data to a four-parameter dose-response inhibition curve. The outcome of curve fitting is shown in Table II. Data points are shown as the mean plus or minus the standard deviation. A legend is inset. (B) Identical experiment to that shown in Panel A, except that SPIN proteins with deleterious mutations in the α-helical bundle domain were investigated within either the SPIN-CYS (solid lines) or the SPIN-WT (dashed lines) framework. A legend is inset.

3.3. Disulfide Insertion Increases Potency by Increasing the Apparent Affinity of the Inhibitor with MPO.

In our earlier study of the SPIN α-helical bundle domain, we found that the L49A, E52A, and Y55A mutants are diminished in MPO inhibition due to a reduction in their apparent affinities for MPO [49]. Therefore, we decided to investigate whether the increased potency of SPIN-CYS against human MPO is due to an increased apparent affinity when compared to SPIN-WT. We used SPR to compare binding of SPIN-CYS, SPIN-WT, and the N-terminal deletion mutant (i.e. SPIN-dN) to immobilized human MPO (Figure 3.4A-C & Table 3.2). Interestingly, we found that SPIN-CYS (K_D 25.2 nM) displays an ~1.8-fold increase in apparent affinity when compared to SPIN-WT (K_D 44.8 nM). Similarly, we found that the N-terminal disulfide results in an overall increase in apparent affinity for the mutants utilized above. Both the L49A-CYS (K_D 211.8 nM) and E52A-CYS (K_D 345.2 nM) mutants display an ~1.4-fold increase in apparent affinity for human MPO over the L49A and E52A mutants (Figure 3.4D-E & Table 3.2). Since Y55A within the SPIN-WT framework fails to bind human MPO in SPR experiments [49], a quantitative comparison of apparent affinities could not be made between the Y55A mutants; however, Y55A within the SPIN-CYS framework does show evidence of binding MPO on its own (Figure 3.4F & Table 3.2). Considered as a whole, these observations show that the N-terminal disulfide results in an increase in apparent affinity for MPO when compared to wild-type SPIN.

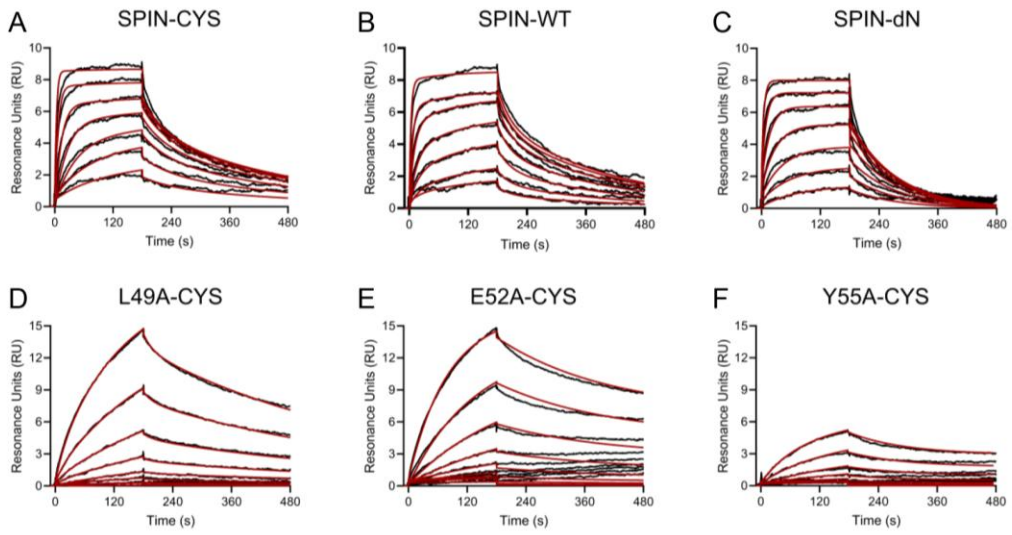

Figure 3.4. MPO Binding Properties of *S. aureus* SPIN Mutants as Determined by SPR.

The binding properties of SPIN-CYS to immobilized human MPO were compared to SPIN-WT and various mutants. Reference-subtracted sensorgrams (black traces) were obtained for each sample following injection of a two-fold dilution series, where 1 μM was used as the highest concentration for each analyte. Sensorgram series were fitted globally to a two-state binding model (red traces). The outcome of fitting is shown in Table II. (A) SPIN-CYS (B) SPIN-WT (C) SPIN-dN (D) L49A-CYS (E) E52A-CYS (F) Y55A-CYS.

Table 3.2. Functional Properties of SPIN Variants as Assessed by Enzyme Assay and Surface Plasmon Resonance[a,b]

SPIN Variant	IC_{50} (nM)[a]	K_D (nM)	k_{a1} ($M^{-1}s^{-1}$) x 10^4	k_{d1} (s^{-1}) x 10^{-3}	k_{a2} (s^{-1}) x 10^{-3}	k_{d2} (s^{-1}) x 10^{-3}
SPIN-WT[c]	6.6 (6.2-7.1)	44.8 ± 9.5	22.6 ± 3.0	22.2 ± 11.7	5.2 ± 3.7	4.6 ± 1.6
SPIN-dN[c,d]	n.d.	48.9 ± 4.2	20.8 ± 1.6	10.2 ± 0.8	-	-
SPIN-CYS[c]	3.6 (3.4-3.9)	25.2 ± 2.8	40.2 ± 6.1	24.7 ± 7.4	9.5 ± 4.8	6.4 ± 1.2
L49A[e]	37.8 (34.3-41.8)	287.0 ± 31.7	2.5 ± 0.4	20.2 ± 2.9	3.8 ± 0.3	2.1 ± 0.3
L49A-CYS	29.1 (25.3-33.9)	211.8 ± 58.5	3.8 ± 1.3	25.0 ± 5.7	9.0 ± 1.4	3.3 ± 0.2
E52A[e]	64.4 (58.9-70.2)	492.0 ± 56.2	1.7 ± 0.4	18.6 ± 5.5	4.1 ± 1.3	3.2 ± 1.0
E52A-CYS	33.5 (30.0-37.7)	345.2 ± 34.9	1.5 ± 0.5	15.0 ± 6.8	4.7 ± 1.7	2.1 ± 1.0
Y55A[e]	181.1 (126.5-321.5)	n.d.	n.d.	n.d.	n.d.	n.d.
Y55A-CYS	83.3 (71.1-100.9)	11590 ± 1202	0.05 ± 0.01	19.6 ± 5.7	2.6 ± 1.1	1.2 ± 0.3

[a]Values in parentheses represent the lower and upper limits for the 95% confidence interval following non-linear curve fitting.
[b]Aside from IC_{50}, all other values are reported as the mean ± standard deviation across replicate measurements (n>4).
[c]SPR parameters determined from experiments using MPO obtained from Elastin Products Corp.
[d]Due to the lack of the N-terminal region, these data were analyzed with a single site kinetic model.
[e]Values taken from a recent study by Fatehi et al. for the sake of comparison [13].

Earlier characterization of certain SPIN mutants revealed that their observed loss of inhibitory potency correlates directly with loss of apparent affinity for MPO [49]. Further examination of the rate constants governing their interaction with MPO revealed that this loss of apparent affinity is due primarily to slowing the association rate of these SPIN variants with MPO. Therefore, we wondered whether the increases in apparent affinity observed for the SPIN-CYS proteins are due to an increase in the association rate with MPO relative to their SPIN-WT counterparts. To address this question, we compared the apparent affinities and various rate constants derived from fitting experimental sensorgrams series to identify potential trends in the data (Figure 3.5 & Table 3.2). It should be noted that SPIN-CYS and SPIN-WT were fit to a two-state binding model owing to the conformational change that occurs in the SPIN N-terminal region following initial binding [23,49] (Figure 3.5A), while the sensorgram series from the SPIN-dN mutant was fit to a single-state binding model as this protein lacks the SPIN N-terminal region [21]. Examination of the apparent affinities (Fig. 5B) and individual rate constants (Fig. 5C-F) revealed that the enhanced affinity of SPIN-CYS seems to arise from an increase in the association rates attributable to both the initial binding of the helical bundle domain (i.e. the second order rate constant, k_{a1}; ~2.4-fold increase) as well as the conformational change of the N-terminus (i.e. the first order rate constant, k_{a2}; ~1.8-fold increase). This is partly offset by an increase in the dissociation rate of the conformational change (i.e. the first order rate constant, k_{d2}; ~1.4-fold increase). Similarly, the enhanced affinity of L49A-CYS appears due to an increase in both association rate constants (k_{a1} ~1.5-fold increase; k_{a2} ~2.4-fold increase) that is partly offset by an increase in the second dissociation rate constant (k_{d2} ~1.6-fold increase). Although E52A-CYS displayed enhanced affinity when compared to E52A alone (Table 3.2), any changes to rate constants could not be discerned due

to too much variability in the data. Despite this limitation, it seems that incorporation of a disulfide bond in the N-terminal region of SPIN provides an enhancement in potency and affinity that arises from an increased association rate of the SPIN protein with MPO.

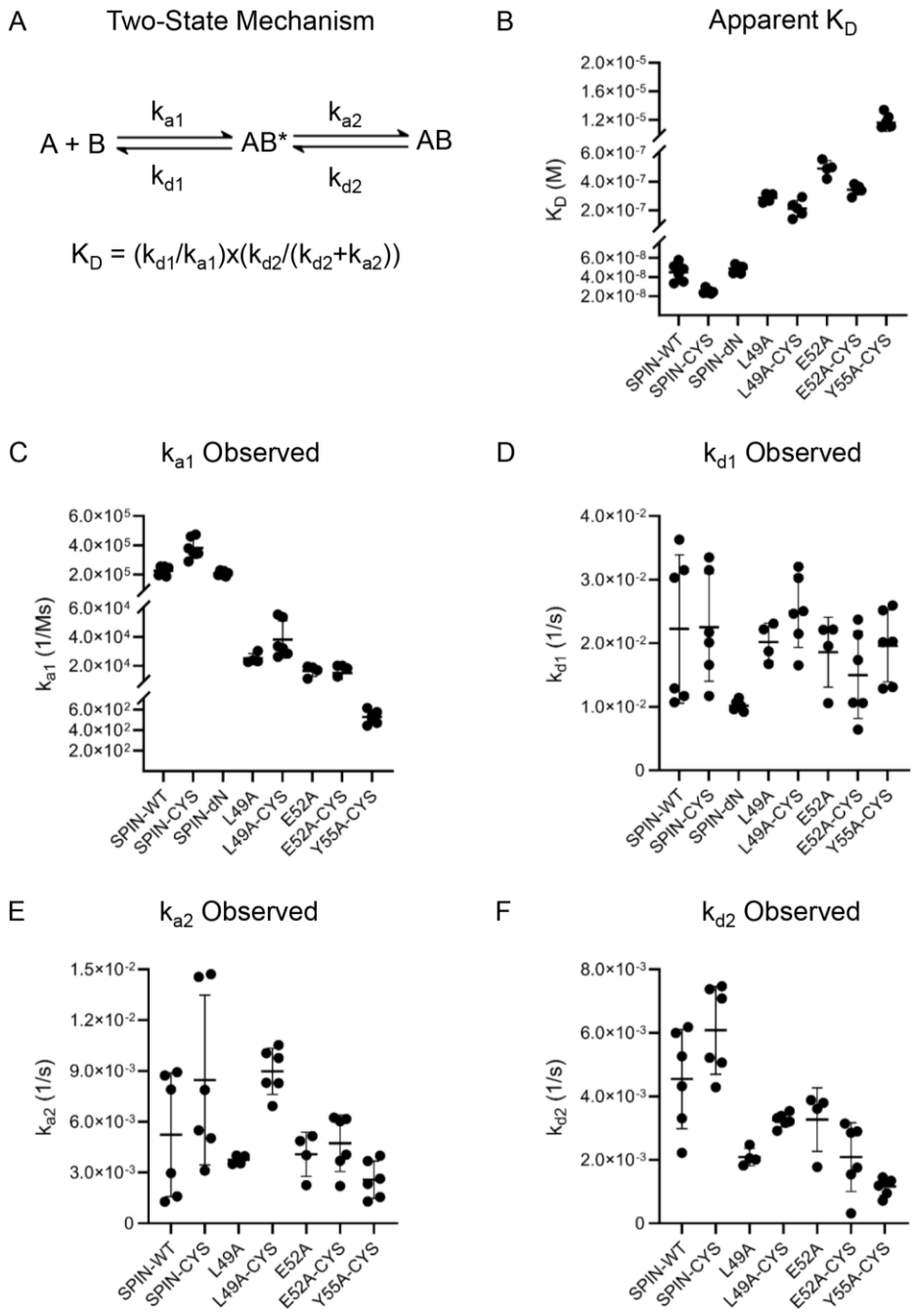

Figure 3.5. Analysis of the MPO-Binding Parameters for Various *S. aureus* SPIN Mutants. (A) Description of the two-state binding mechanism used to analyze interaction of SPIN with immobilized human MPO. Value k_{a1} is a second order rate constant, while values k_{d1}, k_{a2}, and k_{d2} are first order rate constants. The equation for the apparent K_D appears below the mechanism. (B) Comparison of apparent K_D values for SPIN-WT and various SPIN mutants. Error bars show the mean, plus or minus the standard deviation for a minimum of four replicates. (C) Observed k_{a1} for SPIN-WT and various mutants. (D) Observed k_{d1} for SPIN-WT and various mutants. (E) Observed k_{a2} for SPIN-WT and various mutants. (F) Observed k_{d2} for SPIN-WT and various mutants.

4. DISCUSSION

Although the molecular plug model has been a facile way of explaining MPO inhibition by SPIN, emerging evidence has challenged that notion by showing that SPIN only partly blocks halide oxidation [23]. This has raised questions about the SPIN N-terminus and the events that lead to its change from a disordered structure to a folded β-hairpin that inserts into the MPO active site channel. Because separate computational studies have proposed that this binding and folding event is highly cooperative [25], we investigated whether changing the structural properties of this otherwise disordered SPIN N-terminus would impact its ability to inhibit MPO. Our strategy was to insert a stabilizing disulfide bond into the SPIN N-terminus by targeted mutations in two residues, V34 and D44, whose sidechains lie very near one another in the structure of MPO-bound *S. aureus* SPIN [20]. We succeeded in forming a disulfide bond within the SPIN-CYS N-terminus (Fig. S1); however, solution structure calculation on this mutant revealed that the N-terminus did not adopt a defined β-hairpin, but rather an ensemble of lariat-like conformations whose overall dimensions and dynamics were constrained by the presence of the disulfide (Figure 3.1, Figure 3.2, Figure S 3.1 & Table 3.1). We found that this disulfide caused a modest yet statistically meaningful gain in potency of SPIN-CYS against human MPO when compared to SPIN-WT (Fig. 3 & Table II). We also showed that this

increase was retained in the presence of otherwise deleterious mutations (Fig. 3 & Table II). Using SPR, we determined that the increase in potency of each disulfide-containing mutant arises from increasing its apparent affinity for MPO, apparently through enhancement of its association rate with MPO (Figure 3.4, Figure 3.5 & Table 3.2). Therefore, we conclude that restricting the conformational space accessible to the SPIN N-terminus promotes binding to MPO, leading to the gain of function we observed in these experiments. In the future, it may prove interesting to test if the increased potency of these disulfide-containing mutants is also retained in assays that interrogate the halogenation cycle of MPO.

Inserting a disulfide had the intended effect of restricting the conformational space accessible to the SPIN N-terminus, however, it failed to trap this region in the β-hairpin structure seen in the MPO-bound inhibitor. There may be at least two plausible explanations for this observation. On one hand, the β-hairpin may result from simple spatial restrictions imposed on SPIN by the MPO active site channel when the two proteins interact. On the other hand, the β-hairpin could also arise through formation of key hydrogen bonds between groups from the SPIN N-terminus and others from the MPO active site channel. In either scenario, the presence of the binding partner (in this case, MPO) would necessarily play such a fundamental role in folding the inhibitory N-terminus that it cannot be replicated by trivial modifications of the SPIN protein alone. It might be informative, however, to investigate alternative locations for disulfide insertions and assess their consequences. One such option is S36 and V41, whose sidechains are similarly distant to those of V34 and D44. Interestingly, preliminary characterization of an S36C/V41C disulfide insertion revealed that this mutant was ~1.5-fold diminished in potency compared to SPIN-WT (Figure S3.2). Another possibility would be a combinatoric mutant V34C/S36C/V41C/D34, which would result in two pairs of disulfide

bonds within the N-terminus. Presumably, the second disulfide bond would further constrain the SPIN N-terminus within conformational space and perhaps lead to additional gain of function. Unfortunately, incorporating four reactive cysteine residues within such a small region of polypeptide could potentially cause problems like incorrect and/or partial disulfide bonding. While these concerns highlight the limitations of the approach we used in this study, it still provided useful insights into how the structure of the SPIN N-terminus influences its function.

There are several orthologs of *S. aureus* SPIN that also bind and inhibit human MPO [22,24]. The best characterized of these is SPIN from *S. delphini* [24], which inhibits human MPO ~6.5-fold less effectively than *S. aureus* SPIN and which we utilized here as a control for reproducibility of our assay (Figure 3.3). SPIN-delphini is 53% identical to SPIN-aureus, and their overall structures when bound to recombinant human MPO are essentially identical [24]. Yet, recent computational studies by Zhang et al. suggest that the mechanisms underlying the coupled binding and folding of their respective N-termini are fundamentally different [25]. Whereas the N-terminus of SPIN-aureus obeys a highly cooperative binding and folding process, the same region of SPIN-delphini seems to follow instead a conformational selection mechanism [25]. Zhang et al. further observed that the SPIN-delphini N-terminus has a much greater tendency to adopt β-hairpin-type structures in the absence of MPO [25]. During our initial characterization of SPIN-delphini we found that the weaker affinity of this ortholog for human MPO is largely due to a slower association rate with MPO when compared to SPIN-aureus [24]. Intriguingly, these data seem to argue that preforming β-hairpin structures like those seen in the MPO-bound form of SPINs may be counterproductive to inhibitor binding. In the early stages of this work, we attempted to create a disulfide-insertion variant of SPIN-delphini to serve as a comparator for SPIN-CYS; unfortunately, that protein was prone to

incomplete intramolecular disulfide bond formation, which precluded further study. An alternative approach for investigating this issue was to create a chimeric protein wherein the SPIN-delphini N-terminus was appended to the SPIN-aureus α-helical bundle domain. We hypothesized that this chimera ought to have a reduced potency for human MPO due to a slower association rate, presumably resulting from a preformed β-hairpin character in its N-terminal region. Indeed, when we prepared and preliminarily characterized a SPIN-delphini-aureus chimera, we found that its potency was ~5-fold diminished when compared to SPIN-WT (Fig. S2). Although we did not perform a detailed structural analysis on this chimera, our observations support the idea that the reduced potency of SPIN-delphini may be partly due to the preformed β-hairpin character of its N-terminus.

Considering the information in the previous paragraph, we may have been fortunate that our disulfide insertion in SPIN-aureus resulted in a more physically constrained ensemble rather than a fixed β-hairpin *per se*. Although the gain in function of SPIN-CYS was modest, we found that it was reproducible not only within individual experiments, but across various assays for SPIN activity (e.g. MPO inhibition vs MPO binding). The gain of function we observed for SPIN-CYS could be attributed to an increase in its affinity for MPO that appeared commensurate with the increase in its association rate (Table 3.2). We suspect this occurs because the SPIN-CYS protein is more physically compact than SPIN-WT when it first encounters MPO, leading to an increased rate of productive binding events. Although that is largely conjecture, the gain in function in terms of potency, affinity, and association rate was comparable across a panel of SPIN-CYS mutants that had distinct deleterious mutations within their α-helical bundle domains. How these experimental observations correlate with computational studies suggesting a highly cooperative binding and folding mechanism of SPIN-

aureus is not clear at this time [25]. Nevertheless, our previous observations on the H43A/D44A/D45A mutant of SPIN-aureus that binds MPO with wild-type affinity but fails to inhibit its activity strongly suggest that the N-terminal region requires a guide to fold into the MPO active channel [21]. In the future, it might prove informative to examine mutations in H43 and D55 within the SPIN-CYS framework to further investigate this issue and how it is influenced by the conformational properties of the SPIN N-terminus.

CONFLICTS OF INTEREST

The authors declare that they have no conflicts of interest with the contents of this article.

ACKNOWLEDGEMENTS

This work was supported by grant R35GM140852 from the National Institute for General Medical Sciences to B.V.G. and grant S10OD026726 from the U.S. National Institutes of Health to O.P. We also thank the K-INBRE program P20GM103418 from the U.S. National Institutes of Health and Johnson Cancer Research Center of Kansas State University for supporting the NMR studies described here.

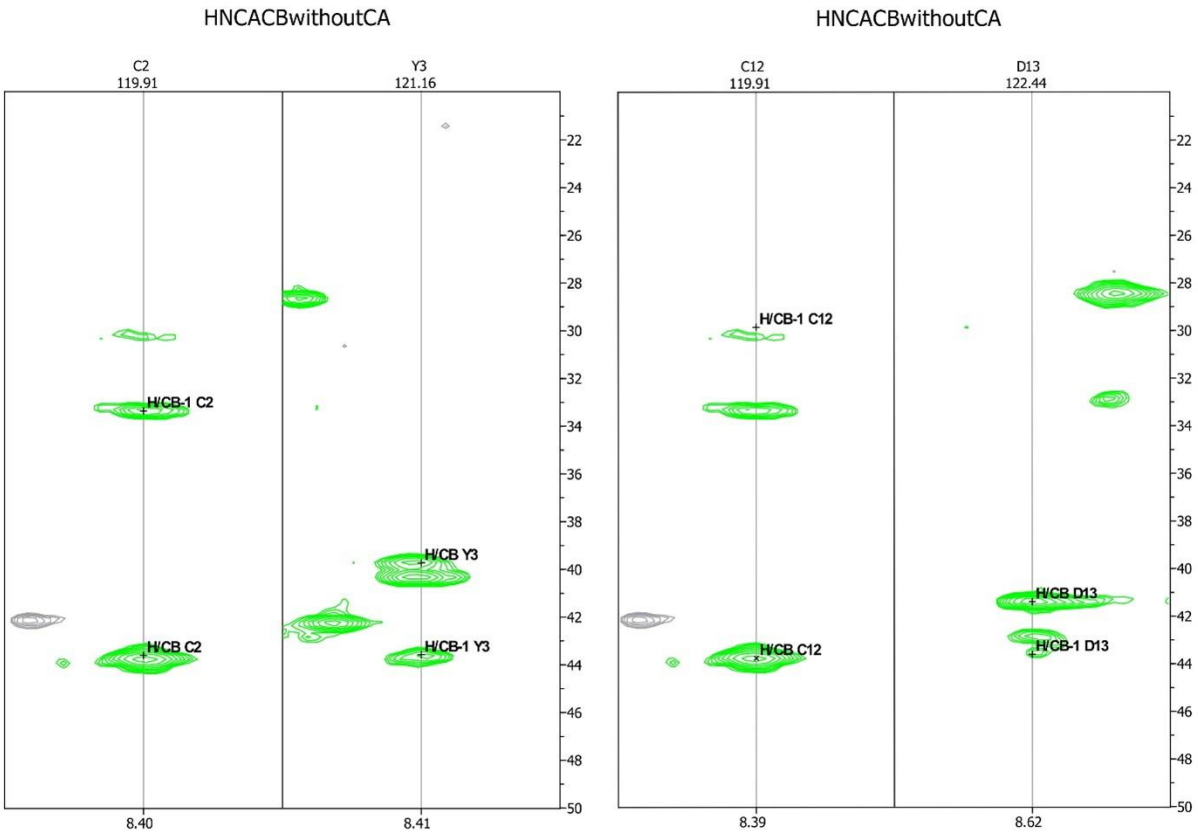

Figure S 3.1. Confirmation of a Disulfide Bond between C34 and C44 in the SPIN-CYS Protein.

Visualization of segments within the HNCACB spectrum collected on a sample of 15N/13C-labeled SPIN-CYS protein. The chemical shift values of the Cβ resonances for C34 (left panel, referred to therein as C2; 43.6 ppm) and C44 (right panel, referred to therein as C12; 43.5 ppm) correspond well to the expected value of about 43 ppm (^{13}C) if the residue participates in a disulfide bond. For a reduced cysteine, the expected value for the Cβ resonance is about 29 ppm. The peak annotated as H/CB-1 represents the Cβ resonance for the previous residue in both panels.

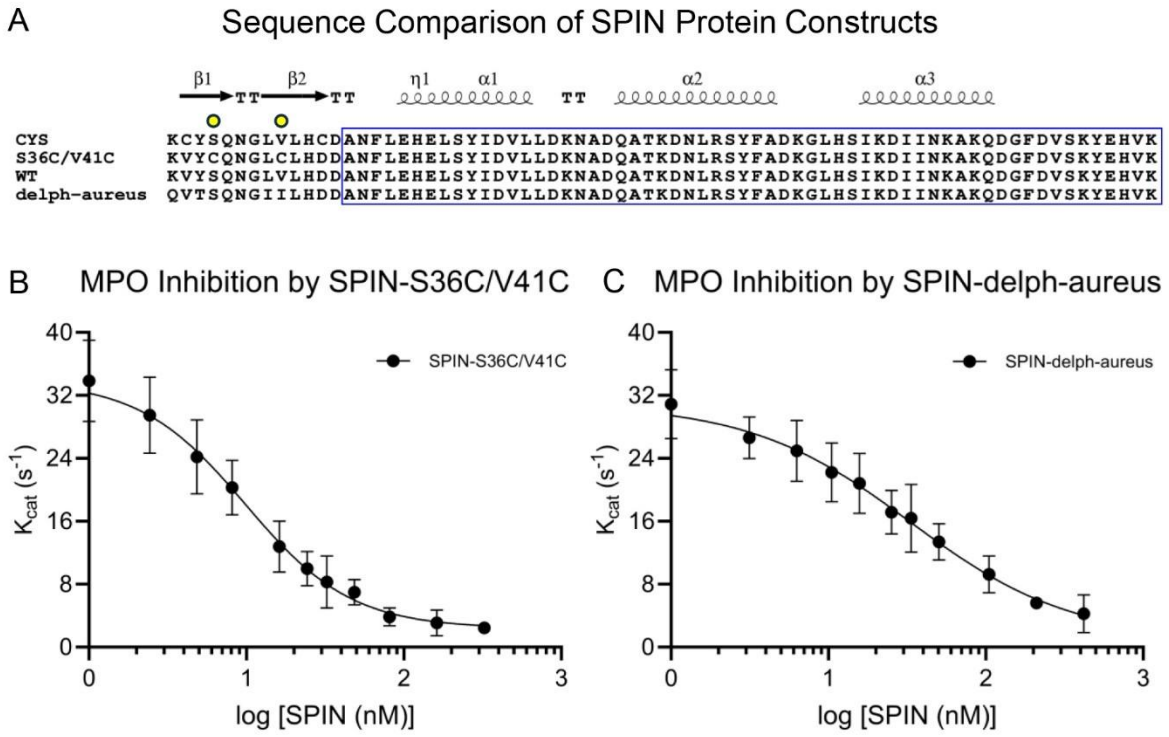

Figure S 3.2. Sequence Information and Partial Characterization of Two Additional SPIN Mutants.

(A) Sequence alignment of wild-type SPIN-aureus, SPIN-CYS, an S36C/V41C disulfide-insertion mutant and a chimeric SPIN consisting of the N-terminal region from SPIN-delphini and the C-terminal region of SPIN-aureus. Secondary structure elements of the MPO-bound form of *S. aureus* SPIN are shown above the sequence alignment, where the residues corresponding to the α-helical bundle domain are enclosed in a blue rectangle. The locations of positions 36 and 41 are highlighted with yellow circles. (B) The inhibitory properties of SPIN-S36C/V41C were investigated using an MPO activity assay. 15 independent replicates were conducted prior to fitting the respective data to a four-parameter dose-response inhibition curve. The outcome of curve fitting is shown as a solid line, while the data points are shown as the mean plus or minus the standard deviation. The apparent IC_{50} value is 9.9 nM (8.8 - 11.2 nM). (C) The inhibitory properties of SPIN-delph-aureus were investigated using an MPO activity assay. 15 independent replicates were performed prior to curve fitting. The apparent IC_{50} value is 33.1 nM (25.1 – 48.9 nM).

Chapter 4 - Studies on the Host Selectivity of the Staphylococcal Innate Immune Evasion Protein SPIN

Abstract

Staphylococcus aureus and related species are highly adapted to their hosts and have evolved numerous strategies to evade the immune system. The Staphylococcal Peroxidase Inhibitor (SPIN) is a small, secreted protein that inhibits myeloperoxidase (MPO) activity. SPIN blocks the MPO active site and prevents production of cytotoxic hypochlorous acid within the neutrophil phagosome, thereby enabling evasion of innate immunity by bacteria. *S. aureus* is primarily a human pathogen, and its SPIN protein cannot inhibit MPO from many non-human species. This raised questions as to whether staphylococci that prefer alternative mammalian species might produce SPIN proteins with strict binding preferences for MPO from those hosts. We tested this hypothesis by isolating canine MPO (cMPO) using samples of canine pus obtained for veterinary diagnostic purposes and exploring its inhibition profile by different SPIN orthologs. The inhibition profile analysis of cMPO obtained in both isolations demonstrated that SPIN proteins from known canine pathogens bind more tightly to and inhibit canine MPO more potently than human MPO. We also find that the increased affinity and potency arise from increases in the second order (i.e. association rate constant (k_a)) rate constant. A 2.1 Å resolution co-crystal structure of SPIN-delphini bound to canine MPO allowed us to explain the physical basis for our observation structural and to propose sequence-dependent physical explanations for why SPIN-delphini binds canine MPO with higher affinity than human MPO. This work alongside our previous studies on SPIN/MPO interaction can be developed into a valuable model system for understanding the structure/function principles that underlie host-specific evolution of virulence proteins.

1. INTRODUCTION

Human neutrophils, the most abundant leukocytes in circulation, serve as the primary responders in the innate immune defense against bacterial pathogens [1,2]. Following the opsonization of bacteria by antibodies or complement fragments, neutrophils execute killing through both extracellular traps (NETs) and intracellular phagocytosis [4]. While neutrophils employ a diverse arsenal of granule-resident defenses including proteases, lysozymes, and antimicrobial peptides, their oxidative killing system is paramount to bacterial clearance [1,2]. This oxidative process is centered on the heme-containing enzyme myeloperoxidase (MPO), the most abundant protein within the neutrophil [5,18]. As the phagosome matures, membrane-resident NADPH oxidase generates H_2O_2, which MPO subsequently utilizes to convert halide or pseudohalide anions (Cl^-, SCN^-) into potent cytotoxic oxidants like hypochlorous acid (HOCl) [5,18]. Given the exceptionally high intraphagosomal concentration of MPO, HOCl can be generated at rates reaching approximately 134 mM/min, creating a lethal antimicrobial environment that forms a cornerstone of a robust immune response [19].

To survive the hostile environment of the neutrophil phagosome, *Staphylococcus aureus* along with closely related staphylococcal species produce nearly two dozen distinct proteins to inhibit complement-mediated opsonization, chemotaxis, and phagocytosis [28,55]. Beyond these extracellular defenses, *S. aureus* employs an elaborate intraphagosomal evasion program, which includes EAP proteins that inhibit Neutrophil Serine Proteases (NSPs) and a novel class of inhibitors known as SPIN (Staphylococcal Peroxidase Inhibitor) [20,29]. Through phage display screening, de Jong et al. discovered SPIN, a small (~8.4 kDa) secreted protein that binds human MPO with high affinity and potently inhibits its peroxidase activity [20]. It blocks the

MPO active site and prevents production of cytotoxic hypochlorous acid within the neutrophil phagosome, thereby enabling evasion of innate immunity by bacteria [20].

Structural investigations into *S. aureus* SPIN (SPIN-aureus hereafter), both free or in complex with recombinant human MPO, identified two functionally distinct domains [20,21]. The C-terminal region, spanning approximately 60 residues, forms an α-helical bundle that facilitates high-affinity binding with MPO; however, this domain lacks inhibitory capability on its own [21]. In contrast, the ~13-residue N-terminal domain remains intrinsically disordered until it binds MPO, at which point it adopts a structured β-hairpin conformation [20,21]. While synthetic peptides mimicking this N-terminal sequence fail to bind or inhibit MPO independently, this domain is indispensable for the SPIN's inhibition of MPO [20,21]. Crystal structures demonstrate that the SPIN N-terminus physically occupies the MPO active site channel and obstructs substrate access [20]. These findings collectively established the "bind-fold-inhibit" model as a foundational framework for SPIN structure-function studies [21,22].

Following characterization of SPIN-aureus, SPIN orthologs were identified in related staphylococcal species [24]. Characterization of SPIN-delphini demonstrated that it inhibited human MPO with approximately 6.5-fold lower potency than the SPIN-aureus [24]. Comparisons of the crystal structures of rhMPO bound to SPIN-delphini or SPIN-aureus revealed that this diminished potency appeared to arise from subtle shifts in sidechain positions or residue substitutions at the protein-protein interface, raising questions about which specific residues drive the initial high-affinity binding [24]. Alanine scanning site-directed mutagenesis on the α-helical bundle domain including residues L49, E50, H51, E52, Y55, and Y75, revealed that mutants E50A and Y75A maintained wild-type potency [21,49]. However, H51A and Y55A exhibited 161-fold and 24.5-fold decreases in inhibition, respectively, pointing to this

area as a functional "hotspot" for MPO recognition. Consistent with the premise that inhibitory potency is directly proportional to binding affinity [24], Surface Plasmon Resonance (SPR) analysis confirmed that these functional losses were driven by reduced affinity for MPO resulting from impaired association rate constant (k_a) of the mutants with MPO. These findings established that conserved SPIN residues found at the MPO interface are critical for mediating the initial binding of the inhibitor to its target [49].

In addition to SPIN-delphini, evaluation of the inhibitory potency of other SPIN orthologs against hMPO revealed that these proteins also exhibited significantly weaker potency compared to SPIN-aureus [24]. This raised questions as to whether staphylococci that prefer alternative mammalian species might produce SPIN proteins with binding preferences for MPO from those hosts. Here we tested this hypothesis by isolating canine MPO (cMPO) from two separate abscess fluid samples driven from single animal and pooled pus from several animals and exploring its inhibition profile by different SPIN orthologs.

MPO is a heme-containing peroxidase found mainly in the neutrophils azurophilic granules [56]. MPO catalyses the oxidation of chloride by hydrogen peroxide to form the potent antimicrobial agent, hypochlorous acid and plays a prominent role in the innate immune system. Intracellular processing of human MPO in the endoplasmic reticulum produces a 90 kDa inactive form of the enzyme known as apoproMPO [57]. Insertion of heme into the peptide backbone [58] then results in the enzymatically active precursor of MPO, proMPO. ProMPO is then cleaved and generates mature human MPO which is a dimeric glycoprotein [57] and has two heavy chains (59 kDa) and two light chains (13.5 kDa) joined together by disulfide bonds. Both heavy chains contain a protoporphyrin IX group with a central iron ion [56]. The hemes are joined with a threefold linkage to the protein including two ester and one sulfonium ion

linkage which is unique to MPO [56]. It makes the porphyrin ring slightly curved and is discussed as the reason for the red shift of the Soret band to 430 nm in MPO with additional bands at 496, 570, 620 and 690 nm, which are responsible for the characteristic green color of this enzyme [59–61]. Here we obtained canine MPO from two different preparations of myeloperoxidase using individual and pooled pus from several animals. The SDS-PAGE gel analysis of cMPO ran side by side hMPO showed identical pattern for both proteins, yielding three distinct bands with molecular weights of 58.5 kDa, 40 kDa, and 14.5 kDa.

The inhibition profile analysis of cMPO obtained in both tirals demonstrated that SPIN proteins from known canine pathogens bind more tightly to and inhibit canine MPO more potently than human MPO. We also find that the increased affinity and potency arises from increases in the second order (i.e. association rate constant (k_a)) rate constant. Molecular level analysis of SPIN-aureus [20] and SPIN-delphini [24] bound to rhMPO has provided fundamental insights into the structure and function of different SPIN orthologs. However, our current understanding is restricted to sequence/structure features specific to human MPO. To expand our understanding of this matter, we sought to purify MPO from a non-human host and characterize its interaction with its most potent SPIN inhibitor. Here we report here a 2.1 Å cocrystal structure of SPIN SPIN-delphini bound to cMPO. This work alongside our previous studies on SPIN/MPO interaction can be developed into a valuable model system for understanding the structure/function principles that underlie host-specific evolution of virulence proteins.

2. EXPERIMENTAL

2.1. Proteins

2.1.1. Native human myeloperoxidase

Native human myeloperoxidase that had been isolated from quiescent human neutrophils and lyophilized was obtained from Planta Natural Products.

2.1.2. Isolation and Purification of Native Canine Myeloperoxidase

Native canine myeloperoxidase was isolated using samples of individual and pooled canine pus obtained through routine veterinary diagnostics. The isolation protocol established by Harrison et al. [62] was modified to optimize enzyme recovery. Initial processing involved centrifugation of the fluid at 5,000 xg for 10 minutes at 7 °C to precipitate cellular matter containing neutrophils. This was followed by a lysis phase, wherein the resulting pellet was resuspended in 1% cetyltrimethylammonium bromide (CTAB) and 0.2 M K_2HPO_4, supplemented with Halt protease inhibitor cocktail to protect MPO from proteolytic degradation. This suspension was homogenized using a Dounce homogenizer on ice, followed by sonication and a seven-hour solubilization at 4 °C. The solubilized protein was separated from insoluble debris by centrifugation at 13.2 rpm at 4 °C for 15 minutes. MPO was precipitated using 55% ammonium sulfate overnight at 4 °C. The ammonium sulfate precipitate was collected via centrifugation at 4,000 xg for 15 minutes and dissolved in 50 mM KPi buffer (pH 7.8) and dialyzed against 1 L 50 mM KPi buffer for four hours using a 10 kDa molecular weight cut-off cassette. Following dialysis, the protein was further purified using Resource S-1ml cation exchange column followed by Superdex 200 increase 10/300 GL size exclusion chromatography on an AKTA FPLC system. The myeloperoxidase activity was monitored through the purification procedure. The purity of the final product was confirmed using SDS-PAGE and the determination of the Reinheits Zahl ratio (A_{430}/A_{280}), with absorbance values measured using a DeNovix DS-11 spectrophotometer.

2.1.3. SPIN proteins

All SPIN proteins were recombinantly expressed according to the general methods described previously [21]. Gene fragments encoding the matured form of SPIN proteins were subcloned into the prokaryotic expression vector pT7HMT [30] and obtained from GenScript. Following overexpression in *E. coli* strain BL21(DE3), the recombinant SPIN proteins were isolated from a lysed and clarified cell extract using immobilized metal ion affinity chromatography. The target protein was cleaved from the his-tag by digestion with TEV protease and separated from the protease and remaining digestion products by a second round of immobilized metal ion affinity chromatography to collect the unbound fraction. Final purification was achieved by size-exclusion chromatography using a Superdex 30 26/60 column attached to an AKTA format FPLC (Cytiva Life Sciences). Following confirmation of purity by SDS-PAGE, each protein was buffer exchanged to ddH_2O, separated into aliquots, and lyophilized for long-term storage.

2.2. Myeloperoxidase Activity Assay

Myeloperoxidase activity within the peroxidase cycle was measured using a coupled colorimetric assay consisting of MPO, H_2O_2, vanillic acid (VA), and 4-aminoantipyrine (AAP) [32]. In this reaction sequence, the oxidized AAP condenses with VA to form a quinoneimine dye such that two quinoneimines are formed for each molecule of H_2O_2 consumed. Reactions were carried out in a neutral pH buffer system (50 mM sodium phosphate (pH 7.0)) at 25 °C and followed spectrophotometrically in a $Versa_{max}$ tunable microplate reader at 510 nm (Ɛ: 6.98 $mM^{-1}cm^{-1}$) [33].

2.3. Steady-State Kinetic Analysis of Myeloperoxidase

Initial velocities of the MPO reaction (2.12 nM enzyme) were measured spectrophotometrically via a plate-based assay outlined above. Briefly, 170 µL of a mixture containing 4.24 nM MPO, 7 mM VA and 5mM AAP were added to 170 µL of buffer containing

H_2O_2 concentrations ranging from ~ 5 µM to ~ 1.1 mM and the formation of the quinoneimine product at 25 °C was followed at 510 nm. From these data, initial velocities were determined and converted to k_{cat} values using the extinction coefficient of the quinoneimine, MPO concentration and the stoichiometry of substrate to product (1 H_2O_2:2 quinoneimine). Replicate data (a minimum of n=3 technical replicates) were fitted to the Michaelis-Menten equation with an additional substrate inhibition component (uncompetitive inhibition) to determine the k_{cat}, K_m and K_I with respect to H_2O_2 using GraphPad Prism [49,63].

$$y = \frac{k_{cat}*[S]}{K_m + ([S] * [1 + \frac{[S]}{K_I}])}$$

2.4. Steady-State Inhibition of Myeloperoxidase by SPIN proteins

The half-maximal inhibitory concentration (IC_{50}) for various SPIN proteins was determined using the plate-based assay described above. Briefly, MPO (4 nM), VA (7 mM), AAP (5 mM) and various concentrations of SPIN proteins were incubated for 90 min at room temperature in sodium phosphate buffer. Following the incubation, 170 µL of each sample above were mixed with 170 µL of sodium phosphate buffer containing ~112 µM H_2O_2. 170 µL of the complete reaction mixture were added to the read plate and the formation of the quinoneimine product at 25 °C was followed at 510 nm. Initial velocities were converted to k_{cat} values as described above, and then the replicate data (a minimum of n=3 technical replicates) were expressed as percent activity using the no-inhibition K_{cat} as 100 % activity. The normalized data then were fitted to an IC_{50} equation of log (inhibitor) vs. normalized response (variable slope) using GraphPad Prism v10.6.1 [49,63].

2.5. Surface Plasmon Resonance

Surface Plasmon Resonance (SPR) was used to investigate interactions between each SPIN protein and immobilized human and canine MPO during according to the general methods described previously [20,21,24,49,63]. All experiments were conducted using a Biacore T-200 instrument (Cytiva Life Sciences) at 25°C. HBS-T was used as a running buffer (20 mM HEPES (pH 7.4), 140 mM NaCl, and 0.005% (v/v) Tween-20) with a flow rate of 30 µL/min.

The biosensor surface was established on a CMD-200M sensor chip (Xantec Bioanalytics GmbH) by coupling human MPO (as control) to flow cell #2 and canine MPO to flow cells #3 and #4 via amine coupling according to the manufacturer's recommendations. To activate the surface, equal volumes of N-hydroxysuccinimide (NHS; 0.1 M in ddH_2O) and N-ethyl-N'-(dimethylaminopropyl) carbodiimide hydrochloride (EDC; 0.4 M in ddH_2O) were mixed immediately prior to injection onto a naïve surface. Subsequently, 20 µg/mL human and canine MPO (prepared in 10 mM sodium acetate pH 5.5) were injected to allow the coupling of protein-borne amine groups to the surface esters through amide bond formation. Finally, 1 M ethanolamine (pH 8.5) was injected to deactivate any uncoupled NHS-esters. The levels of MPO immobilization for protein purified from the pus driven from an individual animal were as follows: hMPO flow cell #2, 794; cMPO flow cell #3, 1030.2 and cMPO flow cell #4, 599.3 Resonance Units (RU). The levels of MPO immobilization for protein purified from the pooled pus were as follows: hMPO flow cell #2, 326.3; cMPO flow cell #3, 616.6 and cMPO flow cell #4 156.1 RU. Flow cell #1 was activated but immediately inactivated by ethanolamine and served as the reference in both experimental setups.

Serial two-fold dilutions (1.93-1000 nM) of each SPIN protein were injected over the flow cells. A contact time of 3 min was used, followed by a 5 min dissociation phase. To regenerate the surface following each injection, a 0.5 min pulse of 0.1 M glycine (pH 10.0)

containing 1 M NaCl was applied. Reference subtracted sensorgram series were processed using Biacore T-200 Evaluation Software v3.2.1 (Cytiva Life Sciences). Data were analyzed globally using Langmuir binding model with global fitting of R_{max}. The fitted binding curves were then imported and graphed using GraphPad Prism v10.6.1.

2.6. Miscellaneous

Amino acid sequence alignments were performed using Clustal Omega [34]. Representations of secondary structure as a function of amino acid sequence were generated using EsPript [35]. Images of protein structures were rendered using PyMol (https://pymol.org/). Analyses of protein-protein interfaces were carried out using the EBI-PISA server (https://www.ebi.ac.uk/pdbe/pisa/) [36]. Statistical analyses were performed using GraphPad Prism v10.6.1 (https://www.graphpad.com/).

2.7. Crystallization, structure determination and refinement

A sample of the SPIN-delphini/cMPO complex was prepared by mixing the purified proteins in a 2:1 molar ratio. The sample was buffer exchanged to 10 mM HEPES (pH 7.4), 50mM NaCl and the concentration was adjusted to 1.5 mg/ml total protein. The Initial crystallization trials were carried out by vapor diffusion of sitting drops at 20 °C using Hampton Research Crystal Screen Index HT and PEGRx, and thereafterof hanging drops using various customized buffers. Single crystals suitable for X-ray diffraction studies were grown over the course of 7–10 days from drops consisting of either 1 µL of complex mixed with 0.5 µL distilled water and 0.5 µL of a precipitant solution (0.1 M sodium acetate trihydrate (pH 4.1, 4.3 and 4.5) and 2 M ammonium sulfate) or drops consisting of 1 µL of complex mixed with 1 µL of the precipitant solution, and were equilibrated over 0.5 mL of precipitant solution.

Individual crystals for analysis were briefly soaked in a cryoprotectant consisting of precipitant solution supplemented with 25% (v/v) glycerol, prior to flash cooling in liquid N2.

X-ray diffraction data were collected at beamline BL-5.0.1 of the Advanced Light Source at Lawrence Berkeley National Laboratory. A total of 1440 images were collected with an oscillation angle of 0.25°, an exposure time of 0.25 s, radiation of λ=0.9774 Å, and a sample to detector distance of 225 mm. The reflections were indexed, integrated, and scaled using the HKL-2000 package. The structure was solved by molecular replacement using the refined polypeptide coordinates of SPIN-delphini/rhMPO (PDB entry 6BMT) as a search model and PHASER as implemented in the PHENIX software suite. The final model was constructed by an iterative combination of automated and manual rebuilding, followed by crystallographic refinement using PHENIX.REFINE. 94.87% of the modeled polypeptide residues lie in favored regions of the Ramachandran plot, with only 0.47% in regions classified as outliers. The asymmetric unit of the crystal contained a homodimer of cMPO bound to SPIN-delphini. We performed our downstream interface analyses using a single enzyme/inhibitor complex (Chains A and C). This selection was justified by several factors. First, the two complexes within the asymmetric unit exhibited high structural identity when superimposed (RMSD of 0.142 Å over the total 481 C_α atoms). Second, a comparative analysis of the displacement parameters (B-factors) revealed that the complex defined as Chains A and C possessed lower overall thermal mobility compared to the second complex defined as Chains B and D. Consequently, this complex was utilized for EBI-PISA interface calculations and evaluations. Beyond the polypeptides, the final model also includes 930 ordered solvent molecules. Each MPO polypeptide also contains a covalently bound heme prosthetic group within the active site, a single Cl^- ion and a Ca^{2+} ion which is coordinated entirely by residues derived from MPO. A more detailed description of the cell constants, diffraction data quality, and properties of the final model can be found in Table 4.5. All structural analyses, including calculation of buried

surface areas and identification of potential hydrogen bonds and salt bridges, were performed using EBI-PISA (http://www.ebi.ac.uk/msd-srv/prot_int/cgi-bin/piserver). Representations of protein structures were generated by PyMol (http://www.pymol.org/).

3. RESULTS

3.1. SPIN orthologs display a preference for cMPO compared to hMPO

Most of innate immune strategies employed by *S. aureus* show clear human specificity [13]. De Jong et al. documented the species-specificity of SPIN-aureus, noting its potent inhibition of human myeloperoxidase (MPO) while remaining ineffective against MPO from other mammals such as mice, rabbits, bovines, or equines [20]. Given the identification of various SPIN orthologs within staphylococcal species that primarily colonize livestock and companion animals (including *S. intermedius*, *S. pseudintermedius*, and *S. delphini*) [26], Ploscariu et al. evaluated the inhibitory potency of these orthologs against hMPO and revealed that each protein exhibited significantly weaker potency compared to SPIN-aureus [24]. Specifically, while SPIN-aureus inhibited hMPO activity with a potent IC_{50} of 6.6 nM, SPIN-delphini exhibited a nearly 6.5-fold reduction in potency (IC_{50} 44 nM). Furthermore, SPIN-schleiferi and SPIN-intermedius displayed even lower inhibitory potency, with IC_{50} values of 102 nM and 125 nM, respectively [24]. Therefore, they hypothesized that these inhibitors might demonstrate a comparable selectivity for the MPO from their respective hosts.

Despite the theoretical significance of this hypothesis, experimental validation was restricted by the limited availability of MPO derived from these specific animal hosts. In this study, we addressed this question by successfully isolating and purifying canine MPO from its native biological environment, canine pus, and sought to investigate whether these SPIN orthologs exhibit any preference for canine MPO. We extracted the enzyme from abscess fluid through a combination of cell lysis using 1% CTAB and homogenization, followed by

precipitation via ammonium sulfate. The crude extract was then purified using dialysis and two-stage FPLC chromatography including cation exchange and size exclusion, to ensure high enzymatic purity. Finally, we verified the purity and heme-group integrity of the isolated MPO through SDS-PAGE and spectrophotometric Reinheits Zahl (RZ) ratio analysis. The final purified cMPO achieved a purity of 82%. When analyzed via SDS-PAGE alongside a commercial hMPO, the cMPO displayed a migration pattern consistent with hMPO. Specifically, both samples yielded three distinct bands at molecular weights of 58.5 kDa, 40 kDa, and 14.5 kDa (Figure 4.1A).

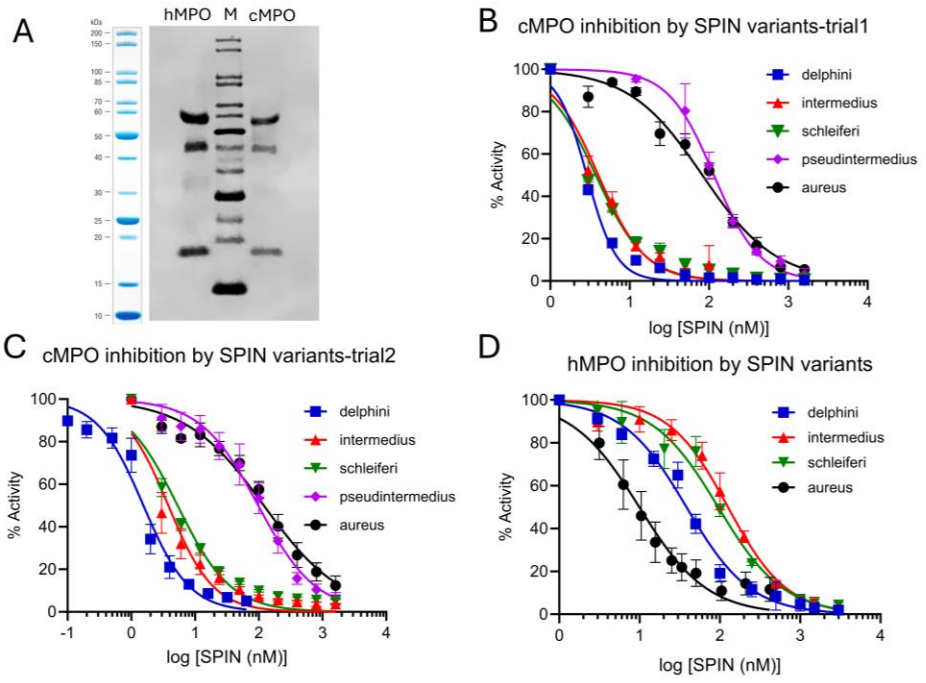

Figure 4.1. cMPO inhibitory properties of different SPIN variants.

The inhibitory properties of SPIN orthologs against cMPO was assessed using a colorimetric enzyme assay designed to track the production of quinoneimine dye resulting from consumption of H_2O_2 as MPO substrate. A minimum of nine replicates were conducted on each ortholog prior to fitting the data to an IC_{50} equation of log (inhibitor) vs. normalized response (variable slope). The outcome of curve fitting is shown in Table 4.1 & Table 4.3. Data points are shown as the mean plus or minus the standard deviation. (A) SDS-PAGE of purified human and canine MPO. Two micrograms of each protein were loaded in each well, separated, and visualized by staining with Coomassie blue. A mixture of standard proteins was loaded in the center with sizes indicated in kDa. Left lane corresponds to commercially obtained hMPO and right lane represents the cMPO purified from pooled pus. (B) cMPO inhibition profile by SPIN orthologs (trial 1). A legend is inset. (C) cMPO inhibition profile by SPIN orthologs (trial 2). A legend is inset. (D) hMPO inhibition profile by SPIN orthologs [24,63]. A legend is inset.

To quantify the potency of these SPIN orthologs against cMPO, we used a colorimetric assay, with two trials conducted independently. Our analysis in first trial revealed that SPIN-delphini, SPIN-intermedius, and SPIN-schleiferi exhibited profound selectivity for cMPO (Figure 4.1B). Notably, SPIN-delphini was the most potent inhibitor of cMPO with an IC_{50} of 2.88 nM, which represented a 16-fold increase in potency compared to hMPO (IC_{50} 45.4 nM) (Figure 4.1B & D, Table 4.1) [24,63]. SPIN-intermedius and SPIN-schleiferi demonstrated

approximately 33-fold (IC_{50} 4.02 nM) and 28-fold (IC_{50} 3.73 nM) greater potency against cMPO relative to hMPO, respectively (Figure 4.1B & D, Table 4.1) [24,63]. SPIN-aureus, which is a hallmark inhibitor of hMPO (IC_{50} 6.6 nM), exhibited nearly 12-fold weaker potency against cMPO (IC_{50} 82.5 nM) (Figure 4.1B & D & Table 4.1) [24,63]. Although SPIN-pseudintermedius displayed no detectable inhibition of hMPO even at high micromolar concentrations, it inhibited cMPO with an IC_{50} of 115.5 nM (Figure 4.1B & D & Table 4.1) [24,63].

Table 4.1. Functional Properties of SPIN Variants over canine MPO purified in first trial as Assessed by Enzyme Assay and SPR

SPIN Variant	IC_{50} (nM)	K_D (nM)	k_a ($M^{-1}s^{-1}$) x 10^4	k_d (s^{-1}) x 10^{-3}	$\chi 2$/Rmax
delphini	2.88 (2.67-3.1)	7.96 ± 3.19	26.55 ± 8.16	1.92 ± 0.19	2.74 ± 1.16
intermedius	4.02 (3.53-4.57)	13.78 ± 2.24	18.82 ± 3.3	2.54 ± 0.03	1.7 ± 0.61
schleiferi	3.73 (3.24-4.3)	26.8 ± 5.9	6.4 ± 1.15	1.6 ± 0.08	1.16 ± 0.24
pseudintermedius	115.5 (103.7-128.3)	182.3 ± 23.8	1.42 ± 0.05	2.5 ± 0.24	0.16 ± 0.08
canis	n.d.	n.d.	n.d.	n.d.	n.d.
aureus	82.5 (71.72-94.75)	17.95 ± 2.24	22.05 ± 0.55	3.96 ± 0.55	2.5 ± 0.3

Table 4.2. Functional Properties of SPIN Variants over human MPO (as control) Assessed by SPR (first trial)

SPIN Variant	K_D (nM)	k_a ($M^{-1}s^{-1}$) x 10^4	k_d (s^{-1}) x 10^{-3}	$\chi 2$/Rmax
delphini	129 ± 5.65	1.65 ± 0.03	2.14 ± 0.04	0.36 ± 0.24
intermedius	71.95 ± 9.12	1.78 ± 0.04	1.27 ± 0. 1	1.43 ± 0.02
schleiferi	181.5 ± 26.16	1.12 ± 0.01	2.03 ± 0.26	0.2 ± 0.07
pseudintermedius	n.d.	n.d.	n.d.	n.d.
canis	n.d.	n.d.	n.d.	n.d.
aureus	15.88 ± 0.99	18.25 ± 0.33	2.9 ± 0.14	2.04 ± 0.11

Subsequent evaluations conducted during second trial yielded results consistent with our previous observations. SPIN-delphini, SPIN-intermedius, and SPIN-schleiferi remained the most potent inhibitors of cMPO. These orthologs demonstrated highest inhibition potency with IC_{50} values of 1.54 nM, 3.8 nM, and 5.31 nM, respectively. This represented approximately 29-, 35-, and 20-fold increase in their inhibitory potency relative to human MPO (Figure 4.1C & D) [24,63].

3.2. SPIN Variants Show Higher Affinities for cMPO compared to hMPO

Prior research has established a direct correlation between weakened inhibitory potency and diminished binding affinity among SPIN orthologs to human MPO [24]. This relationship was further elucidated through residue-level analyses of the *S. aureus* SPIN α-helical bundle

and its N-terminal domain [49,63]. Specifically, site-directed mutagenesis involving L49A, E52A, and Y55A substitutions within the α-helical bundle resulted in a significant reduction in hMPO inhibition which was attributed to a decline in their apparent affinities for the enzyme [49]. Subsequent investigations of the SPIN-aureus N-terminal inhibitory domain by insertion of a stabilizing disulfide bridge (the SPIN-Cys mutant) provided further evidence for this biochemical correlation. It was observed that the enhanced potency of the SPIN-Cys variant was driven by an increase in its apparent affinity for hMPO [63].

Table 4.3. Functional Properties of SPIN Variants over canine MPO purified in second trial as Assessed by Enzyme Assay and SPR

SPIN Variant	IC_{50} (nM)	K_D (nM)	k_a ($M^{-1}s^{-1}$) x 10^4	k_d (s^{-1}) x 10^{-3}	χ2/Rmax
delphini	1.54 (1.46-1.63)	8.95 ± 1.16	27.12 ± 7.42	2.36 ± 0.33	3.13 ± 1.92
intermedius	3.8 (3.28-4.41)	9.25 ± 0.5	31 ± 4.71	2.87 ± 0.32	2.87 ± 1.56
schleiferi	5.31 (4.68-6.04)	26.15 ± 3.97	8.12 ± 1.35	2.08 ± 0.2	1.44 ± 0.62
pseudintermedius	97.9 (90.67-105.6)	157.3 ± 51.37	1.7 ± 0.14	2.62 ± 0.66	0.47 ± .25
canis	n.d.	n.d.	n.d.	n.d.	n.d.
aureus	119.8 (106.1-135.3)	22.48 ± 8.57	34.25 ± 17.91	6.71 ± 1.9	4.43 ± 1.72

Table 4.4. Functional Properties of SPIN Variants over human MPO (as control) Assessed by SPR (second trial)

SPIN Variant	K_D (nM)	k_a ($M^{-1}s^{-1}$) x 10^4	k_d (s^{-1}) x 10^{-3}	χ2/Rmax
delphini	100 ± 0.0	1.64 ± 0.21	2 ± 0.0	3.13 ± 0.21
intermedius	107.5 ± 2.12	1.46 ± 0.02	1.58 ± 0.0	4.88 ± 0.12
schleiferi	200 ± 100	1.26 ± 0.3	2.25 ± 0.57	1.62 ± 1.49
pseudintermedius	n.d.	n.d.	n.d.	n.d.
canis	n.d.	n.d.	n.d.	n.d.
aureus	14.75 ± 5.65	33.83 ± 15.46	4.61 ± 0.38	7.34 ± 2.47

Therefore, we asked the question whether the functional/inhibitory preference for cMPO exhibited by certain SPIN orthologs is primarily driven by an increased binding affinity for the enzyme. To address this, we employed SPR to characterize the interactions between each SPIN

ortholog and immobilized human or canine MPO, through two independent assessments. Injections of an increasing concentration of each recombinant SPIN ortholog including SPIN-delphini, SPIN-intermedius and SPIN-schleiferi and SPIN-pseudintermedius gave clear evidence of their binding preference for cMPO compared to hMPO (Figure 4.2 & Figure 4.3). We utilized a simplified Langmuir binding model to evaluate SPIN/MPO binding in our SPR study, rather than a two-state model, as it resulted in fitting of the sensorgram series with normalized residual values of less than 10% in all cases (i.e. $\chi 2/R_{max}$) [64,65]. Data obtained during the first trial revealed that SPIN-delphini displayed a nearly 16-fold higher affinity for cMPO (K_D 7.96 nM) relative to hMPO (K_D 129 nM) (Figure 4.2A-B, Table 4.1) [24,63]. Similarly, SPIN-intermedius and SPIN-schleiferi demonstrated 5- and 7-fold stronger binding to cMPO, respectively (Figure 4.2E-F, Table 4.1 & Table 4.2). In contrast, SPIN-aureus exhibited comparable affinities for both canine and human MPO (17.95 nM vs 15.88 nM) (Figure 4.2I-J, Table 4.1 & Table 4.2). Furthermore, while SPIN-pseudintermedius failed to produce any detectable binding signal with hMPO, its apparent affinity for cMPO was calculated at 182.3 nM (Figure 4.2G-H, Table 4.1 & Table 4.2).

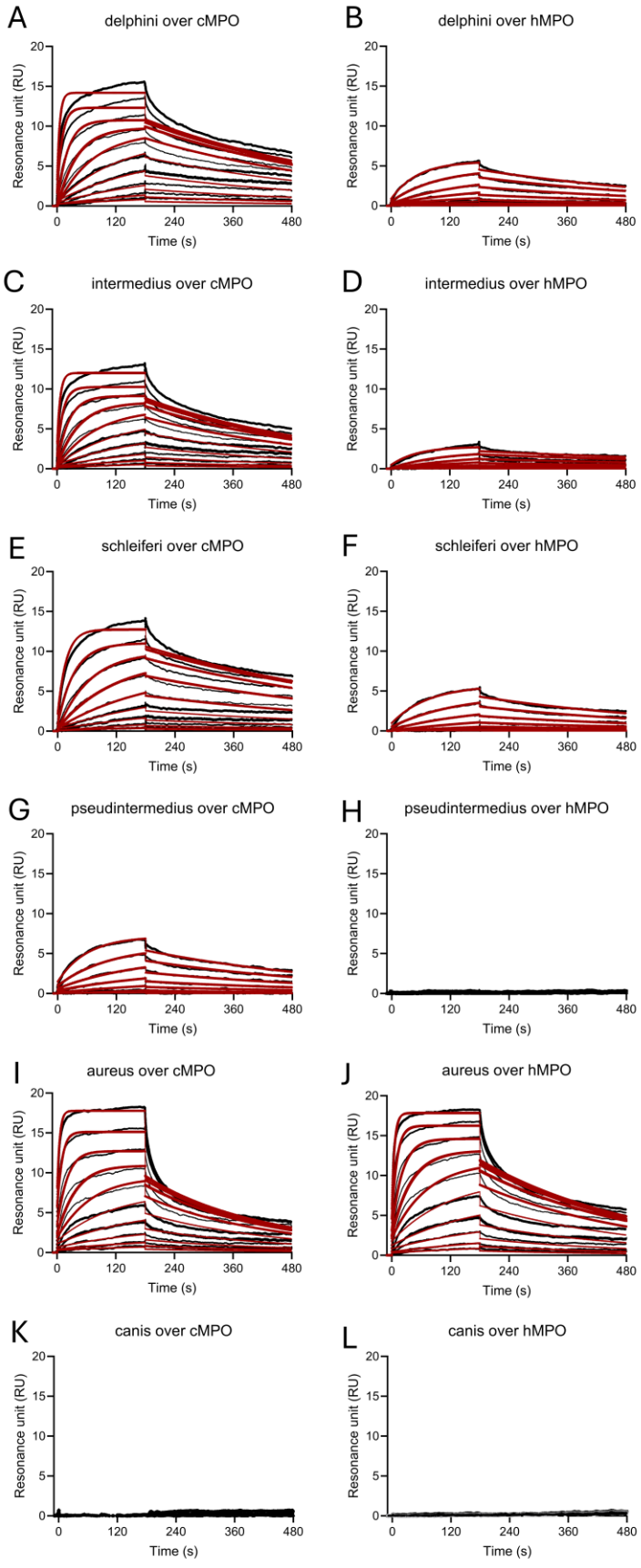
A
delphini over cMPO
B
delphini over hMPO
C
intermedius over cMPO
D
intermedius over hMPO
E
schleiferi over cMPO
F
schleiferi over hMPO
G
pseudintermedius over cMPO
H
pseudintermedius over hMPO
I
aureus over cMPO
J
aureus over hMPO
K
canis over cMPO
L
canis over hMPO
Resonance unit (RU)
Time (s)
0
5
10
15
20
0
120
240
360
480

Figure 4.2. MPO Binding Properties of Various SPIN Orthologs as Assessed by SPR in first trial.

The binding properties of SPIN orthologs to immobilized canine MPO purified in first trial were compared to those of immobilized human MPO. Reference-subtracted sensorgrams (black traces) were obtained for each sample following injection of a two-fold dilution series, using 1 μM as the highest concentration. Sensorgram series were fitted globally to a Langmuir binding model (red traces). The outcome of fitting is shown in Table 4.1 & Table 4.2.

The findings derived from the cMPO purified during the second trial resembled our previous observations and aligned with the results of the inhibition assays (Figure 4.1B-D, Figure 4.3, Table 4.1 & Table 4.2). Specifically, the apparent affinity of SPIN-delphini for cMPO was estimated at 8.95 nM, contrasting with its 11-fold weaker interaction with hMPO (K_D 100 nM) (Figure 4.3A-B, Table 4.3 & Table 4.4). This selectivity was observed in SPIN-intermedius and SPIN-schleiferi, which exhibited approximately 12-fold (K_D 9.25 nM) and 8-fold (K_D 26.15 nM) greater binding affinities for cMPO relative to their respective interactions with hMPO (K_D 107.5 nM and 200 nM) (Figure 4.3C-F, Table 4.3 &Table 4.4). Furthermore, SPIN-pseudintermedius maintained its profile, associating with cMPO with an apparent affinity of 157.3 nM despite showing no detectable evidence of binding to the human ortholog (Figure 4.3G-H, Table 4.3 & Table 4.4). This reproducibility across two independent biological replicate experiments reinforces the premise that these SPIN variants have evolved refined host-specific molecular recognition properties.

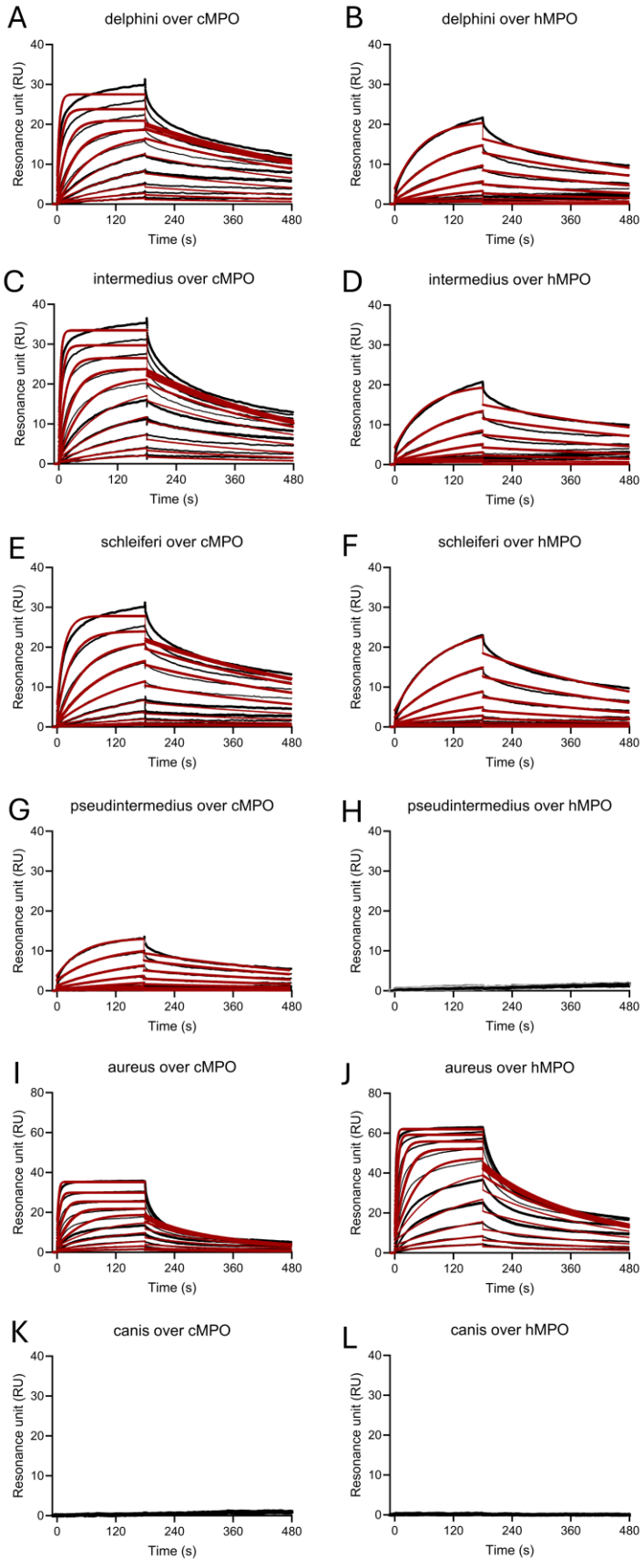
A
delphini over cMPO
B
delphini over hMPO
C
intermedius over cMPO
D
intermedius over hMPO
E
schleiferi over cMPO
F
schleiferi over hMPO
G
pseudintermedius over cMPO
H
pseudintermedius over hMPO
I
aureus over cMPO
J
aureus over hMPO
K
canis over cMPO
L
canis over hMPO
Resonance unit (RU)
Time (s)

Figure 4.3. MPO Binding Properties of Various SPIN Orthologs as Assessed by SPR in second trial.

The binding properties of SPIN orthologs to immobilized canine MPO purified in second trial were compared to those of immobilized human MPO. Reference-subtracted sensorgrams (black traces) were obtained for each sample following injection of a two-fold dilution series, using 1 μM as the highest concentration. Sensorgram series were fitted globally to a Langmuir binding model (red traces). The outcome of fitting is shown in Table 4.3 & Table 4.4.

3.3. Binding Preferences of SPIN Variants for MPOs from Known Host Species arise from Increased Association Rates

Characterization of SPIN-aureus loss-of-function mutants demonstrated that the observed decline in apparent affinity for hMPO was primarily attributable to a significant reduction in the association rate of these variants [49]. This fundamental role of association rate was further confirmed by investigation of the N-terminal domain of SPIN-aureus [63]. In that study, the incorporation of a stabilizing disulfide bond-the SPIN-Cys mutant-yielded a simultaneous enhancement in inhibitory potency and binding affinity driven by an accelerated association rate with hMPO [63]. This prompted us to consider the underlying mechanism driving the increased potency of these SPIN orthologs. Specifically, we sought to determine whether the increased affinity displayed by these SPIN variants for cMPO similarly resulted from an increased association rate.

To address this question, we compared the individual rate constants derived from fitting experimental sensorgram series to identify potential trends in the data. Examination of the individual rate constants revealed that the enhanced affinity of SPIN orthologs arises from an increase in their association rates with cMPO (Figure 4.4, Figure 4.6). If there is a statistically significant difference in binding affinity (K_D), there is a statistically significant difference in association rate (k_a) (Figure 4.5).

The 16-fold higher affinity of SPIN-delphini for cMPO is driven by a commensurate increase in its association rate (Figure 4.4B & E, Figure 4.5A-B, Table 4.1 & Table 4.2), as its

dissociation rates from both canine and human MPO remain nearly identical (Figure 4.4 C & F, Figure 4.5B-C, Table 4.1 & Table 4.2). In contrast, the enhanced affinity of SPIN-intermedius is a cumulative result of an 11-fold faster initial binding of the helical bundle domain (Figure 4.4B & E, Figure 4.5E, Table 4.1 & Table 4.2) combined with a 2-fold slower dissociation rate from cMPO (Figure 4.4C & F, Figure 4.5F, Table 4.1 & Table 4.2). Similarly, SPIN-schleiferi interacts with cMPO with a 7-fold accelerated association rate (Figure 4.4B & E, Figure 4.5H, Table 4.1 & Table 4.2)but a comparable dissociation rate from both enzymes (Figure 4.4B & E, Figure 4.5 I, Table 4.1 & Table 4.2). While SPIN-aureus maintains similar binding affinities for both enzymes due to similar association rates (Figure 4.2I-J, Figure 4.4A-B & D-E, Figure 4.5J-K, Table 4.1 & Table 4.2), its 1.4-fold faster dissociation from cMPO could account for its diminished inhibitory potency against the cMPO (Figure 4.4C & F, Figure 4.5L, Table 4.1 & Table 4.2).

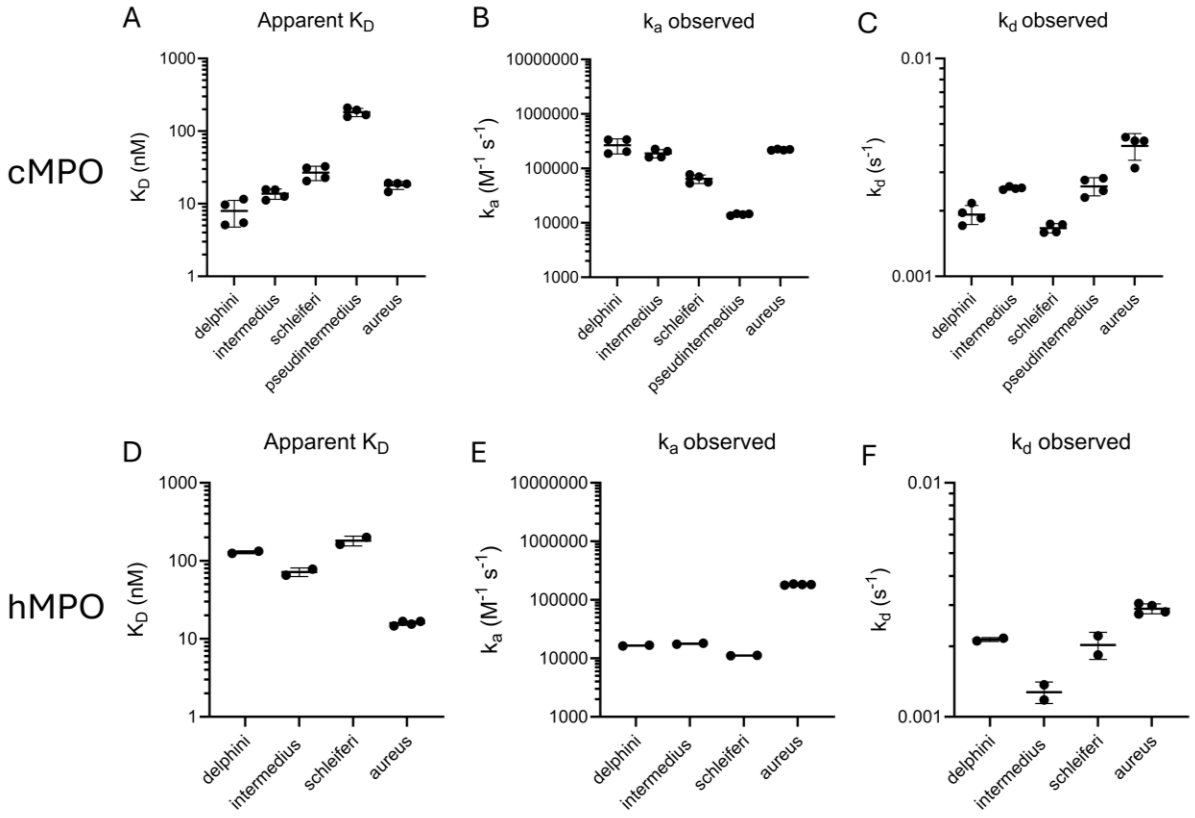

Figure 4.4. Comparative Analysis of the Binding Parameters for Various SPIN Variants over canine MPO (purified in first trial) and human MPO.

(A) Comparison of apparent K_D values for SPIN orthologs over cMPO. Error bars show the mean, plus or minus the standard deviation for a minimum of four replicates. (B) Observed k_a for SPIN orthologs over cMPO (C) Observed k_d for SPIN orthologs over cMPO (D) Comparison of apparent K_D values for SPIN orthologs over hMPO. Error bars show the mean, plus or minus the standard deviation for a minimum of four replicates. (E) Observed k_a for SPIN orthologs over hMPO. (F) Observed k_d for SPIN orthologs over hMPO.

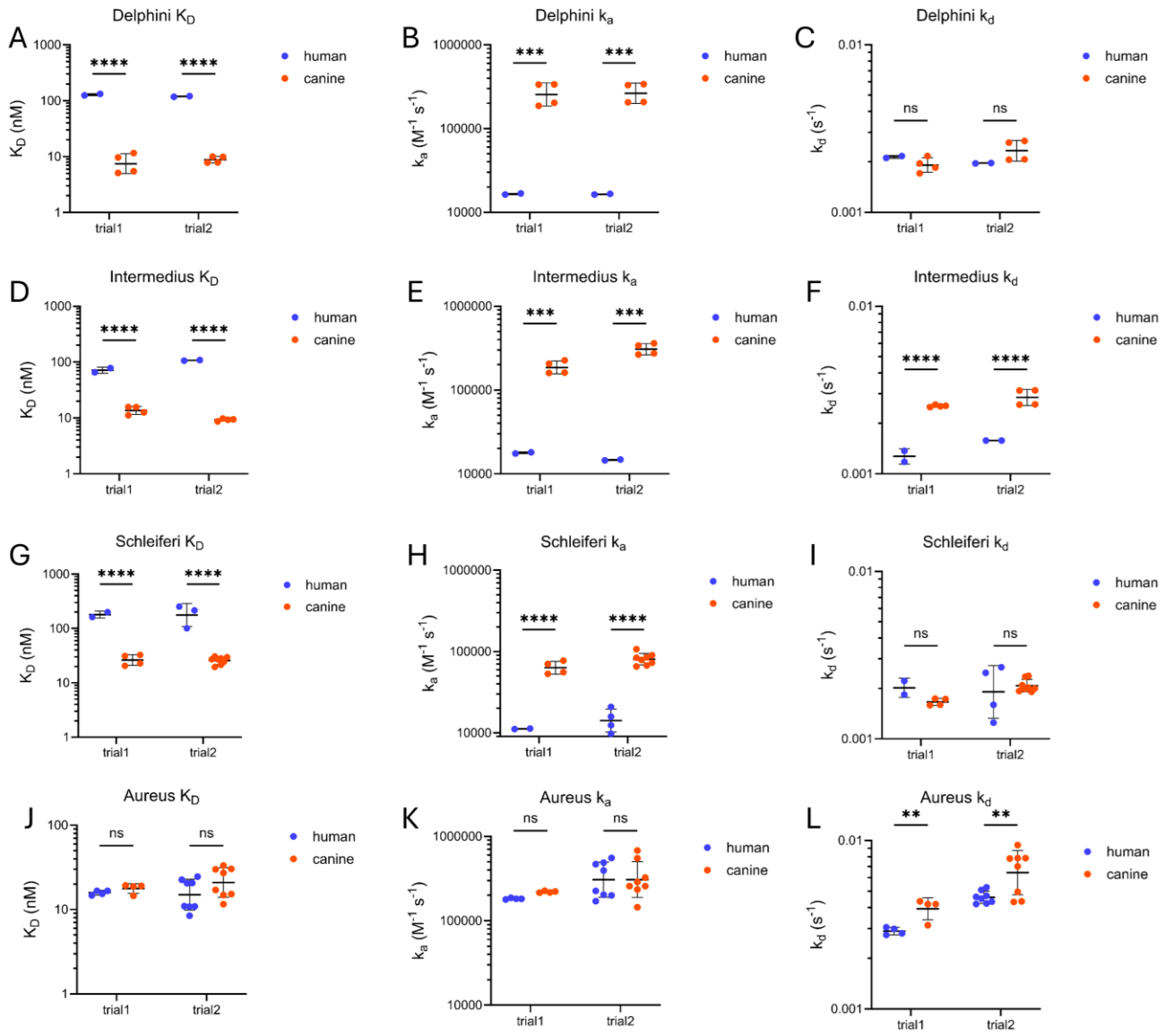

Figure 4.5. Pairwise Comparison of Binding Parameters for SPIN Variants over canine MPO with human MPO.

(Panels A, D, G and J) Comparison of apparent K_D values for SPIN-delphini, -intermedius, -schleiferi and -aureus over cMPO (obtained in first and second trial) with that of hMPO. Error bars show the mean, plus or minus the standard deviation for a minimum of two replicates. (Panels B, E, H and K) Comparison of observed k_a values for SPIN-delphini, -intermedius, -schleiferi and -aureus over cMPO (obtained in first and second trial) with that of hMPO. Error bars show the mean, plus or minus the standard deviation for a minimum of two replicates. (Panels C, F, I and L) Comparison of observed k_d values for SPIN-delphini, -intermedius, -schleiferi and -aureus over cMPO (obtained in first and second trial) with that of hMPO. Error bars show the mean, plus or minus the standard deviation for a minimum of two replicates.

Our subsequent observations remained consistent with the first trial dataset. SPIN-delphini maintained a 16-fold elevation in its association rate with cMPO (Figure 4.6B & E, Figure 4.5A-B, Table 4.3 & Table 4.4), whereas its dissociation rate exhibited no significant difference between the two enzymes (Figure 4.6 C & F, Figure 4.5B-C, Table 4.3 & Table 4.4). SPIN-intermedius displayed a 21-fold increase in association rate (Figure 4.6B & E, Figure 4.5E, Table 4.3 & Table 4.4) coupled with a 1.8-fold reduction in dissociation rate when interacting with cMPO relative to hMPO (Figure 4.6C & F, Figure 4.5F, Table 4.3 & Table 4.4). Similarly, SPIN-schleiferi demonstrated an ~6-fold acceleration in its association with the cMPO (Figure 4.6B & E, Figure 4.5H, Table 4.3 & Table 4.4), though it dissociated from both enzymes comparably (Figure 4.6B & E, Figure 4.5 I, Table 4.3 & Table 4.4). In contrast, the association rate for SPIN-aureus remained similar across both enzymes (Figure 4.6A-B & D-E, Figure 4.5J-K, Table 4.3 & Table 4.4); however, it dissociated ~1.4-fold faster from cMPO.

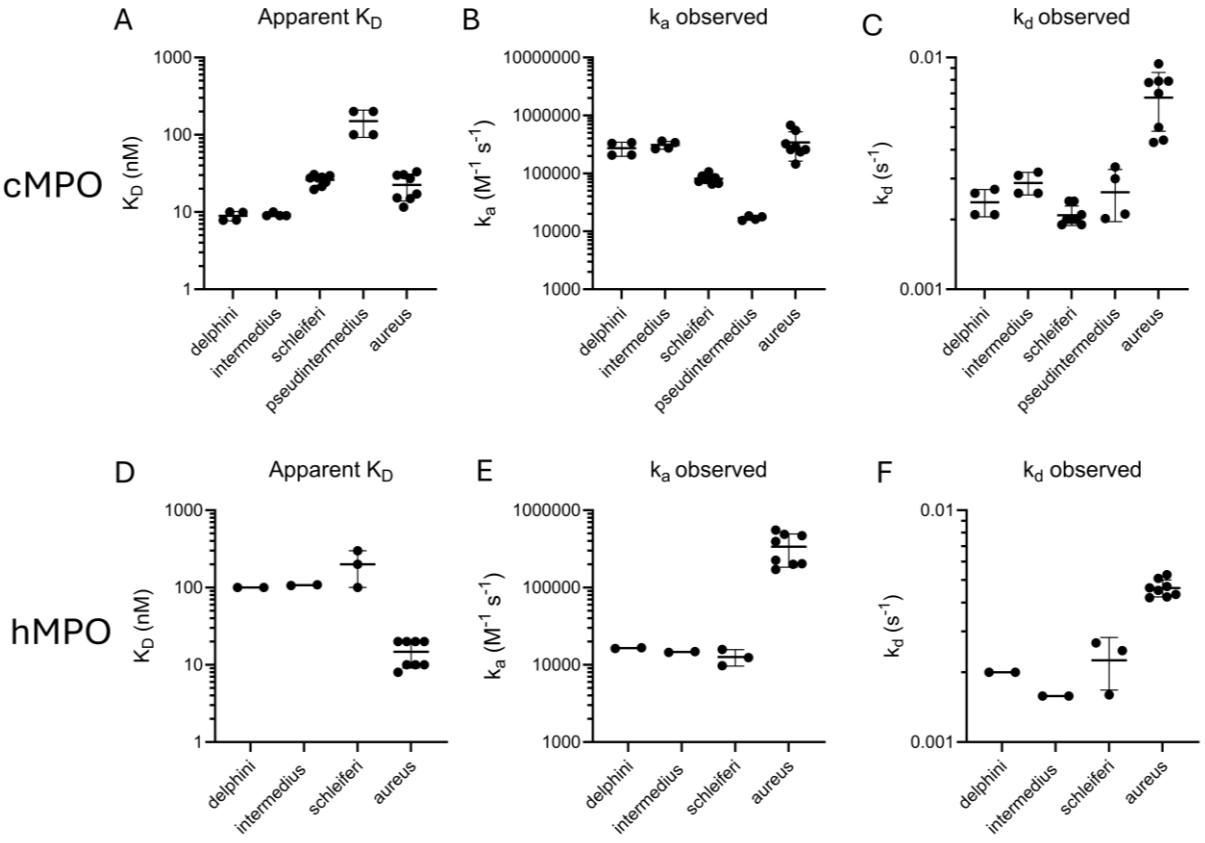

Figure 4.6. Comparative Analysis of the Binding Parameters for Various SPIN Variants over canine MPO (purified in second trial) and human MPO.

(A) Comparison of apparent K_D values for SPIN orthologs over cMPO. Error bars show the mean, plus or minus the standard deviation for a minimum of four replicates. (B) Observed k_a for SPIN orthologs over cMPO (C) Observed k_d for SPIN orthologs over cMPO (D) Comparison of apparent K_D values for SPIN orthologs over hMPO. Error bars show the mean, plus or minus the standard deviation for a minimum of four replicates. (E) Observed k_a for SPIN orthologs over hMPO. (F) Observed k_d for SPIN orthologs over hMPO.

3.4. The crystal structure of SPIN-delphini bound to cMPO at 2.1 Å resolution

The purification procedure outlined in Materials and Methods yielded peroxidase which was pure by 82% analyzed by SDS-PAGE as well as the ratio of the absorbance at 430 nm to that of 280 nm. Electrophoretic examination revealed the presence of components of apparent molecular weights 14500 and 57500 (heavy and light components). Different preparations of myeloperoxidase, either from individual animal (first trial) or from pooled pus (second trial),

gave a reproducible pattern in electrophoretic analysis. This pattern was similar to that observed in native human myeloperoxidase. SPIN orthologs from *S. delphini*, *S. intermedius*, *S. schleiferi*, and *S. pseudintermedius* fail to bind with or inhibit human MPO with the same affinity or potency as the S. aureus SPIN. Therefore, we hypothesized that these SPIN variants may instead exhibit a similar selectivity for MPO derived from their preferred hosts. Additional structural and functional information was required to determine whether or not this is the case. To test this hypothesis, we crystallized SPIN-delphini bound to cMPO to better understand the host species specificity of these SPIN proteins at the structural level. We succeeded in growing single crystals of SPIN-delphini bound to cMPO that diffracted synchrotron X-rays to 2.1 Å limiting resolution and solved and refined this structure to R_{work}/R_{free} (%) values of 17.8 / 20.1. The final $2F_o$-F_c electron density maps were consistent with the existence of four covalent bonds between SPIN-delphini bound cMPO and the heme group: H^{502} to heme Fe at 2.1 Å, M^{409} to heme CBB at 2.6 Å, D^{260} to heme CMD at 2.4 Å and E^{408} to heme CMB at 2.6 Å. In all mammalian peroxidases each half of dimeric MPO contains one iron, present as covalently bound heme, one calcium and one chloride [59]. Our predicted model confirmed this composition, locating a single Cl^- and Ca^{2+} in each monomer, coordinated entirely by residues within the MPO polypeptide chain. We identified four N-linked glycosylation sites within the large polypeptide, conforming to the Asn-X-Ser/Thr consensus motif at residues N^{355}, N^{391}, N^{483}, and N^{729}. Of these, N^{355}, N^{483}, and N^{729} exhibited extensive glycan chains (PDB entry TBD).

Table 4.5. X-ray Diffraction Data, Structure Solution, and Refinement Statistics[a]

	SPIN-delphini/cMPO
PDB Accession Code	12CL
Data Collection	
Beamline	ALS-5.0.1
Space Group	*C*2
Wavelength (Å)	0.9775
Cell Dimensions	
a, b, c (Å)	132.70, 145.38, 107.61
α, β, γ (º)	90, 114.85, 90
Resolution (Å)	50.00-2.10
Wilson B-Factor (Å^2)	27.6
Completeness (%)	100.0 (99.8)
I / σI	12.4 (1.9)
R_{pim}	0.060 (0.404)
$CC_{1/2}$	0.992 (0.658)
Redundancy	6.8 (6.0)
Refinement	
Resolution (Å)	49.42-2.09 (2.17-2.09)
Number of Reflections	107,489
R_{work} / R_{free} (%)	16.7 / 19.9
Atoms Modeled	11,582
Ordered Solvent	866
Ramachandran Plot	
Favored/Allowed (%)	97.16 / 2.76
Average B-Factors (Å^2)	36.79
R.M.S. Deviations	
Bond Lengths (Å)	0.008
Bond Angles (°)	0.95

[a]Values in parentheses are for the highest-resolution shell.

3.5. Sequence-dependent structural differences between human and canine MPO explain preference of SPIN-delphini for canine MPO

Whereas MPO from human and canine share about 90% identity, the affinity of SPIN-delphini for these two MPOs differ by nearly 14-fold at 114.5 nM and 8.4 nM, respectively. Therefore, we considered whether the differences in affinities observed by SPR were due to alterations of key sidechains found at the respective SPIN/cMPO interfaces. We analyzed the SPIN-delphini/cMPO complex using the EBI-PISA server and used the output to construct both an interface map and a list of likely intermolecular interactions. We then compared these data

from SPIN-delphini/cMPO to analogous results obtained for SPIN-delphini/rhMPO [24]. We determined that the total number of inhibitor-derived residues at the SPIN-delphini/cMPO interface (30) is identical to that of SPIN-delphini/rhMPO (30) (Table 4.6). Out of the 30 residues found at the interface, 28 interfacing residues are identical between SPIN-delphini/cMPO and SPIN-delphini/hMPO [24] (Table 4.6). We found that 13 residues driven from SPIN-delphini are involved in polar interactions (i.e. hydrogen bonds and salt bridges) with residues derived from cMPO, whereas only 10 residues formed polar contacts with residues derived from hMPO [24] (Table 4.6). Eight of these residues are identical between the two complexes and were deemed to form equivalent interactions (i.e. S^{31}, Q^{32}, N^{33}, H^{38}, R^{42}, M^{43}, Y^{50} and D^{89}) [24] (Table 4.6).

By contrast, residues D^{40}, H^{46}, Q^{47}, Q^{62} and T^{63} form polar contacts only in SPIN-delphini/cMPO while residues D^{45} and Y^{70} do so only in complex with rhMPO [24] (Table 4.6). D^{40}, which resides in the SPIN-delphini beta-hairpin domain, is involved in hydrogen bonding with L^{349} and R^{352} of cMPO (Table 4.6 & Figure 4.7A) while there is no such interaction between SPIN-delphini and rhMPO (Table 4.6 & Figure 4.7B) [24]. Separately, SPIN-delphini H^{46} is involved in a hydrogen bond with R^{352} and R^{354} of cMPO, but lacking an equivalent interaction with hMPO (Table 4.6 & Figure 4.7A & B) [24]. E^{47} from SPIN-delphini forms two strong H-bonds with R^{352} of cMPO (Table 4.6, Figure 4.7A & B). H^{46} forms two H-bonds with R^{352} and R^{354} in cMPO, lacking an equivalent interaction with hMPO (Table 4.6, Figure 4.7A & B). SPIN-delphini Y^{50} forms stronger hydrogen bonds with residues R^{354} and L^{356} from cMPO (3 Å and 2.9 Å, respectively) compared to those of rhMPO (3.2 Å and 3.1 Å, respectively) (Table 4.6, Figure 4.7A-B). In summary, while SPIN-delphini maintains an ability to bind human MPO and inhibit its activity, the quantitative differences between its affinity for and

inhibition of human and canine MPO appear to be predicated upon sequence/structure changes that affect both the overall orientation and positioning of functional groups at the MPO binding site.

Table 4.6: Comparative interface analysis of SPIN-delphini/cMPO and SPIN-delphini/rhMPO [24].

		Interface with cMPO		Interface with hMPO	
	SPIN residue	**Bond type**	**MPO residue**	**Bond type**	**MPO residue**
29	VAL				
30	THR				
31	**SER**	H	**GLU268/PRO269**	H	**GLU268/PRO269**
32	**GLN**	H	**SER266**	H	**THR266/GLU268**
33	**ASN**	H	**GLU268**	H	**GLU268**
34	GLY				
35	ILE				
36	ILE				
37	LEU				
38	**HIS**	HS	**ASP380**	H/S/S	**ASP380**
39	ASP				
40	ASP	H/HS	LEU349/ARG352		
42	**ARG**	H/H	**ARG352/ASN381**	H	**ASN381**
43	**MET**	H	**ASN381**	H	**ASN381**
44	LEU				
45	ASP			H/S	ARG368
46	HIS	H	ARG354		
47	GLU	HS	ARG352		
49	GLN				
50	**TYR**	H	**ARG354/LEU356**	H	**ARG354/MET356**
53	VAL				
60	ASN				
62	GLN	H	ASP438		
63	THR	H	GLN359		
66	ARG				
67	LEU				
70	TYR			H	ASN352
74	GLN				
89	**ASP**	H	**ASN381**	H	**ASN381**
91	LEU				
92	ASP				

Identical interactions in bold typeface	residues at the interface with MPO
H: hydrogen bond	bond forming residues with cMPO only
S: salt bridge	bond forming residues with hMPO only
	bond forming residues with both MPOs

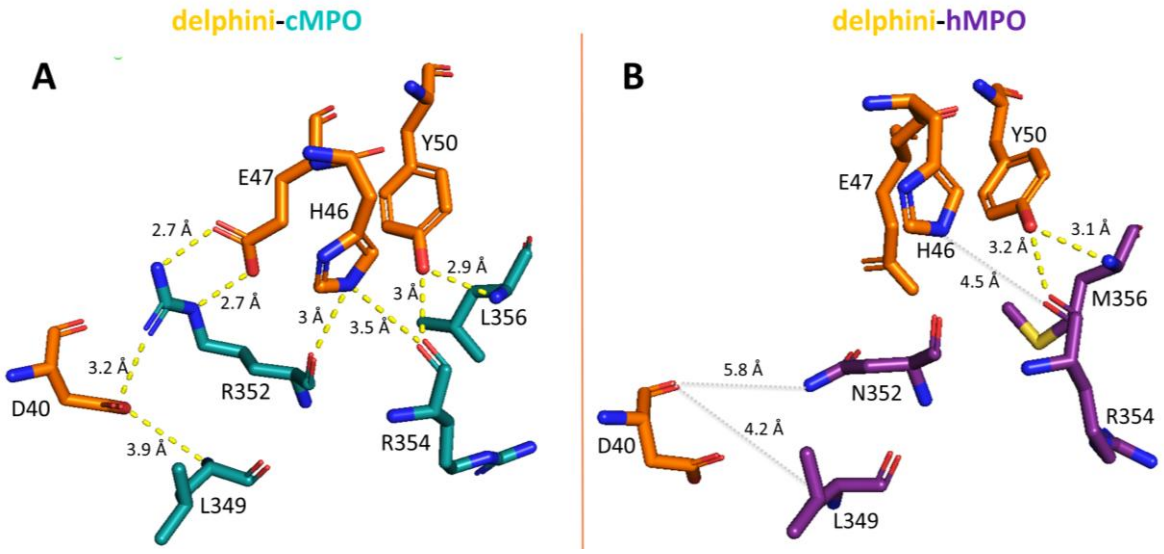

Figure 4.7. Molecular Analysis of the SPIN-delphini/cMPO Interface and Comparsion with SPIN-delphini/rhMPO.

(A) Polar interactions between residues driven from SPIN-delphini to those of canine MPO. D^{40} sidechain (orange) forms two hydrogen bonds with L^{349} and R^{352} of cMPO (aqua green). Likely interactions (yellow dashes) and their corresponding distances are labeled. H46 is involved in two H-bonds with R^{352} and R^{354} of cMPO. Likely interactions (yellow dashes) and their corresponding distances are labeled. E^{47} H-bonds R^{352} of cMPO. Likely interactions (yellow dashes) and their corresponding distances are labeled. Y^{50} forms two strong H-bonds with R^{354} and L^{356} from cMPO. Likely interactions (yellow dashes) and their corresponding distances are labeled. (B) SPIN-delphini D^{40} sidechain (orange) distances from L^{349} and N^{352} of rhMPO (purple) shown in grey dashes representing interactions not formed due to excessive distance between donor and acceptor groups. H^{46} sidechain (orange) distance from M^{356} of rhMPO (purple) shown in grey dashes representing interactions not formed due to excessive distance between donor and acceptor groups. Polar interactions between SPIN-delphini Y^{50} sidechains (orange) with R^{354} and M^{356} of rhMPO (purple). Likely interactions (yellow dashes) and their corresponding distances are labeled.

4. DISCUSSION

Majority of the immune evasion molecules secreted by *S. aureus* at infection sites, demonstrate a pronounced specificity for human [13]. This species-selectivity is notably evident in the bi-component pore-forming leukocidins of *S. aureus* and related staphylococci as they exhibit strong preference for cellular receptors from specific species, thereby dictating their divergent cytotoxic effects across target leukocytes from various hosts [66]. Similarly, the *S.*

aureus SCIN (Staphylococcal Complement Inhibitor) protein family effectively neutralizes the alternative complement pathway in humans while remaining inactive in murine models [67,68]. SPIN, as an *S. aureus* immune evasion protein, also shows strong selectivity for MPO from its biologically relevant host [20].

SPIN orthologs are distributed across several bacterial species closely related to *S. aureus* [24]. While *S. aureus* is recognized as a versatile pathogen capable of colonizing both humans and livestock (such as dairy cattle), multiple staphylococcal species encoding SPIN-like sequences, including *S. delphini*, *S. intermedius*, *S. schleiferi*, and *S. pseudintermedius*, are primarily known as pathogens of livestock and/or companion animals [26]. Consistent with this, SPIN-aureus demonstrates a pronounced binding selectivity and inhibitory potency toward myeloperoxidase derived from its human host, yet it lacks any detectable interaction with or inhibition of murine MPO and many others [20]. Additionally, it is noteworthy that SPIN orthologs from *S. delphini*, *S. intermedius*, *S. schleiferi*, and *S. pseudintermedius* fail to bind with or inhibit human MPO with the same affinity or potency as the *S. aureus* SPIN [24]. Therefore, we hypothesized that these SPIN variants may instead exhibit a similar selectivity for MPO derived from their preferred hosts.

To evaluate this hypothesis, we successfully isolated cMPO and characterized its inhibitory profile against a diverse array of SPIN orthologs. Leveraging canine abscess fluid samples collected independently for veterinary diagnostic purposes, we purified the native enzyme through a combination of purification strategies including CTAB extraction, sonication and ammonium sulfate precipitation, followed by cation exchange and gel filtration chromatographies. Our preliminary efforts to isolate native MPO from canine pus were significantly hindered by a dramatic loss of enzymatic activity due to extensive proteolytic

degradation within the sample. To mitigate this issue, we incorporated a potent protease inhibitor cocktail into the extraction mix prior to cellular lysis. The progressive enrichment of the catalytically active enzyme was monitored following each purification step via validation of both protein concentration and enzymatic activity through determination of the Reinheit Zahl ratio (A_{430}/A_{280}) and the colorimetric activity assay. During the purification process, the enzyme's distinctive green color served as a visual indicator to identify MPO-rich fractions following each chromatographic step.

Our preliminary findings substantiated our hypothesis, revealing that SPIN orthologs from other staphylococcal species exhibit significantly higher affinity and potency toward cMPO relative to hMPO (Figure 4.1, Figure 4.2 & Figure 4.3). Across both independent experimental series, we observed that SPIN-delphini, SPIN-intermedius, and SPIN-schleiferi suppressed cMPO activity with greater potency than hMPO. Specifically, during the first trial, these orthologs demonstrated approximately 16-, 33- and 28-fold increase in potency, respectively (Figure 4.1B, Table 4.1 & Table 4.2); this trend was reproduced in the second trials with corresponding shifts of 29-, 35-, and 20-fold (Figure 4.1C, Table 4.3 & Table 4.4). The notable increase in the fold-difference observed for SPIN-delphini during the second trial is likely a result of methodological refinement, as the use of lower inhibitor concentrations allowed for a more precise generation of the dose-response curve. Furthermore, despite SPIN-pseudintermedius failure to bind to or inhibit hMPO (Figure 4.2 & Figure 4.3), it inhibited cMPO with IC_{50} values of 115.5 nM and 97.9 nM in the first and second trials, respectively (Figure 4.1B-C).

S. aureus is a known pathogen of both humans and livestock [25]. In our SPR analysis across both trials, SPIN-aureus demonstrated nearly identical association rates for both human

and canine MPO (Figure 4.4B & E, Figure 4.5K & Figure 4.6B& E), resulting in overall comparable binding affinities (Figure 4.2I-J, Figure 4.3I-J & Figure 4.5J). However, we observed a significantly faster dissociation rate (k_d) from cMPO compared to hMPO (Figure 4.4C & F, Figure 4.5L, Figure 4.6C & F). This increased off-rate likely explains the observed reduction in inhibitory potency against canine MPO. Even though the protein recognizes both targets with equal rate, the resulting cMPO/SPIN-aureus complex is shorter-lived and less stable than that of hMPO/SPIN-aureus. The increased affinity and potency of SPIN-delphini and SPIN-schleiferi are driven by a statistically significant enhancement in the initial association rate (k_a) with cMPO (Figure 4.4B&E, Figure 4.5B&H, Figure 4.6B&E). The increased affinity of SPIN-intermedius for cMPO also resulted from a significant improvement in the association rate (k_a) (Figure 4.4B&E, Figure 4.5E, Figure 4.6B&E), but further displayed a modest, but significant, 2-fold decrease in the dissociation rate (k_d) (Figure 4.4C&F, Figure 4.5F, Figure 4.6C&F).

The comparative structural analysis of SPIN-delphini in complex with cMPO versus hMPO (Figure 4.7A & B) reveals that while the total number of interfacing residues remains identical (30 residues) (Table 4.6), the specific network of polar interactions is distinct and likely dictates the differential binding affinities. We observed that SPIN-delphini forms 13 polar contacts with cMPO compared to only 10 with hMPO (Table 4.6). Notably, D^{40}, which resides in the SPIN-delphini beta-hairpin domain, is involved in hydrogen bonding with L^{349} and R^{352} of cMPO (Table 4.6 & Figure 4.7A) while there is no such interaction between SPIN-delphini and rhMPO (Table 4.6 & Figure 4.7B) [24] since this position is N^{352} instead. This could partly explain the increased potency of SPIN-delphini against cMPO when compared to hMPO. Separately, SPIN-delphini H^{46} is involved in two hydrogen bonds with R^{352} and R^{354} of cMPO,

but lacking an equivalent interaction with hMPO (Table 4.6 & Figure 4.7A & B) [24]. The residue H^{51} of SPIN-aureus has been found to be the most critical residue in SPIN C-terminal domain for binding to MPO and its loss results in 160-fold weaker inhibition of MPO [49]. E^{47} forms two strong hydrogen bonds with R^{352} of cMPO, lacking such interaction with hMPO (Table 4.6, Figure 4.7A & B). Loss of E^{52} in SPIN-aureus has shown an order of magnitude loss in its affinity and potency against hMPO [49]. It can be inferred that the H^{46} (H^{51} in SPIN-aureus) interaction with R^{352} and R^{354} in cMPO, could also contribute to the 14-fold increased affinity of SPIN-delphini for cMPO when compared to hMPO (Table 4.6, Figure 4.7A-B). It seems that residues D^{40} and E^{47} from SPIN-delphini may be collaborating to engage R^{352} in canine MPO, but this isn't possible in human MPO, since this position is N^{352} instead.

SPIN-delphini Y^{50} forms stronger hydrogen bonds with residues R^{354} and L^{356} from cMPO (3 Å and 2.9 Å, respectively) compared to those of rhMPO (3.2 Å and 3.1 Å, respectively) (Table 4.6, Figure 4.7A & B). In earlier studies on SPIN-aureus, removal of the Y^{50} sidechain (Y^{55} based on SPIN-aureus numbering) resulted in a roughly 24-fold loss of function when compared to SPIN-WT [49]. Thus, shortening of the hydrogen bond distances for this functionally-important position may also contribute to the increased affinity of SPIN-delphini for cMPO compared to rhMPO.

Taken together, these data suggest that while the global binding mode is conserved, the increased potency of SPIN-delphini against canine MPO is predicated upon a more sophisticated network of polar interactions and the strategic positioning of functional groups within the MPO binding pocket. Our quantitative biochemical, functional, and comparative structural information on SPIN orthologs bound to MPO from their preferred host species, can

be developed into a valuable model system for understanding the structure/function principles that underlie host-specific evolution of virulence proteins.

Chapter 5 - Conclusions

The work in this dissertation has clarified the specific molecular interactions that enable *S. aureus* to evade the host innate immune system via the SPIN. Here we investigated the contribution of individual residues in SPIN C-terminal helical bundle binding using sequence conservation and existing structures of SPIN bound to human MPO as a guide. Among selected residues, we found that loss of L49 or E52 reduced SPIN activity by roughly an order of magnitude, but that loss of Y55 or H51 caused progressively greater loss of inhibitory potency. SPR analysis showed that loss of inhibitory potency in these SPIN mutants resulted from a diminished initial interaction between the inhibitor and human MPO. This study identified positions Y55 and H51 as critical determinants of SPIN function.

We showed that SPIN-CYS mutant exhibited a gain in inhibitory potency against human MPO when compared to wild-type SPIN which persisted even in the presence of deleterious mutations within the C-terminal domain. Our SPR studies showed that the gain in potency arose through an increase in apparent affinity of SPIN-CYS for human MPO, which was driven by an increased association rate with MPO when compared to wild-type SPIN. This work provided new information on the coupled binding and folding events required to manifest biological activity of SPIN.

In this dissertation we investigated the species specificity of SPIN proteins using canine MPO and explored its inhibition profile by different SPIN orthologs. We found that SPIN proteins from known canine pathogens bind more tightly to and inhibit canine MPO more potently than human MPO. We also found that the increased affinity arose from increases in the association rate constant. We solved a 2.1 Å resolution co-crystal structure of SPIN-delphini

bound to canine MPO and explained the sequence-dependent physical basis for why SPIN-delphini binds canine MPO with higher affinity than human MPO.

Future research will expand the investigation of host selectivity within the SPIN protein family by leveraging an extensive library of orthologs and purified MPO from diverse host species. We aim to characterize the inhibitory profiles across these variants and elucidate the physical basis for host-specific interactions by solving co-crystal structures of the resulting complexes. Ultimately, this data will be used to establish a model system for understanding the structure-function principles that govern the host-specific evolution of bacterial virulence factors.

Acknowledgements

We extend our sincere gratitude to the Kansas State Veterinary Diagnostic Laboratory, with special thanks to Dr. Kittana and Ms. Amy Burklund, Dr. Renberg and Dr. Celliers for continuously providing us with abscess fluid samples. We are also grateful to the Wildcats Veterinary Clinic and the Little Apple Veterinary Hospital, particularly Dr. Kvasnica and Dr. Lindquist, for providing the abscess samples used in this study. This research would not have been possible without their kind and heartwarming contributions.

5. REFERENCES

[1] W.M. Nauseef, How human neutrophils kill and degrade microbes: An integrated view, Immunol. Rev. 219 (2007) 88–102. https://doi.org/10.1111/j.1600-065X.2007.00550.x.

[2] B. Amulic, C. Cazalet, G.L. Hayes, K.D. Metzler, A. Zychlinsky, Neutrophil Function: From Mechanisms to Disease, Annual Review of Immunology 30 (2012) 459–489. https://doi.org/10.1146/annurev-immunol-020711-074942.

[3] W.L. Lee, R.E. Harrison, S. Grinstein, Phagocytosis by neutrophils, Microbes and Infection 5 (2003) 1299–1306. https://doi.org/10.1016/j.micinf.2003.09.014.

[4] M. Faurschou, N. Borregaard, Neutrophil granules and secretory vesicles in inflammation, Microbes and Infection 5 (2003) 1317–1327. https://doi.org/10.1016/j.micinf.2003.09.008.

[5] W.M. Nauseef, Myeloperoxidase in human neutrophil host defence, Cellular Microbiology 16 (2014) 1146–1155. https://doi.org/10.1111/cmi.12312.

[6] C.T.N. Pham, Neutrophil serine proteases: specific regulators of inflammation, Nat Rev Immunol 6 (2006) 541–550. https://doi.org/10.1038/nri1841.

[7] B. Korkmaz, M.S. Horwitz, D.E. Jenne, F. Gauthier, Neutrophil Elastase, Proteinase 3, and Cathepsin G as Therapeutic Targets in Human Diseases, Pharmacological Reviews 62 (2010) 726–759. https://doi.org/10.1124/pr.110.002733.

[8] H. Odeberg, I. Olsson, Microbicidal mechanisms of human granulocytes: synergistic effects of granulocyte elastase and myeloperoxidase or chymotrypsin-like cationic protein, Infect Immun 14 (1976) 1276–1283. https://doi.org/10.1128/iai.14.6.1276-1283.1976.

[9] V. Brinkmann, U. Reichard, C. Goosmann, B. Fauler, Y. Uhlemann, D.S. Weiss, Y. Weinrauch, A. Zychlinsky, Neutrophil Extracellular Traps Kill Bacteria, Science 303 (2004) 1532–1535. https://doi.org/10.1126/science.1092385.

[10] V. Papayannopoulos, A. Zychlinsky, NETs: a new strategy for using old weapons, Trends in Immunology 30 (2009) 513–521. https://doi.org/10.1016/j.it.2009.07.011.

[11] V. Papayannopoulos, K.D. Metzler, A. Hakkim, A. Zychlinsky, Neutrophil elastase and myeloperoxidase regulate the formation of neutrophil extracellular traps, Journal of Cell Biology 191 (2010) 677–691. https://doi.org/10.1083/jcb.201006052.

[12] Van de Velde: Etude sur le mécanisme de la virulence... - Google Scholar, (n.d.). https://scholar.google.com/scholar_lookup?title=Etude%20sur%20le%20m%C3%A9canisme%20de%20la%20virulence%20du%20staphylocoque%20pyog%C3%A8ne&author=H.%20van%20de%20Velde&publication_year=1894&pages=403-460 (accessed February 17, 2026).

[13] A.N. Spaan, B.G.J. Surewaard, R. Nijland, J.A.G. Van Strijp, Neutrophils Versus *Staphylococcus aureus* : A Biological Tug of War, Annu. Rev. Microbiol. 67 (2013) 629–650. https://doi.org/10.1146/annurev-micro-092412-155746.

[14] C.J.C. De Haas, K.E. Veldkamp, A. Peschel, F. Weerkamp, W.J.B. Van Wamel, E.C.J.M. Heezius, M.J.J.G. Poppelier, K.P.M. Van Kessel, J.A.G. Van Strijp, Chemotaxis Inhibitory Protein of *Staphylococcus aureus* , a Bacterial Antiinflammatory Agent, The Journal of Experimental Medicine 199 (2004) 687–695. https://doi.org/10.1084/jem.20031636.

[15] C. Prat, J. Bestebroer, C.J.C. De Haas, J.A.G. Van Strijp, K.P.M. Van Kessel, A New Staphylococcal Anti-Inflammatory Protein That Antagonizes the Formyl Peptide Receptor-Like 1, The Journal of Immunology 177 (2006) 8017–8026. https://doi.org/10.4049/jimmunol.177.11.8017.

[16] C. Prat, P.-J. Haas, J. Bestebroer, C.J.C. De Haas, J.A.G. Van Strijp, K.P.M. Van Kessel, A Homolog of Formyl Peptide Receptor-Like 1 (FPRL1) Inhibitor from *Staphylococcus aureus* (FPRL1 Inhibitory Protein) That Inhibits FPRL1 and FPR, The Journal of Immunology 183 (2009) 6569–6578. https://doi.org/10.4049/jimmunol.0801523.

[17] A.N. Spaan, T. Henry, W.J.M. van Rooijen, M. Perret, C. Badiou, P.C. Aerts, J. Kemmink, C.J.C. de Haas, K.P.M. van Kessel, F. Vandenesch, G. Lina, J.A.G. van Strijp, The Staphylococcal Toxin Panton-Valentine Leukocidin Targets Human C5a Receptors, Cell Host & Microbe 13 (2013) 584–594. https://doi.org/10.1016/j.chom.2013.04.006.

[18] S.J. Klebanoff, A.J. Kettle, H. Rosen, C.C. Winterbourn, W.M. Nauseef, Myeloperoxidase: a front-line defender against phagocytosed microorganisms, J Leukoc Biol. 93 (2013) 185–198. https://doi.org/10.1189/jlb.0712349.

[19] C.C. Winterbourn, M.B. Hampton, J.H. Livesey, A.J. Kettle, Modeling the Reactions of Superoxide and Myeloperoxidase in the Neutrophil Phagosome: IMPLICATIONS FOR MICROBIAL KILLING*, Journal of Biological Chemistry 281 (2006) 39860–39869. https://doi.org/10.1074/jbc.M605898200.

[20] N.W.M. de Jong, K.X. Ramyar, F.E. Guerra, R. Nijland, C. Fevre, J.M. Voyich, A.J. McCarthy, B.L. Garcia, K.P.M. van Kessel, J.A.G. van Strijp, B.V. Geisbrecht, P.-J.A. Haas, Immune evasion by a staphylococcal inhibitor of myeloperoxidase, Proceedings of the National Academy of Sciences 114 (2017) 9439–9444. https://doi.org/10.1073/pnas.1707032114.

[21] N.W.M. de Jong, N.T. Ploscariu, K.X. Ramyar, B.L. Garcia, A.I. Herrera, O. Prakash, B.B. Katz, K.G. Leidal, W.M. Nauseef, K.P.M. van Kessel, J.A.G. van Strijp, B.V. Geisbrecht, A structurally dynamic N-terminal region drives function of the staphylococcal peroxidase inhibitor (SPIN), Journal of Biological Chemistry 293 (2018) 2260–2271. https://doi.org/10.1074/jbc.RA117.000134.

[22] M. Allison, N. Mishra, B.V. Geisbrecht, Structure, Function, and Mechanistic Insights into a Novel Family of Myeloperoxidase Inhibitory Proteins Expressed by Staphylococci, in: Mammalian Heme Peroxidases, CRC Press, 2021.

[23] U. Leitgeb, P.G. Furtmüller, S. Hofbauer, J.A. Brito, C. Obinger, V. Pfanzagl, The staphylococcal inhibitory protein SPIN binds to human myeloperoxidase with picomolar affinity but only dampens halide oxidation, Journal of Biological Chemistry 298 (2022) 102514. https://doi.org/10.1016/j.jbc.2022.102514.

[24] N.T. Ploscariu, N.W.M. de Jong, K.P.M. van Kessel, J.A.G. van Strijp, B.V. Geisbrecht, Identification and structural characterization of a novel myeloperoxidase inhibitor from *Staphylococcus delphini*, Archives of Biochemistry and Biophysics 645 (2018) 1–11. https://doi.org/10.1016/j.abb.2018.03.007.

[25] Y. Zhang, X. Liu, J. Chen, Coupled binding and folding of disordered SPIN N-terminal region in myeloperoxidase inhibition, Front. Mol. Biosci. 10 (2023). https://doi.org/10.3389/fmolb.2023.1130189.

[26] T. Sasaki, K. Kikuchi, Y. Tanaka, N. Takahashi, S. Kamata, K. Hiramatsu, Reclassification of Phenotypically Identified Staphylococcus intermedius Strains, J Clin Microbiol 45 (2007) 2770–2778. https://doi.org/10.1128/JCM.00360-07.

[27] N.W.M. De Jong, K.P.M. Van Kessel, J.A.G. Van Strijp, Immune Evasion by *Staphylococcus aureus*, Microbiol Spectr 7 (2019) 7.2.20. https://doi.org/10.1128/microbiolspec.GPP3-0061-2019.

[28] K.J. Koymans, M. Vrieling, R.D. Gorham, J.A.G. van Strijp, Staphylococcal immune evasion proteins: Structure, function, and host adaptation, in: Current Topics in Microbiology and Immunology, Springer Verlag, 2017: pp. 441–489. https://doi.org/10.1007/82_2015_5017.

[29] D.A.C. Stapels, K.X. Ramyar, M. Bischoff, M. von Köckritz-Blickwede, F.J. Milder, M. Ruyken, J. Eisenbeis, W.J. McWhorter, M. Herrmann, K.P.M. van Kessel, B.V. Geisbrecht, S.H.M. Rooijakkers, Staphylococcus aureus secretes a unique class of neutrophil serine protease inhibitors, Proceedings of the National Academy of Sciences 111 (2014) 13187–13192. https://doi.org/10.1073/pnas.1407616111.

[30] B.V. Geisbrecht, S. Bouyain, M. Pop, An optimized system for expression and purification of secreted bacterial proteins, Protein Expression and Purification 46 (2006) 23–32. https://doi.org/10.1016/j.pep.2005.09.003.

[31] P. Sukthankar, S.K. Whitaker, M. Garcia, A. Herrera, M. Boatwright, O. Prakash, J.M. Tomich, Thermally Induced Conformational Transitions in Nascent Branched Amphiphilic Peptide Capsules, Langmuir 31 (2015) 2946–2955. https://doi.org/10.1021/la504381y.

[32] A. Holt, D.F. Sharman, G.B. Baker, M.M. Palcic, A Continuous Spectrophotometric Assay for Monoamine Oxidase and Related Enzymes in Tissue Homogenates, Analytical Biochemistry 244 (1997) 384–392. https://doi.org/10.1006/abio.1996.9911.

[33] E.-J. Kim, E.-K. Oh, J.K. Lee, Peroxidase and Photoprotective Activities of Magnesium Protoporphyrin IX, 24 (2014) 36–43. https://doi.org/10.4014/jmb.1311.11088.

[34] F. Sievers, A. Wilm, D. Dineen, T.J. Gibson, K. Karplus, W. Li, R. Lopez, H. McWilliam, M. Remmert, J. Söding, J.D. Thompson, D.G. Higgins, Fast, scalable generation of high-quality protein multiple sequence alignments using Clustal Omega, Mol. Syst. Biol. 7 (2011). https://doi.org/10.1038/msb.2011.75.

[35] X. Robert, P. Gouet, Deciphering key features in protein structures with the new ENDscript server, Nucleic Acids Res 42 (2014) W320–W324. https://doi.org/10.1093/nar/gku316.

[36] E. Krissinel, K. Henrick, Inference of Macromolecular Assemblies from Crystalline State, Journal of Molecular Biology 372 (2007) 774–797. https://doi.org/10.1016/j.jmb.2007.05.022.

[37] M. Hammel, G. Sfyroera, D. Ricklin, P. Magotti, J.D. Lambris, B.V. Geisbrecht, A structural basis for complement inhibition by Staphylococcus aureus, Nat Immunol 8 (2007) 430–437. https://doi.org/10.1038/ni1450.

[38] M. Hammel, G. Sfyroera, S. Pyrpassopoulos, D. Ricklin, K.X. Ramyar, M. Pop, Z. Jin, J.D. Lambris, B.V. Geisbrecht, Characterization of Ehp, a Secreted Complement Inhibitory Protein from Staphylococcus aureus, Journal of Biological Chemistry 282 (2007) 30051–30061. https://doi.org/10.1074/jbc.M704247200.

[39] D. Ricklin, A. Tzekou, B.L. Garcia, M. Hammel, W.J. McWhorter, G. Sfyroera, Y.-Q. Wu, V.M. Holers, A.P. Herbert, P.N. Barlow, B.V. Geisbrecht, J.D. Lambris, A Molecular Insight into Complement Evasion by the Staphylococcal Complement Inhibitor Protein Family, The Journal of Immunology 183 (2009) 2565–2574. https://doi.org/10.4049/jimmunol.0901443.

[40] H. Chen, D. Ricklin, M. Hammel, B.L. Garcia, W.J. McWhorter, G. Sfyroera, Y.-Q. Wu, A. Tzekou, S. Li, B.V. Geisbrecht, V.L. Woods, J.D. Lambris, Allosteric inhibition of complement function by a staphylococcal immune evasion protein, Proc. Natl. Acad. Sci. U.S.A. 107 (2010) 17621–17626. https://doi.org/10.1073/pnas.1003750107.

[41] J.L. Woehl, D.A.C. Stapels, B.L. Garcia, K.X. Ramyar, A. Keightley, M. Ruyken, M. Syriga, G. Sfyroera, A.B. Weber, M. Zolkiewski, D. Ricklin, J.D. Lambris, S.H.M. Rooijakkers, B.V. Geisbrecht, The Extracellular Adherence Protein from *Staphylococcus aureus* Inhibits the Classical and Lectin Pathways of Complement by Blocking Formation of the C3 Proconvertase, The Journal of Immunology 193 (2014) 6161–6171. https://doi.org/10.4049/jimmunol.1401600.

[42] D.A.C. Stapels, J.L. Woehl, F.J. Milder, A.T. Tromp, A.A. Van Batenburg, W.C. De Graaf, S.C. Broll, N.M. White, S.H.M. Rooijakkers, B.V. Geisbrecht, Evidence for multiple modes of neutrophil serine protease recognition by the EAP family of Staphylococcal innate immune evasion proteins, Protein Science 27 (2018) 509–522. https://doi.org/10.1002/pro.3342.

[43] T.J. Herdendorf, D.A.C. Stapels, S.H.M. Rooijakkers, B.V. Geisbrecht, Local structural plasticity of the Staphylococcus aureus evasion protein EapH1 enables engagement with multiple neutrophil serine proteases, Journal of Biological Chemistry 295 (2020) 7753–7762. https://doi.org/10.1074/jbc.RA120.013601.

[44] T.J. Herdendorf, B.V. Geisbrecht, Staphylococcus aureus evasion proteins EapH1 and EapH2: Residue-level investigation of an alternative binding motif for human neutrophil elastase, Archives of Biochemistry and Biophysics 676 (2019) 108140. https://doi.org/10.1016/j.abb.2019.108140.

[45] T.J. Herdendorf, B.V. Geisbrecht, Investigation of Human Neutrophil Elastase Inhibition by *Staphylococcus aureus* EapH1: The Key Role Played by Arginine 89, Biochemistry 57 (2018) 6888–6896. https://doi.org/10.1021/acs.biochem.8b01134.

[46] N. Mishra, T.J. Herdendorf, O. Prakash, B.V. Geisbrecht, Simultaneous inhibition of two neutrophil serine proteases by the S. aureus innate immune evasion protein EapH2, Journal of Biological Chemistry 299 (2023) 104878. https://doi.org/10.1016/j.jbc.2023.104878.

[47] C.D. Gido, T.J. Herdendorf, B.V. Geisbrecht, Characterization of two distinct neutrophil serine protease–binding modes within a Staphylococcus aureus innate immune evasion protein family, Journal of Biological Chemistry 299 (2023) 102969. https://doi.org/10.1016/j.jbc.2023.102969.

[48] N.T. Ploscariu, A.I. Herrera, S. Jayanthi, T.K. Suresh Kumar, B.V. Geisbrecht, O. Prakash, Backbone and side-chain 1H, 15N, and 13C resonance assignments of a novel Staphylococcal inhibitor of myeloperoxidase, Biomol NMR Assign 11 (2017) 285–288. https://doi.org/10.1007/s12104-017-9764-5.

[49] S. Fatehi, T.J. Herdendorf, N.T. Ploscariu, B.V. Geisbrecht, Staphylococcal peroxidase inhibitor (SPIN): Residue-level investigation of the helical bundle domain, Archives of Biochemistry and Biophysics 756 (2024) 110023. https://doi.org/10.1016/j.abb.2024.110023.

[50] F. Delaglio, S. Grzesiek, GeertenW. Vuister, G. Zhu, J. Pfeifer, A. Bax, NMRPipe: A multidimensional spectral processing system based on UNIX pipes, J Biomol NMR 6 (1995). https://doi.org/10.1007/BF00197809.

[51] Y. Shen, A. Bax, Protein backbone and sidechain torsion angles predicted from NMR chemical shifts using artificial neural networks, J Biomol NMR 56 (2013) 227–241. https://doi.org/10.1007/s10858-013-9741-y.

[52] P. Güntert, L. Buchner, Combined automated NOE assignment and structure calculation with CYANA, J Biomol NMR 62 (2015) 453–471. https://doi.org/10.1007/s10858-015-9924-9.

[53] RomanA. Laskowski, J.AntoonC. Rullmann, MalcolmW. MacArthur, R. Kaptein, JanetM. Thornton, AQUA and PROCHECK-NMR: Programs for checking the quality of protein structures solved by NMR, J Biomol NMR 8 (1996). https://doi.org/10.1007/BF00228148.

[54] D. Sharma, K. Rajarathnam, 13C NMR chemical shifts can predict disulfide bond formation, J Biomol NMR 18 (2000) 165–171. https://doi.org/10.1023/A:1008398416292.

[55] Immune Evasion by Staphylococcus aureus | Microbiology Spectrum, (n.d.). https://journals.asm.org/doi/full/10.1128/microbiolspec.gpp3-0061-2019 (accessed February 9, 2026).

[56] J. Arnhold, Properties, functions, and secretion of human myeloperoxidase, in: Biochemistry Moscow, Springer Netherlands, 2004: pp. 4–9. https://doi.org/10.1023/B:BIRY.0000016344.59411.ee.

[57] W.M. Nauseef, Insights into myeloperoxidase biosynthesis from its inherited deficiency, Journal of Molecular Medicine 76 (1998) 661–668. https://doi.org/10.1007/s001090050265.

[58] K. Arnljots, I. Olsson, Myeloperoxidase precursors incorporate heme., Journal of Biological Chemistry 262 (1987) 10430–10433. https://doi.org/10.1016/S0021-9258(18)60977-9.

[59] P.G. Furtmüller, M. Zederbauer, W. Jantschko, J. Helm, M. Bogner, C. Jakopitsch, C. Obinger, Active site structure and catalytic mechanisms of human peroxidases, Arch Biochem Biophys 445 (2006) 199–213. https://doi.org/10.1016/j.abb.2005.09.017.

[60] P.C. Andrews, N.I. Krinsky, The reductive cleavage of myeloperoxidase in half, producing enzymically active hemi-myeloperoxidase, J Biol Chem 256 (1981) 4211–4218.

[61] R. Wever, H. Plat, Spectral properties of myeloperoxidase and its ligand complexes, Biochim Biophys Acta 661 (1981) 235–239. https://doi.org/10.1016/0005-2744(81)90009-7.

[62] J.E. Harrison, S. Pabalan, J. Schultz, The subunit structure of crystalline canine myeloperoxidase, Biochim Biophys Acta 493 (1977) 247–259. https://doi.org/10.1016/0005-2795(77)90181-7.

[63] S. Fatehi, N. Mishra, T.J. Herdendorf, O. Prakash, B.V. Geisbrecht, Staphylococcal peroxidase inhibitor (SPIN): Investigation of the inhibitory N-terminal domain via a

stabilizing disulfide insertion, Archives of Biochemistry and Biophysics 758 (2024) 110060. https://doi.org/10.1016/j.abb.2024.110060.

[64] S.S. Khaligh, F. Khalid-Salako, H. Kurt, M. Yüce, Exploring the Interaction of Biotinylated FcGamma RI and IgG1 Monoclonal Antibodies on Streptavidin-Coated Plasmonic Sensor Chips for Label-Free VEGF Detection, Biosensors 14 (2024). https://doi.org/10.3390/bios14120634.

[65] M. Collins, N. Ibeanu, W.R. Grabowska, S. Awwad, P.T. Khaw, S. Brocchini, H. Khalili, Bispecific FpFs: a versatile tool for preclinical antibody development, RSC Chem Biol 5 (2024) 1147–1164. https://doi.org/10.1039/d4cb00130c.

[66] A.N. Spaan, J.A.G. van Strijp, V.J. Torres, Leukocidins: staphylococcal bi-component pore-forming toxins find their receptors, Nat Rev Microbiol 15 (2017) 435–447. https://doi.org/10.1038/nrmicro.2017.27.

[67] S.H.M. Rooijakkers, M. Ruyken, A. Roos, M.R. Daha, J.S. Presanis, R.B. Sim, W.J.B. van Wamel, K.P.M. van Kessel, J.A.G. van Strijp, Immune evasion by a staphylococcal complement inhibitor that acts on C3 convertases, Nat Immunol 6 (2005) 920–927. https://doi.org/10.1038/ni1235.

[68] I. Jongerius, J. Köhl, M.K. Pandey, M. Ruyken, K.P.M. van Kessel, J.A.G. van Strijp, S.H.M. Rooijakkers, Staphylococcal complement evasion by various convertase-blocking molecules, J Exp Med 204 (2007) 2461–2471. https://doi.org/10.1084/jem.20070818.